

CONSEIL INTERNATIONAL DES UNIONS SCIENTIFIQUES

UNION GEODESIQUE ET GEOPHYSIQUE INTERNATIONALE

ASSOCIATION DE SÉISMOLOGIE
ET DE
PHYSIQUE DE L'INTÉRIEUR DE LA TERRE

PUBLICATIONS DU BUREAU CENTRAL SÉISMOLOGIQUE INTERNATIONAL

Sous la direction de J. P. ROTHÉ

SECRÉTAIRE DE L'ASSOCIATION DE SÉISMOLOGIE ET DE PHYSIQUE DE L'INTÉRIEUR DE LA TERRE

SÉRIE A
TRAVAUX SCIENTIFIQUES

Fascicule 24

Assemblée Générale de Zürich 1967



TOULOUSE
ÉDOUARD PRIVAT & C^o Libraire-Éditeur
14, RUE DES ARTS, 14

1968



AVERTISSEMENT

Dans le présent fascicule on trouvera le texte de quelques-unes des communications scientifiques qui ont été présentées au cours de l'Assemblée Générale de Zurich (25 septembre au 6 octobre 1967).

Les communications publiées se rapportent aux sujets suivants :

Stations complexes (Arrays);

Tables de temps de propagation (Travel-Time Tables).

Les autres communications présentées sont destinées à paraître dans les différents périodiques scientifiques. On en trouvera les références bibliographiques dans les Comptes Rendus n° 15, Association de Séismologie et de Physique de l'Intérieur de la Terre; Comptes Rendus des séances de la XIV^e conférence réunie à Zurich du 25 septembre au 6 octobre 1967, Strasbourg, 1968 (sous presse).

J.-P. ROTHÉ,

Secrétaire général

*de l'Association Internationale de Séismologie
et de Physique de l'Intérieur de la Terre.*

1880

1881

1882

1883

1884

1885

1886

1887

1888

1889

1890

1891

1892

1893

1894

1895

1896

1897

1898

1899

1900

1901

1902

1903

1904

1905

1906

1907

1908

1909

1910

1911

1912

1913

1914

1915

ASSEMBLEE GENERALE DE ZURICH

(25 septembre au 6 octobre 1967)

COMMUNICATIONS PUBLIÉES DANS LE FASCICULE 24 DES TRAVAUX SCIENTIFIQUES DU BUREAU CENTRAL INTERNATIONAL DE SÉISMOLOGIE

TABLE DES MATIÈRES

ARRAYS

	PAGES
P. E. GREEN, Recent experiments with a large aperture seismic array	7
K. WHITHAM, D. H. WEICHERT, Geophysical results from digital processing of Yellowknife arrays signals	29
G. NEWSTEAD and J. CLEARY, Preliminary results from the Warrawunga array	45
P. MECHLER and Y. ROCARD, Limitation géologique dans l'utilisation d'un réseau de sismographes	57
B. A. BOLT and T. Mc EVILLY, Earth structure and focal mechanism: Evidence from the Berkeley array	65
L. P. VINNIK, The use of arrays for the investigations in micro-seisms	83

TRAVEL TIMES TABLES

Z. SUZUKI, Travel-times of P in Japan in the distance range of 0-15°	89
E. P. ARNOLD, P and S times in Japan	103
N. V. KONDORSKAYA, The Analysis of P. Waves at USSR stations in relation to Jeffreys-Bullen tables. Part. I	137
N. V. KONDORSKAYA and L. B. SLAVINA, Some results of investigation of P waves travel-times. Part II	149
S. D. KOGAN, Travel-times and amplitudes of PcP waves from surface foci	153
H. JEFFREYS and M. L. GOGNA, Times of P in Pacific Explosions ..	163
I. LEHMANN, Discontinuous velocity changes in the mantle as derived from seismic travel-times and amplitudes	167

4000

4000

4000

4000

4000

4000

4000

4000

4000

4000

4000

4000

4000

4000

4000

4000

4000

4000

4000

4000

4000

4000

4000

4000

4000

4000

4000

4000

4000

4000

4000

4000

4000

4000

4000

4000

4000

4000

4000

RECENT EXPERIMENTS WITH A LARGE APERTURE SEISMIC ARRAY

P. E. GREEN, Jr.*
Lincoln Laboratory**, Massachusetts Institute of Technology
Lexington, Massachusetts (U.S.A.)

ABSTRACT

This paper will present the most recent results obtained from the Large Aperture Seismic Array in Montana. Experiments have shown that this station is able to measure seismogram parameters with improved accuracy because of several factors; the large signal-to-noise gain, the directivity which aids in rejecting unwanted components, and the "diversity" or spatial averaging afforded by sampling the arriving signal at a number of separated locations. The interesting parameters include rough epicenter location, magnitude, depth phases, complexity and energy ratios between phases both long period and short period. By the use of digital signal processing techniques, these parameter measurements are being automated one by one. Raw digital seismogram data and rapid epicenter lists are being widely distributed to the seismological community. The data obtained with the array have led to high resolution measurements of the microseismic noise directional properties, to new data on spatial irregularities of crust and upper mantle, and to the accumulation of interesting data on many teleseismic events below magnitude 4.0.

Introduction

In 1965 an experimental Large Aperture Seismic Array (LASA) was installed in Montana to investigate the extension of existing array techniques to a new order of size, number of sensors and signal processing sophistication. This paper will discuss what we have learned to date in using this array. Details may be found elsewhere on the structure and design of the system [1] and the operation of the array as a facility [2].

Figure 1 shows the geometrical layout of the array. There are 525 short-period vertical (SPZ) instruments installed in twenty-one 7 km subarrays of 25 elements each. Near the center of each subarray a set of three mutually perpendicular long-period instruments (LPZ, LPX, LPY) has been installed. The response characteristics of the SP and LP instruments are shown in Fig. 2.

Before this array was built there were a number of conjectures regarding the spatial properties of the *signal*, and the *noise* as

* Paper presented at the International Union of Geodesy and Geophysics General Assembly, Special ASPEI Session on Arrays, October 4, 1967, Zurich, Switzerland.

** Operated with support from the U. S. Advanced Research Projects Agency.

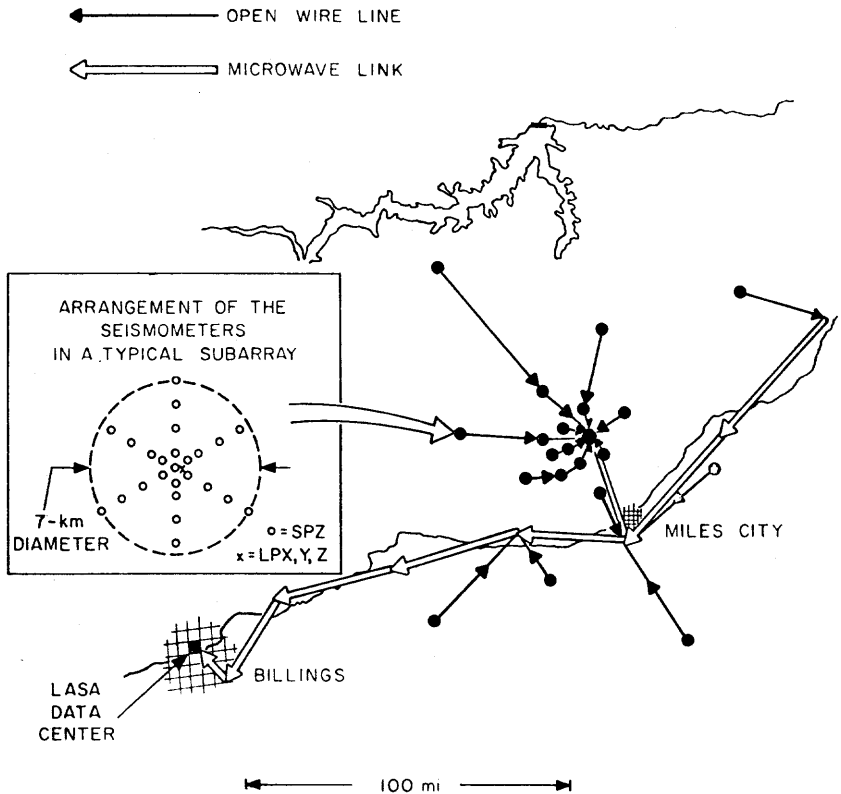


Fig. 1. — Arrangement of seismometers in the experimental large array in Montana.

observed over this large aperture. These properties affect the amount of *signal enhancement* to be extracted from the array processing, and this in turn affects the ability to do blast-earthquake *discrimination* — the primary purpose for which this development was undertaken. In what follows we will discuss in order our current understanding of these four questions, signal properties, noise properties, signal enhancement and discrimination.

Properties of the signal

As the separation between sensors increases, the properties of the arriving seismic signals at any two outputs may be expected to differ increasingly. Inequalities may be expected in signal amplitude, in time of arrival, and in fact in the shape of the entire waveform.

Departures of arrival time from the theoretical values have proved to be the most interesting so far. Consider the difference in arrival time of say the short-period P-phase at individual seismometers. If one makes a least-squares fit to these arrival times of

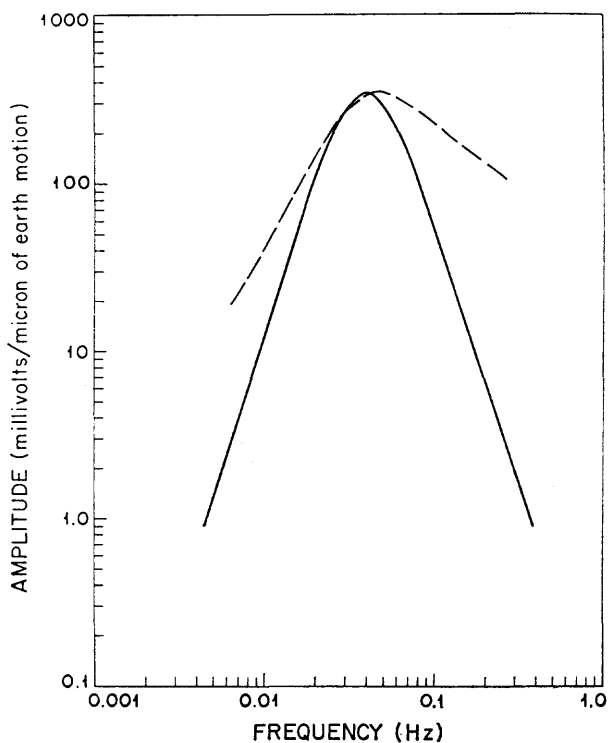
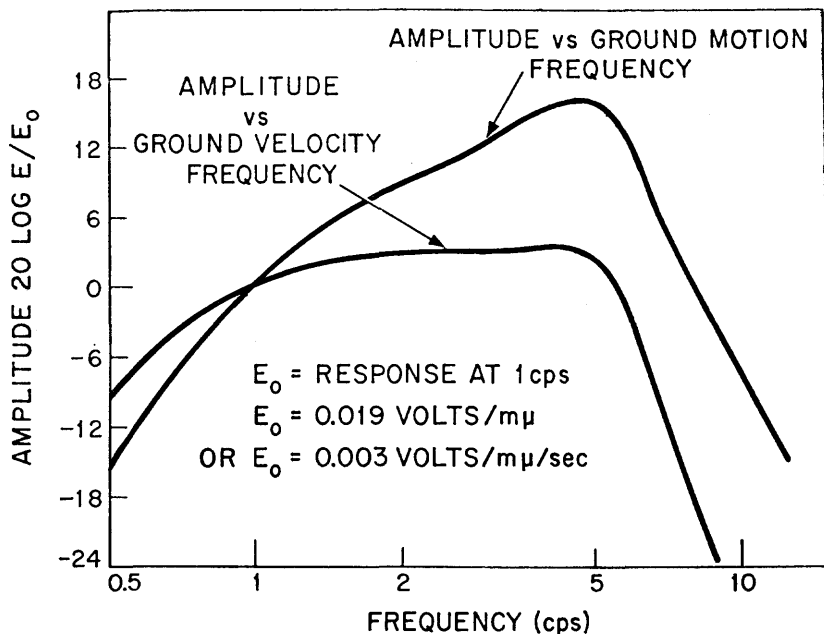


FIG. 2. — Response curves of LASA instruments. (A) Short-period sensor plus input filter, (B) Long-period (dotted curve shows a special wideband characteristic we have not normally used).

a plane wave travelling across the array, it is found [3] that (i) the plane wave implies an azimuth and a $dT/d\Delta$ that differ slightly from the true azimuth and the $dT/d\Delta$ given by various standard travel time curves (as much as 7 or 8 degrees and 0.25 sec. per degree, respectively), (ii) a different best-fit plane wave is found for different parts of the 200 km circular aperture, and (iii) there are residual errors remaining between the observed inter-station travel time differences and those implied by the plane wave model. These residual « time anomalies » are negligible fractions of a cycle within one 7 km subarray and are also negligible for the 200 km array of long-period sensors, but they may amount to as much as 0.5 second for the entire 200 km short-period array at certain azimuths and distances. For example, Fig. 3 shows data on the

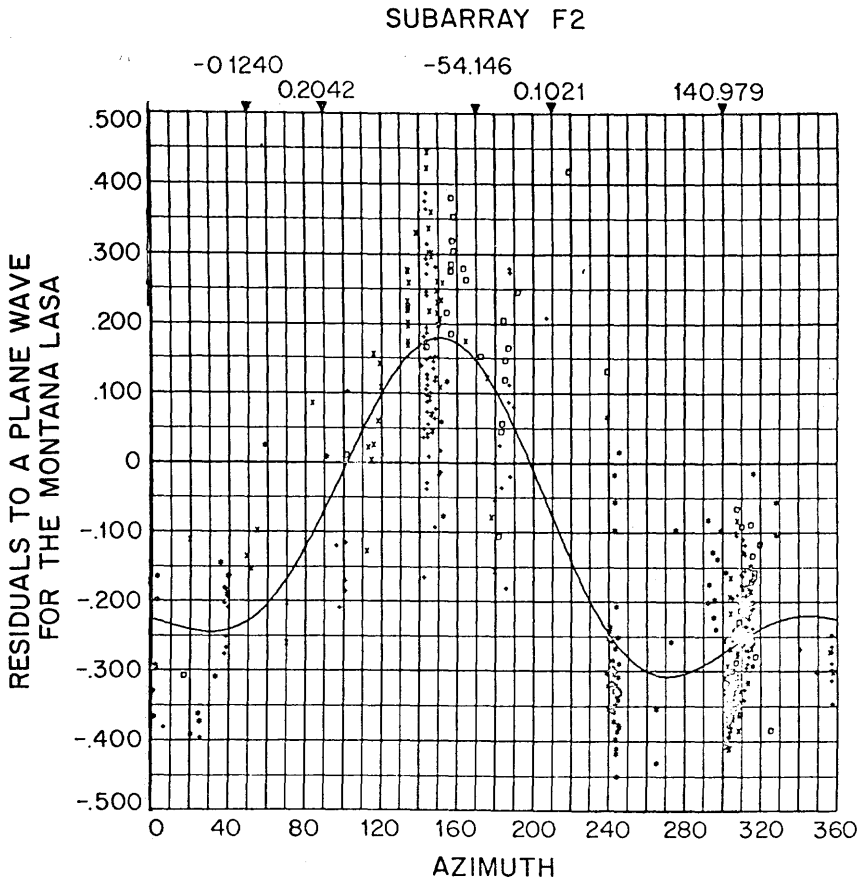


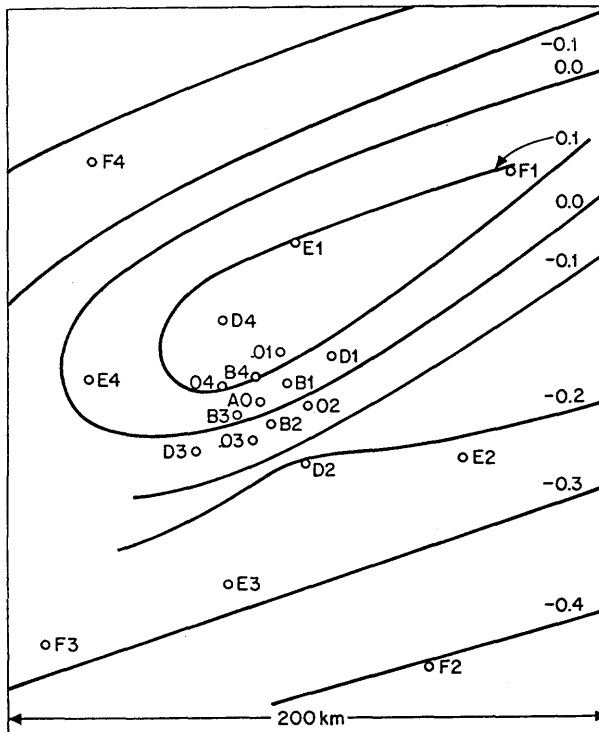
FIG. 3. — Departure of observed arrival time at subarray F2 from best-fit plane wave, as a function of true azimuth to source, for various distance ranges (\square = 0—3 900 km, \times = 3 900—6 100 km, $+$ = 6 100—9 500 km, $*$ = 9 500—11,500 km).

departure from the best fit plane wave of the arrival time at one of the outer sub-arrays, as a function of azimuth and distance.

Continuing efforts are being made to infer the physical sources of these time anomalies in terms of earth structure, either in the velocity profile with depth of the earth's mantle [4] or in terms of local structure underlying the Montana array [3]. Figure 4 shows a sample interpretation of the station delays in terms of an underlying structural feature in the crust or upper mantle [3].

The anomalies are quite important from the point of view of array operation. In aiming the 200 km short-period array by delaying and then summing the individual traces, the anomalies must be applied as station corrections to the theoretical plane wave delays in order to prevent an excessive loss of signal output.

In addition to the time anomalies there are inequalities in signal amplitude between sensors. Some data on this are presented in Table I, from which it is seen for example that short-period P



CONTOURS OF THE AVERAGE VALUE
OF THE STATION CORRECTION TO A PLANE WAVE

FIG. 4. — Contours of the average value of the station correction to a plane wave. The numbered subarray points are those shown in Fig. 1.

amplitudes scatter over a range of 4 to 1 among the sensors of the entire LASA, but only 1.8 to 1 within one subarray. This is for a typical event; occasionally the spread is higher. At long periods, amplitude inequalities between sites appear to be very small. Attempts are being made by various groups working with LASA data to associate the specific amplitude anomalies across the array with models of physical structure underlying it. To date these have been less successful than similar studies of time anomalies.

As part of a series of studies of structure underlying the Montana array, several series of measurements have been made, including local magnetotelluric field strength [5], a magnetometer survey [6] and seismic profiles of the area [6, 7].

TABLE I
COMPARISON OF AMPLITUDE SCATTER OVER
7 - AND 200 - KM APERTURES

	Ratio of Standard Deviation to Mean		Ratio of Strongest to Weakest Sensor	
	Typical Event	Worst-Case Event	Typical Event	Worst-Case Event
<i>Short Period P</i> (25 events) 7 km Subarray (16 sensors in F4)15	.30	1.8:1	2.6:1
200 km Array (center sensors from each of 16 subarrays)40	.80	4:1	9:1
<i>Long Period 200 km Array</i> (1 event) Body wave phases08		1.3:1	
Rayleigh20		2.5:1	

From the point of view of array operation the amplitude anomalies have two consequences. First of all, since repeated events from the same epicentral region will exhibit the same known pattern of short-period P amplitude inequalities across the array, it is possible to take this into account in the array processing so as to emphasize those subarrays having a strong response and de-emphasize the weak ones. A systematic rule is available for doing this optimally [8], knowing the relative levels of noise and signal from each subarray. Application of such differential gains to subarray

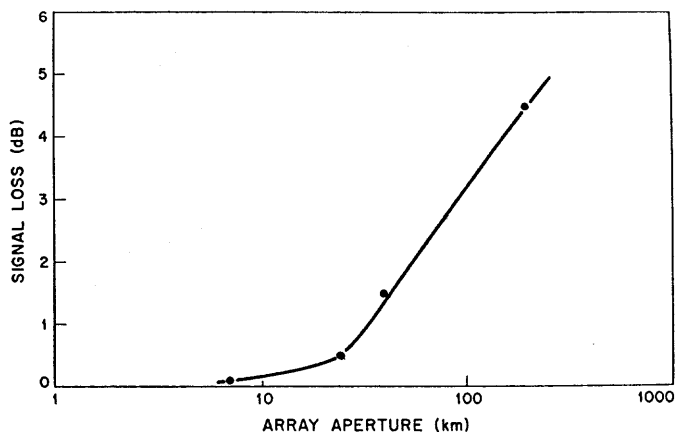
outputs before delaying and summing has been found to give, on the average event, a 2 db improvement in signal-to-noise ratio, compared to the equal-weight case.

The second consequence of the amplitude anomalies has to do with estimation of the body-wave magnitude of a seismic event, a crucial step in the identification of its possible artificial origin, as will be discussed under « discrimination ». It has long been known that seismic signal amplitudes vary notoriously between widely spaced teleseismic observing points, more so than could be explained by the source radiation pattern. Estimates of magnitude have thus, wherever possible, been averages of the readings at many observatories. In comparing the amplitude scatter data in the first row of Table I with that of a similar number of worldwide stations supplying data to the U. S. Coast and Geodetic Survey, we concluded that an average of magnitudes at LASA subarrays is considerably more reliable than that from a single seismometer or subarray and almost as reliable as that from a worldwide net.

We have used the term « space diversity » to denote loosely the beneficial effect of averaging over the differences in waveform from site to site. The advantage of the LASA structure in magnitude measurement may be attributed to the space diversity in observed signal amplitude. It is conceivable that the diversity in arrival times might be useful in increasing the precision of absolute arrival time measurements, although this will have to await experiments in which the array is used for precise location jointly with other stations.

In addition to time and amplitude differences between sensors there are additional differences in the waveforms. The portion of the short-period P waveform after the first several cycles (the coda) tends in general to be more dissimilar from site to site than the earlier cycles. Differences within subarrays are minor compared to those between widely separated subarrays. Experiments by Key [9] using the Eskdalemuir array in Scotland attribute such differences to reverberation components travelling coherently from specific physical scatterers of incident P-energy. Such components were found to have a low velocity characteristic of surface wave noise and have been dubbed « signal-generated noise ». We have not observed such coherent signals with the LASA. Evidence seems to be that in Montana the coda dissimilarities are due to different patterns of reverberation associated with the various sites individually rather than with coherent signals reradiated from some structural discontinuity.

Differences in P waveform, apart from differences in initiation time and amplitude, have two important effects on the operation of the array. First, as inter-element spacing increases, the signals become increasingly decorrelated. Thus in adding up the variously delayed subarray outputs there is a loss in peak signal amplitude as total aperture increases, in spite of corrections to the time alignment of the individual traces by application of the time station corrections discussed earlier. Figure 5 shows the magnitude of this



OBSERVED SIGNAL LOSS vs APERTURE

FIG. 5. — P-wave signal loss with aperture for constant number of sensors and geometry.

effect. Secondly, the identification of phases following soon after P (such as pP, sP, sometimes PcP, etc.) is facilitated by the fact that the various subarray outputs have these phases in common whereas the obscuring P-codas are dissimilar. The high detectability using LASA of pP and sP phases, to be discussed in connection with discrimination, is partly due to this waveform space diversity effect.

It was mentioned above that time and amplitude anomalies over the 200 km array aperture were negligible for long-period signals. If aperture were to be increased beyond the 200 km figure, anomalies due to differential underlying structure could presumably appear. Even if this did not occur, however, it is known that waveform differences across the aperture would arise for surface waves because of their dispersed nature. The waveform at the edge of the array farthest from the source would not be a simple

time-translate of the waveform at the near edge, but would be expanded in duration. Figure 6 shows the theoretically calculated

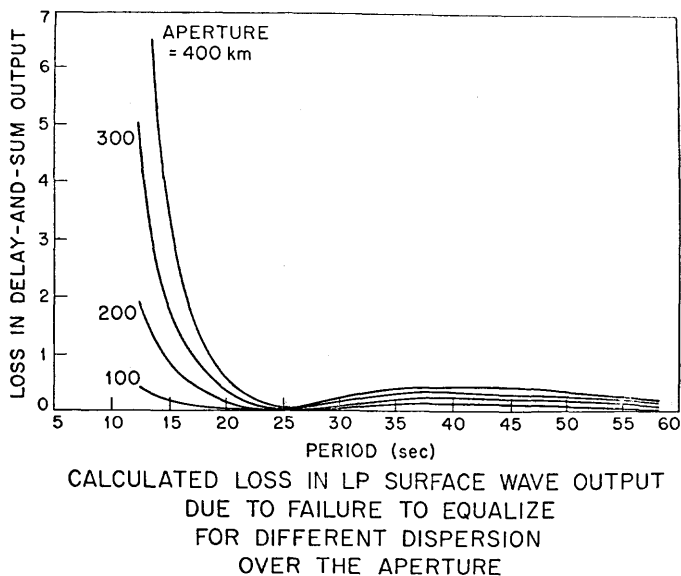


FIG. 6. — Calculated loss in LP surface wave output due to failure to equalize for different dispersion over the aperture.

loss in output in delaying and summing long-period traces as a function of period and aperture. This loss could presumably be avoided by passing the individual traces before delay and summation through filters to correct the differences in dispersion.

Noise properties

The large aperture of the Montana array has provided an unusual opportunity for high resolution studies of seismic noise. In a separate paper [10] of this I.U.G.G. Congress the work that has been done to date is reported in some detail. Therefore results will only be summarized very briefly here.

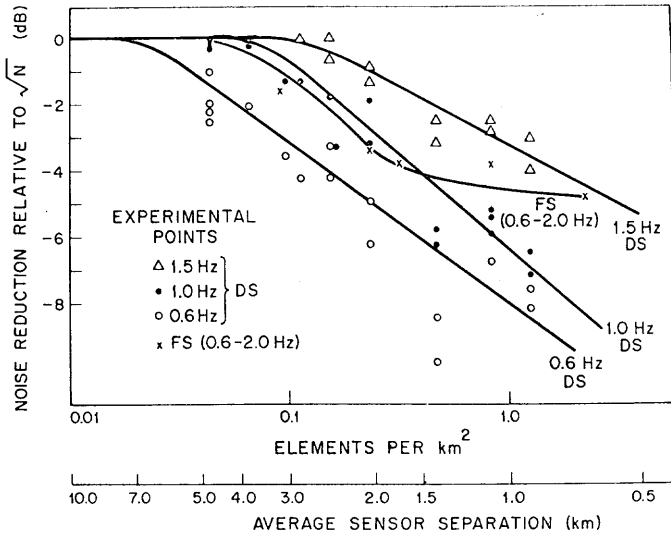
At short periods we were surprised to find that the noise appeared not to be resolvable in direction and velocity to indefinitely increasing detail as the aperture increased, but to be subject to a limit in resolvability corresponding to about 30 km aperture. Beyond this size aperture, the peaks of power as a function, say, of wave number and azimuth (at a given frequency) did not continue to become narrower. This indicates a decorrelation probably due to differential local structure acting as different complex prefilters on the noise into each sensor.

Using a 30 km aperture, the short-period noise was found to consist, during quiet periods, of two clearly resolvable components, energy at around 3.5 km/sec, corresponding to the fundamental Rayleigh velocity, and at around 14 km/sec corresponding usually with identifiable ocean storm activity at teleseismic distances which is thus presumed to be a strong generator of P-energy. The 3.5 km/sec component was consistently weaker from westerly directions than from the east, thus suggesting attenuation under the mountainous regions to the west of the LASA site. These are typical of the results usually observed at short periods for quiet intervals. During periods of high wind, the noise level increases, and in one experiment was associated with a local source; the extreme northwest subarray (see Fig. 1) exhibited highly coherent noise attributable to wave action against the shore at two points in the reservoir lying to the north of the array.

For long periods (say 25 sec) the noise appears to be coherent across the entire LASA. By treating the array as actually three arrays composed of orthogonally oriented sensors, the noise was found to consist typically of fundamental mode Rayleigh and Love energy associated with known storm activity. Unlike the short-period storm-generated surface wave energy, the long-period energy arriving from the west appeared relatively unattenuated.

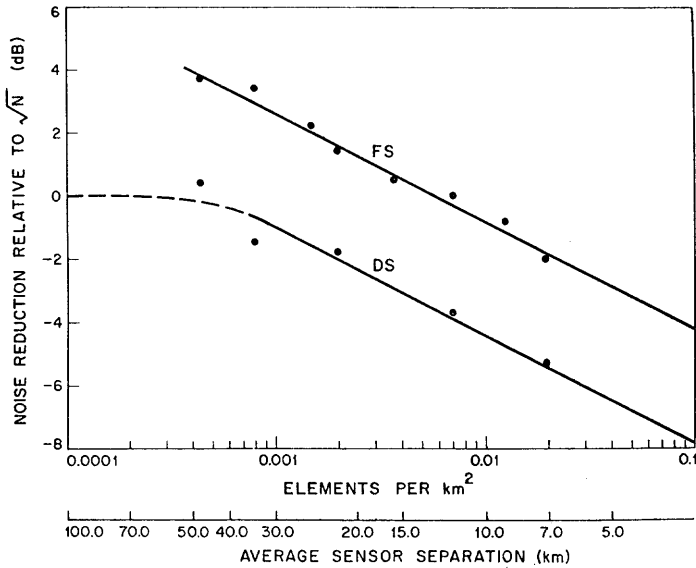
Signal enhancement

Two forms of disturbance are to be suppressed by array processing, noise and interfering teleseisms. A number of experiments were done on SNR gain as a function of inter-element spacing. The gain is defined as the SNR of the single output trace divided by the average SNR of the many traces (seismometer outputs) being combined. Figure 7 summarizes the result for SP signals at several frequencies in the 0.6 — 2.0 Hz band, while Fig. 8 gives similar results for the LP array. The noise suppression is shown relative to the square root of N, the number of sensors; as sensor noises become independent, as they will for large enough inter-element spacing, the gain should equal the square root of N figure. The figures give results for two forms of array combining, delay-and-sum (DS) and filter-and-sum (FS) [11]. DS processing is the conventional « steered sum » or « beamforming » process in which a simple time shift is applied to the N signals which are then added. This has the effect of steering the peak of the array directivity pattern in the desired direction, but it makes no particular attempt



SHORT PERIOD SNR GAIN vs ELEMENT DENSITY

FIG. 7. — Short-period SNR gain vs element density.



LONG PERIOD SNR GAIN vs ELEMENT DENSITY

FIG. 8. — Long-period SNR gain vs element density.

to steer the nulls and small minor lobes of the pattern toward sources of interference. In FS processing, before summation each sensor output is subjected not only to a pure steering delay, but also to a filtering operation. The set of N filters can be synthesized from a theoretical model of the noise, or, as in the « maximum likelihood » procedure we have used, it is synthesized from a sample of observed noise*. In either case the effect is that, frequency by frequency across the operating band, the main lobe is positioned to favor the signal and the pattern nulls and sidelobes are positioned to minimize the noise.

One sees that if closely spaced seismometers are used in the design of an array, then FS processing is required; and if widely spaced elements are used, approximately the same gain can be obtained with the much simpler DS processing. In the LP case, the price paid is a factor of 10 in element density, i.e., a factor of about three in inter-element spacing. In the design of any future large array, we have concluded that FS will be an impractical scheme for SP array operation and that wide inter-element spacing should be used instead. On the other hand, for LP operation the inter-element communication costs are apt to be high enough, while the data rates and therefore processing complexity remain low enough, that FS will continue to be attractive.

The total LP SNR gain of the Montana array averages 10 db for DS and 14 db for FS, respectively. For SP signals prefiltered to a 0.6 — 2.0 Hz passband, the corresponding figures are 6 and 11 db respectively for one subarray and 16** and 22 db respectively for the overall array.

One area in which FS processing has been found to be much more useful than DS processing is in the suppression of interfering LP Rayleigh waves from particular teleseisms. The time duration of these surface waves is usually about 10 to 20 minutes, so that it is quite likely that some event may generate surface waves which interfere with LP observations of a desired event. (This is not nearly so serious a problem with SP data). An experiment was

* For the data of Figs. 7 and 8 the noise measuring interval or "fitting interval" was taken immediately preceding the event, and lasted three minutes for the SP experiments and 60 minutes for the LP experiments. The duration of the synthesized filter impulse responses was 2.0 seconds for the SP case and 40 seconds for the LP case.

** As mentioned in the first section, an additional 2 db is available using known amplitude inequalities between subarrays.

performed to determine the effectiveness of DS and FS processing in suppressing the surface waves of an interfering event while passing the surface waves of the desired event. The interfering event was taken as a 21 November 1966 Kurile Islands event and the desired event as a 12 November 1966 Argentina event. A 12 November 1966 Kurile Islands event was used to design the filters used in the FS processing. The surface waves of the 12 November 1966 Argentina event were hidden in the surface waves of the 21 November 1966 Kurile Islands event, by adding the traces, as indicated in Fig. 9. The results of the DS processing, shown in

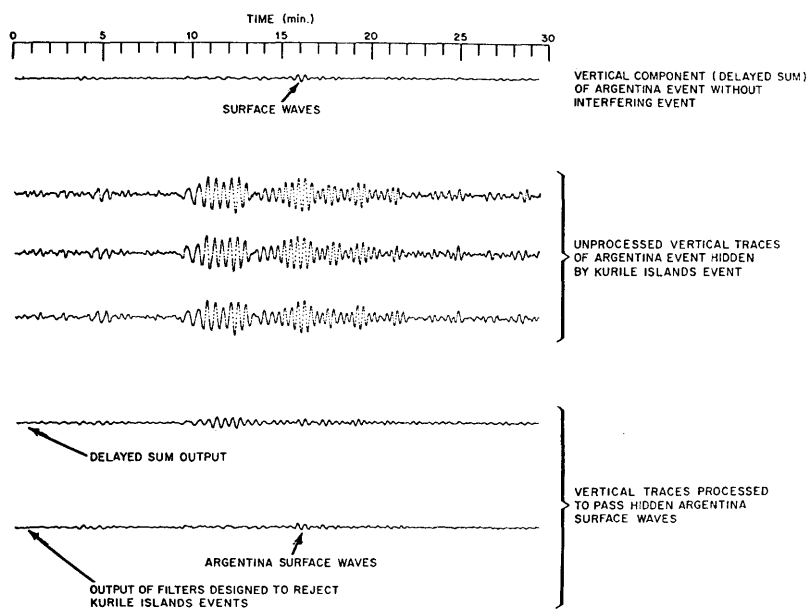


FIG. 9. — Suppression of long-period interfering teleseism.

Fig. 9, indicate that the Argentina surface waves are not visible, since only 11 db of rejection of the interfering surface waves was obtained with this form of processing. However, the Argentina surface waves are visible in the FS processed trace, as this form of processing achieved about 20 db of suppression of the interfering surface waves. Thus, FS processing has a clear superiority over the simpler DS form of processing for the purpose of rejecting interfering surface waves from specific events of widely different azimuth.

We have investigated a method of further increasing signal-to-noise ratio that is effective on the dispersive teleseismic surface waves, but not on the LP or SP undispersed body waves. This procedure is to pass the single output of an array processor (or an individual sensor) through a filter whose impulse response is roughly matched to the surface wave signal. Since the duration of the dispersed signal increases with epicentral distance, the SNR gain of this scheme, being given approximately by the time-bandwidth product of the wave train, is expected likewise to increase with distance. Thus, much of the loss in amplitude due to dispersion can be recovered, although of course the loss due to geometric spreading and dissipation cannot.

It was found that a simple linear frequency-sweep reference waveform gave satisfactory results; this reference waveform is also known as a chirp waveform. It would be a replica of the Rayleigh wave train if the group velocity were a linear function of frequency and if the dissipation loss were uniform with frequency over the seismometer pass band.

Two examples of the application of matched filtering to LP Rayleigh waves generated by presumed nuclear explosions in the Eastern Kazakhstan area are shown in Fig. 10 (a) and (b), along with the autocorrelation function of the reference waveform shown in Fig. 10 (c). Not only does the matched filter technique produce an SNR enhancement but it facilitates the measurement of surface wave magnitude M_s in a physically more meaningful way than the usual method of using the amplitude of the 20 second portion of the wave train, since it measures the energy in the entire wave train.

Identification

The most useful discriminant for distinguishing between natural seismic events and underground nuclear explosions of large magnitude appears to be the one based on the relationship between the surface-wave magnitude and the body-wave magnitude. Theoretical calculations due to Keilis-Borok [12] have shown that the most efficient excitation of surface waves occurs at wavelengths approximately four times the dimension of the source, that is, the source region acts as a quarter-wavelength antenna. The source dimensions for an underground nuclear explosion are usually much

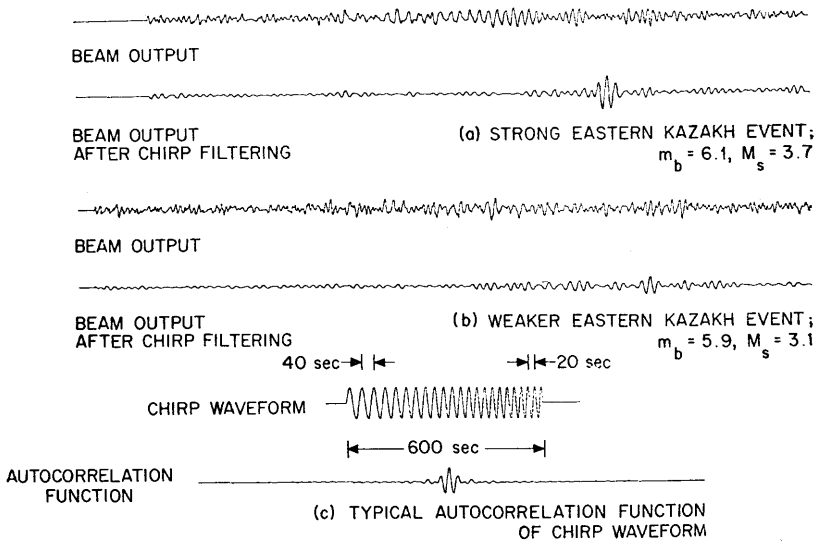


FIG. 10. — Matched filter SNR improvement for long-period Rayleigh waves.

smaller than those of an earthquake of comparable body-wave magnitude. Thus, one would expect the earthquakes to excite longer periods of surface waves more efficiently than the underground nuclear explosions. The surface waves would act as carriers of the information on strength of long-period source excitation. This conclusion has been verified experimentally by several previous investigators [13, 14] at near-zone distances, and at least one teleseismic experiment has been reported [15].

Observations have been made using LASA data to determine how effective a single such array is in using this discriminant teleseismically. The body-wave and surface-wave magnitudes for events from various regions have been computed. The weaker events have been subjected to FS or DS processing (about 14 db and 11 db of signal-to-noise ratio enhancement, respectively) and in addition matched filtering was used if needed to achieve another 6 to 10 db. The body-wave magnitude, m_b , is based on the amplitude of SP waves recorded at teleseismic distances and is computed according to the usual Gutenberg and Richter formula [16] for shallow focus earthquakes. The measurement of surface-wave magnitude, M_s , used the formula of Gutenberg [17] applied to the matched filter output.

The results of the experiment are given in Figs. 11A through D, which show M_s vs m_b for earthquakes in Central Asia, Kurile-

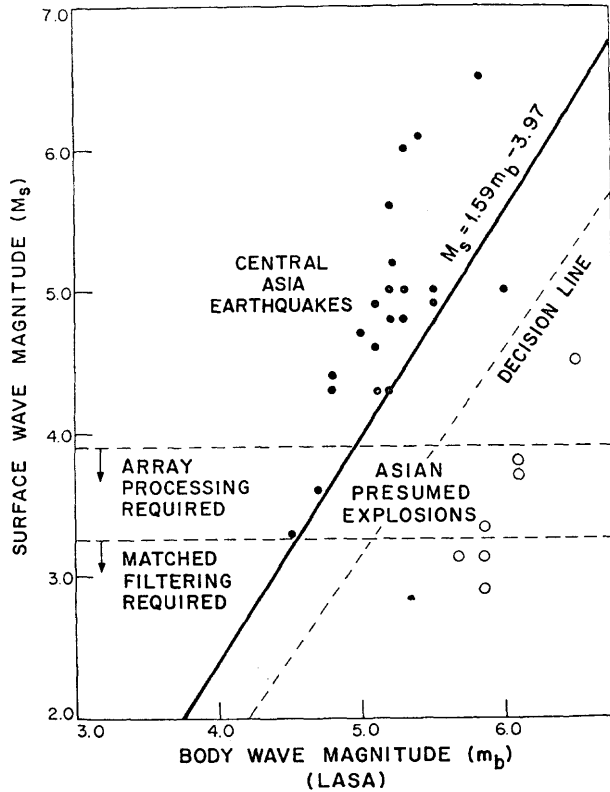


FIG. 11 A. — LASA surface wave magnitudes vs body wave magnitude for Asian presumed explosions and for earthquakes from four seismic regions. (See Figs. 11 B, 11 C and 11 D.)

Kamchatka, Aleutians and the Central Pacific, respectively, as well as the Gutenberg-Richter [16] empirical relationship, $M_s = 1.59 m_b - 3.97$. Eight underground nuclear explosions from Asian sites are included for reference in all three diagrams. The body-wave magnitude shown in Figs. 11A through D was calculated by averaging over several widely-separated sensors at LASA, so that a relatively good determination of body-wave magnitude was obtained, thanks to the space diversity effect. The surface-wave magnitude data were also plotted versus the CGS body-wave magnitude. Although the scatter of the data was slightly diminished by doing this, the separation of the earthquake and explosion populations was somewhat better using LASA, rather than CGS, body-wave magnitudes.

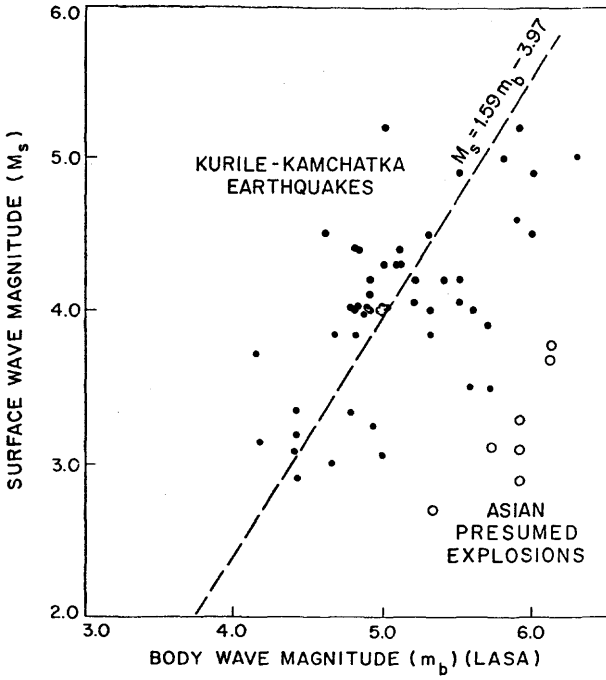


FIG. 11 B.

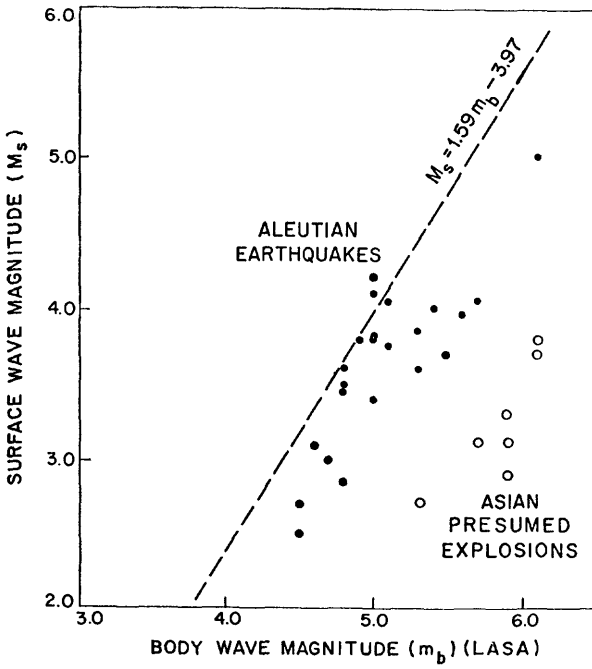


FIG. 11 C.

The separation of explosions and earthquakes is seen to be complete, and is most marked for the continental earthquakes. The body-wave magnitude threshold for the earthquakes is approximately 4.4, even though the LASA is located at teleseismic distances from Central Asia (60° - 90°). The threshold for the bombs is at a body-wave magnitude of approximately 5.3.

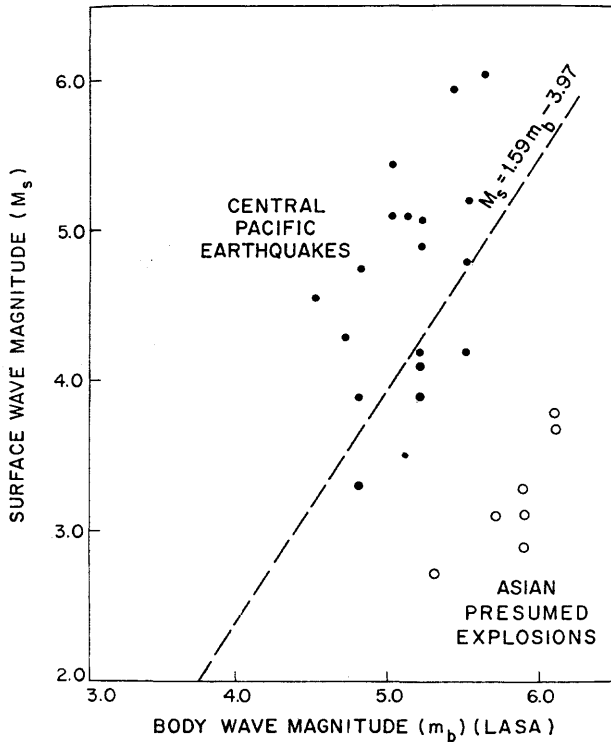


FIG. 11 D.

Below this magnitude level but above the short-period detection threshold*, identification using the single experimental LASA must rely on other less effective discriminants. Data from one of these short-period discriminants are given in Fig. 12. The ordinate is the ratio of energy in two frequency bands of the first 20-30 seconds of the P-phase. This discrimination criterion is seen to be equivalent to the M_s vs m_b criterion just discussed, except that the two frequency bands are not so widely separated. The data for each event in Fig. 11 was measured from the single "beam" (DS) output trace. It is seen that the separation between blasts and earthquakes

* The 50 % cumulative detection threshold using DS ("beamforming") is about $m_b = 3.5$.

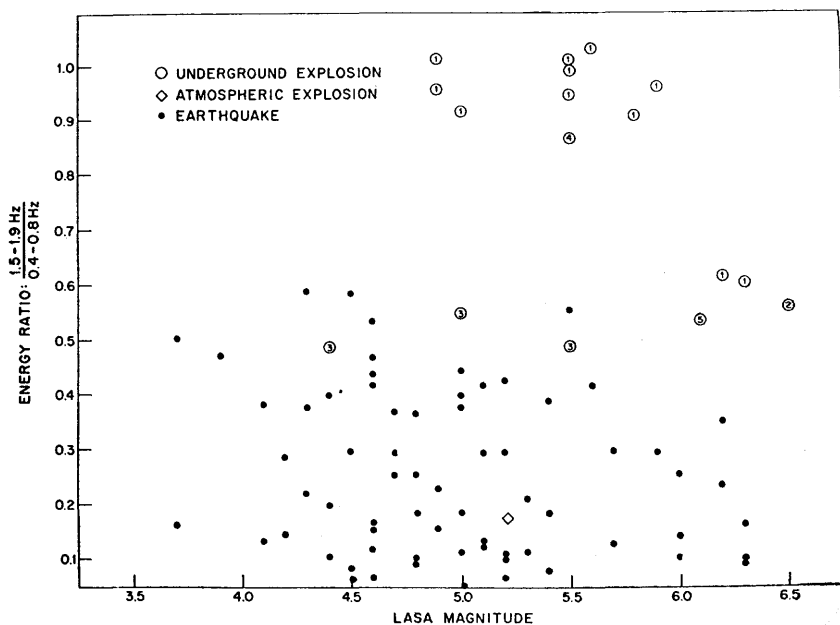


FIG. 12. — Short-period spectral ratio for explosions and earthquakes.

is not as unequivocal as with Fig. 10, but that the lowest magnitude at which the short-period spectral ratio measurement can be made is lower than that for M_s vs m_b .

The "P-coda complexity" criterion [18] is analogous to the two criteria just discussed. The complexity C (as used here) is defined as the ratio of the energy in the interval 5 - 30 seconds after P-initiation to the energy in the interval 0 - 5 seconds. It is thus a measure of the disparity in energy at two parts of the delay axis whereas the two criteria just discussed involve two parts of the frequency axis. The most reasonable explanation of the finding that earthquakes have longer codas (at some azimuths) than explosions is that they radiate more S-energy (at some azimuths) which when converted to P near the source appears as a lengthening of the P-phase. LASA complexity data (Fig. 13) confirm that a separation between source types occurs, but the effect is seen to be dependent on which test site is being observed.

The determination of focal depth is usually done by combining travel times to many stations or by observation of the depth phases pP or sP . We have found that the combined effect of the SNR gain, the velocity discrimination available from the LASA aperture, and the space diversity effect all combine to facilitate the observa-

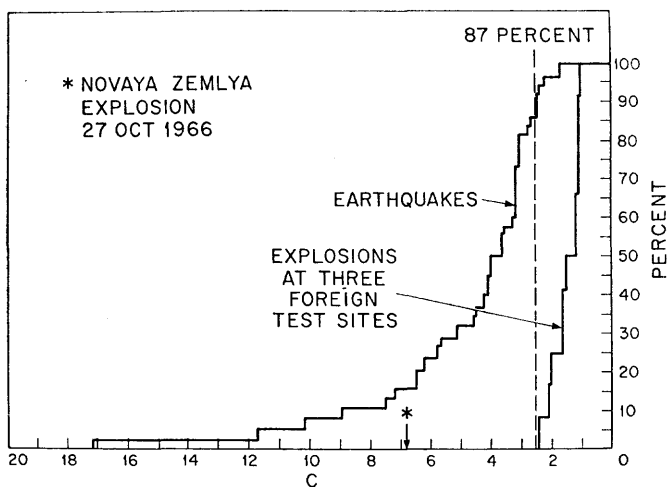
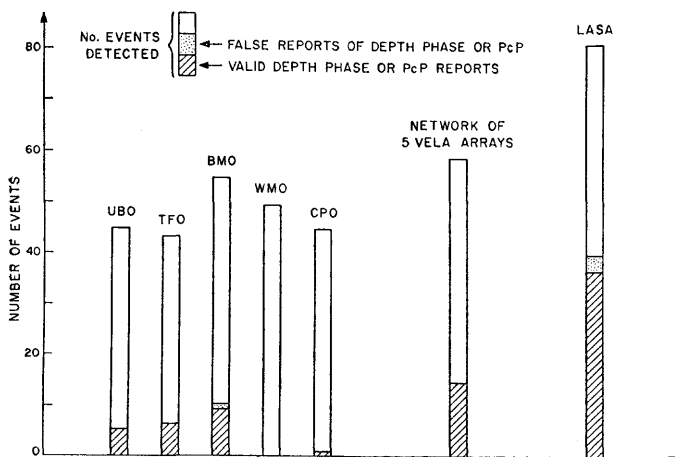


FIG. 13. — Cumulative plots of number of events having complexity factor *C* or greater vs *C*.

tion of depth phases. Figure 14 shows data on the relative efficacy of depth phase observations with the LASA, each of the five U. S. array observatories, and a hypothetical net composed of all five



DEPTH PHASE REPORTING OF LASA vs A 5-STATION NETWORK IN U.S.

1 Aug - 15 Sep, 1966
 $\Delta \leq 90^\circ$, Bloc Countries +6°

FIG. 14. — Results of comparing depth phase reports of LASA and a five station net with USCGS computed depths.

observatories. The data was obtained by comparing station reports of phases within 60 seconds after P with the computed hypocenter depths reported by the U. S. Coast and Geodetic Survey. Unfortunately, it is seen that, even using the large array, at most 40 - 50 % of teleseismic events can be identified in this way.

The mutual application of several criteria, each of which is only partially effective by itself is under study using a large population of natural and explosive events.

REFERENCES

- [1] Four papers on the Large Aperture Seismic Array, Proc. I.E.E.E., 53, 1821-1859, December 1965.
- [2] P. E. GREEN and R. V. WOOD, Jr., Large Aperture Seismic Array Capabilities, M.I.T., Lincoln Laboratory Technical Report 421, July 12, 1966 (DDC 639197).
- [3] R. M. SHEPPARD, Jr., Measurements of LASA Time Station Residuals, Velocity and Azimuth Errors, Thesis submitted for M.S. degree, Boston College, Weston Observatory, Weston, Mass., August 4, 1967.
- [4] M. A. CHINNERY and M. N. TOKSÖZ, P-Wave Velocities in the Mantle Below 700 km, B.S.S.A., 57, 199-226, May 1967.
- [5] G. SIMMONS and E. HERRIN, private communication, 1967.
- [6] L. C. PAKISER, private communication, 1967.
- [7] J. S. STEINHART and R. P. MEYER, Explosion Studies of Continental Structure, Carnegie Institute of Washington, Publ. 622, 1961.
- [8] D. G. BRENNAN, On the Maximal Signal-to-Noise Ratio Realizable From Several Noisy Signals, Proc. I.R.E., 43, 1530, October 1955.
- [9] F. A. KEY, Signal-Generated Noise Recorded at the Eskdalemuir Seismometer Array Station, B.S.S.A., 57, 27-38, February 1967.
- [10] R. T. LACOSS and M. N. TOKSÖZ, Frequency-Wave Number Spectra of Micro-Seismic Noise, paper to be presented at A.S.P.E.I. session, I.U.G.G. General Assembly, Zurich, September 25 - October 7, 1967.
- [11] J. CAPON, R. J. GREENFIELD and R. J. KOLKER, "Multidimensional Maximum-Likelihood Processing of a Large Aperture Seismic Array, Proc. I.E.E.E., 55, 192, February 1967.
- [12] V. I. KEILIS-BOROK, Differences in the Spectra of Surface Waves from Earthquakes and from Explosions, Tr. Inst. Fiz. Zemli, N° 15 (182), p. 88, 1961.
- [13] F. PRESS, G. DEWART and R. GILMAN, A Study of Diagnostic Techniques for Identifying Earthquakes, J. Geophys. Res., 68, 2909, 1963.
- [14] J. N. BRUNE, A. ESPINOSA and J. OLIVER, Relative Excitation of Surface Waves by Earthquakes and Underground Explosions in the California-Nevada Region, J. Geophys. Res., 68, 3501, 1963.
- [15] R. C. LIEBERMANN, C. Y. KING, J. N. BRUNE and P. W. POMEROY, Excitation of Surface Waves by the Underground Nuclear Explosion of Long Shot, J. Geophys. Res., 71, 4333, 1966.
- [16] B. GUTENBERG and C. F. RICHTER, Magnitude and Energy of Earthquakes, Ann. Geophys., 9, 1, 1956.

- [17] B. GUTENBERG, Amplitudes of Surfaces Waves and Magnitudes of Shallow Earthquakes, *Bull. Seismol. Soc. Am.*, 35, 3, 1945.
- [18] J. W. BIRTILL and F. E. WHITEWAY, The Application of Phased Arrays to the Analysis of Seismic Body Waves, *Phil. Trans. Roy. Soc. A*, 258, 421-493, November 25, 1965.

GEOPHYSICAL RESULTS FROM DIGITAL PROCESSING OF YELLOWKNIFE ARRAY SIGNALS

by K. WHITHAM and D. H. WEICHERT
Dominion Observatory, Ottawa Canada

ABSTRACT

Results are described from the automatic digital processing of teleseismic signals from the medium aperture crossed seismic array at Yellowknife, N.W.T. Developments in the automatic processing method are described which increase the speed from that previously described. Epicentral uncertainties from a single array determination are outlined.

Intensive digital processing is described of a tape obtained by the superposition of the signals from the Early Rise chemical explosions at an epicentral distance of about 21° . The results and other observations from chemical explosions at 11° to 17° are compared with the predictions for the average upper mantle structure derived from observations of chemical explosions on the Canadian standard seismic network at long ranges. Preliminary upper mantle structural interpretations are given incorporating phase velocity data with time and distance data. The difficulties in self-consistent interpretations using velocity filtering are outlined. The best model to date requires only a very weak P-wave low velocity layer at considerable depth in the PreCambrian Shield.

Introduction

The Yellowknife medium aperture seismic array was established in 1962 by the United Kingdom Atomic Energy Authority in cooperation with the Department of Energy, Mines and Resources of the Government of Canada. The array consists of two orthogonal lines, one accurately north-south and the other east-west, each line containing one vertical Willmore Mark II seismometer in each of ten vaults emplaced in granite. One vault is common to both lines and the distance between adjacent instruments is 2.5 km, so that each arm of the asymmetric cross is 22.5 km long. The amplified output of each seismometer is carried by an amplitude modulated tone system to a central recording laboratory, where it is recorded on a separate channel of a 24-channel FM magnetic tape. Figure 1 schematically illustrates the geometry of the array.

Since late 1965, facilities have been available in Ottawa for the digital processing of signals recorded by the array and a small group within the Dominion Observatory is now undertaking research into array seismology. The facilities available at the present time include a playback tape deck, demodulators, multi-channel analog switchable filters, a multiplexer and an analog-to-digital converter interfaced to

a general-purpose DDP-124 digital computer with one digital magnetic tape unit and rather limited input-output peripheral equipment. In addition, a digital-to-analog converter and a multitrace pen recorder are available to reform and display digitally processed analog outputs. The computer is a recent acquisition : prior to the spring of 1967, analysis of Yellowknife data could only be undertaken in non-prime time on a CDC-3100 digital computer in the general purpose Scientific Computation Centre of the Department of Energy, Mines and Resources.

Some preliminary results on the detection levels achieved, on epicentral position accuracies and on signal-to-noise gains have been described by WEICHERT et al. (1967). Continuous free search procedures of the half space under the array have been developed whilst processing at twice record-time speed, using the unit weight delay, sum and correlate technique. The methods used have been subject to considerable experiment and refinement (MANCHEE and WEICHERT, 1968).

Major Changes in Continuous Tape Processing

In the work referenced above, an azimuth and apparent velocity was specified for each array beam formed, and the delays calculated for each seismometer, rounded to the nearest integer multiple of the sampling interval, before summing and correlating. With the arrival of the new machine, delays of integer multiples of the sampling interval, up to an arbitrary and useful number, have been applied to the summation of each line, the sums then correlated in all possible combinations, and the best azimuth and apparent velocity interpolated.

This second method developed for economic free teleseismic search takes advantage of the linear rather than general geometry of the Yellowknife array. Detailed analysis of the first method showed that the formation of 168 beams (equivalent to seven velocities in each of 24 uniformly seperated azimuths) at twice record-time speed took 21 ms out of the 25 ms theoretically available, whereas the second method theoretically reduced this time to 13 ms for the CDC-3100 machine. The exact gain for any case depends upon the basic add and multiply times for the computer under consideration. With the DDP-machine, sacrificing memory for processing speed throughout the program, computer studies have now demonstrated that a continuous search of the FM tapes can be made at four times the recording speed, with only a very small

reduction in the number of beams, namely to 121, adequate for P phase coverage at teleseismic distances. The economics of this

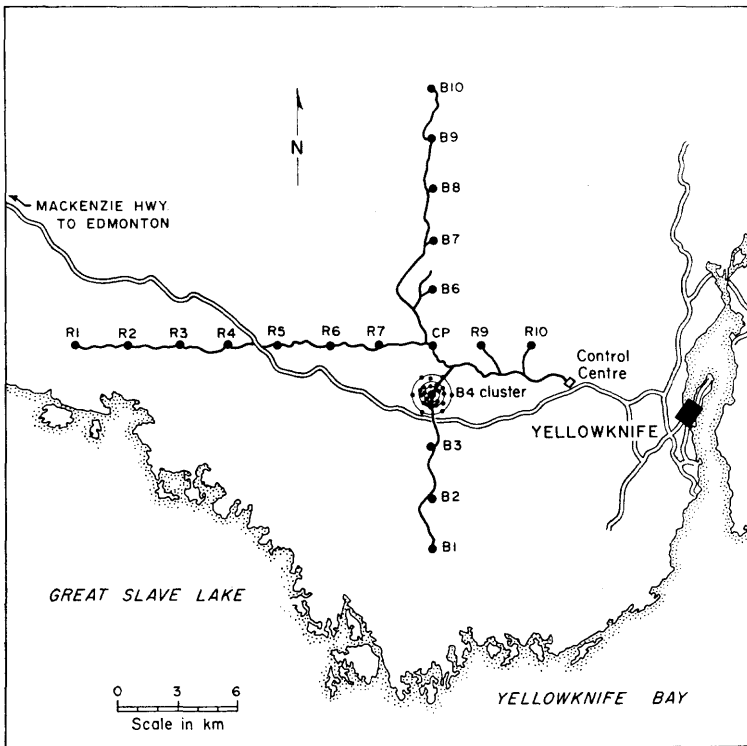


FIG. 1. — Sketch map of Yellowknife Seismic Array.

theoretically demonstrated speed-up to a small organization are quite important, and changes in demodulators, filters, etc., to implement it are underway.

Positional Accuracies of Epicentres Determined from the Free Search Programme

WEICHERT et al. (1967) have shown that, in the Third Zone to Yellowknife, the computer process achieved initially a location accuracy with standard deviations between 3 and 4 degrees in distance and between 2 and 3 degrees in azimuth. These results, of course, are increasingly biased with increasing focal depth, unless a depth correction is independently available.

A second major free search experiment using the first processing technique was conducted on the array tapes for 27 days during November and December, 1966. In this major experiment, particular attention was paid to the source of the epicentral errors obtained

by a parabolic interpolation between the three highest correlogram values, independently in both azimuth and in slowness (reciprocal velocity). A major effort was made to eliminate systematic errors in order to study the errors in detail.

In this digital experiment, the positions published by the USCGS were adopted as correct and error vectors of positions calculated by the computer process relative to them examined. Wherever necessary, depth corrections were made. Systematic differences found between the observed apparent arrival vectors and those calculated from the USCGS data and the J-B tables must then be explained by structure, if the other possible sources of error have been correctly eliminated. The most obvious structural source of bias is a dipping interface of velocity contrast under the array. It can be shown by vector geometry analysis that the evidence for a sloping interface can be directly evaluated from a diagram showing the vector differences between the computer derived and actual positions expressed in the slowness-azimuth plot. A small to moderate dip of a refracting interface with a reasonable velocity contrast is indicated immediately by parallel error vectors of approximately constant magnitude.

Figure 2 shows some of the slowness vector anomalies for a sample of teleseismic events recorded during the November experiment. To avoid overcrowding the figure, the sample has been restricted and many events been omitted from already overcrowded areas. The figure also shows the approximate 3 db contour of the correlator response of the array configuration at 1 cps, and the set of beams used in the numerical experiment.

It is immediately clear that the errors described by WEICHERT et al. (1967) consist of systematic regional errors on which are superposed generally smaller random errors. The systematic regional errors are not consistent with an explanation in terms of a single dipping interface of velocity contrast under the array. A careful analysis of the procedure used has been made in order to estimate arithmetical sources of systematic error, but it can be proved that the following produce insignificant effects compared to the observed regional errors :

- 1) mechanical skew of read and write heads of the tape,
- 2) filter phase shifts,
- 3) the digitization skew in the system used during 1966, which lacked a simultaneous sample-and-hold system,
- 4) the time quantization of the data, and consequent rounding errors in the method of beam formation.

5) errors produced by the effect of the above rounding on the correlogram values being interpolated.

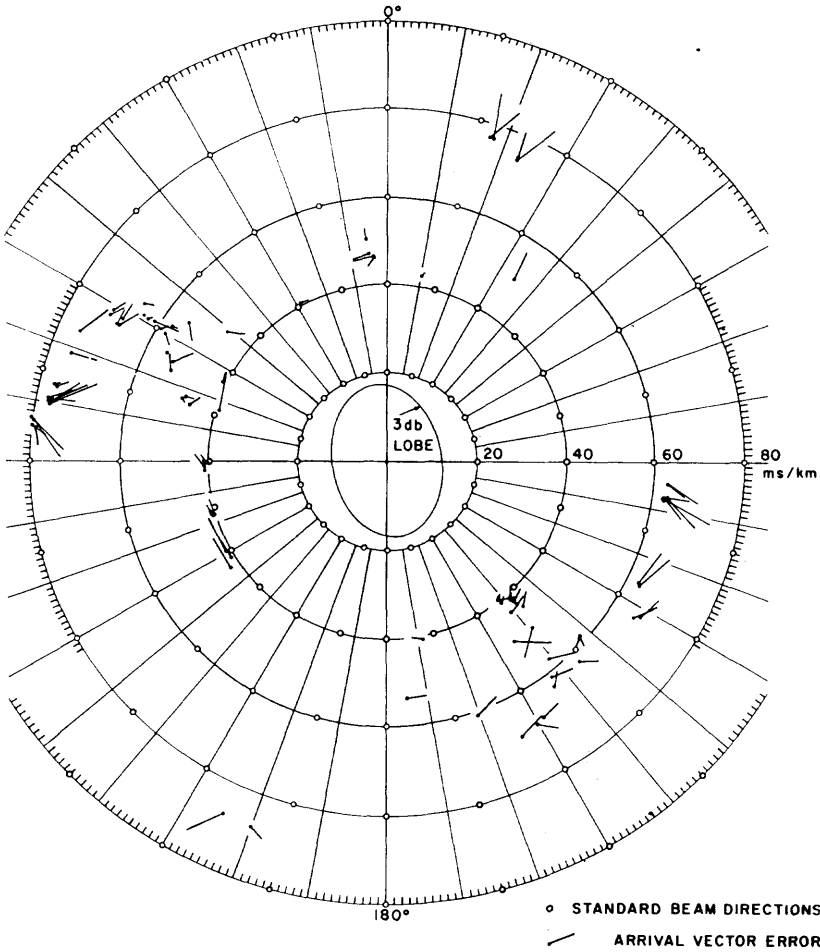


FIG. 2. — Sample of YKA slowness-vector anomalies for the free search experiment.

The apparent velocities used have been automatically corrected for fluctuations of the FM tape speed during recording or playback.

The effect of arithmetic noise consequent upon the particular set of beams adopted was further investigated by making a comparison of error vectors obtained with the usual beams and the results from a limited fine-scan experiment with interpolation between beams about twice as densely spaced. The events which were available for this comparison are not the ones used during the period mentioned above, but ones observed between early September

and late October, 1966. Although there are some differences in the two determinations a similar regional grouping can be distinctly observed, and it is therefore believed at present that the strong regional variation of the arrival vector errors cannot be explained by the computer procedures adopted.

These apparent regional effects in $\frac{dT}{d\Delta}$ and azimuth are being investigated further, with attention paid to the observed travel time. Some preliminary investigations along these lines have already been undertaken by the authors. Results to date are somewhat ambiguous and not given here, since a great deal more carefully treated data is required over a fuller epicentral distance range at many azimuths in order to :

- 1) resolve whether the J-B velocity curve at great depths in the mantle needs adjustment,
- 2) verify the apparent interpretation that at great depths in the mantle there is a lack of lateral uniformity in velocity,
- 3) take into account adequately the azimuthal information often neglected in similar studies conducted in data from LASA,
- 4) clarify the role of velocity structure in the upper mantle beneath Yellowknife and possible complex topography in surfaces between velocity contrasts.

As the upper mantle becomes more laterally differentiated locally, the difficulties in resolving deep velocity from the $\frac{dT}{d\Delta}$ data become greater.

One fact is clear : it would be advantageous to study source regions between two widely separated arrays using effectively reversed observations through the interpreted anomalous regions.

Detection Level of Array in Free Processing Mode

The data analysed in the latest experiment (MANCHEE and WEICHERT, 1967) have indicated a 50 % automatic detection level for events between 30° and 100° from the array to be $m4.0 \pm 0.1$. The 90 % level is $m4.5$. No significant variation in detection level or in body wave magnitude with azimuth has yet been found.

It should be understood that the figures quoted refer to times when the array was fully operational under typical mid-winter ambient noise conditions. Although noise levels do vary significantly throughout the year, a more serious problem in the context of a continuous monitoring problem is that of array serviceability. The Yellowknife array was designed and economically constructed

as a research tool; it is accepted that a few percentage of the time it will be down following lightning or other storm damage, and that for another few percentage of the time not all elements will be fully operational.

Array Processing of Observations from Chemical Explosions with Seismic Paths in the Upper Mantle

Recently, BARR (1967) of the Dominion Observatory studied long range observations on standard Canadian seismic stations from chemical explosions in Hudson Bay and Lake Superior. The coordinates of the cusps observed in the mean travel-time curve were used to define the average structural discontinuities in the Canadian Shield. The P-wave velocity structure deduced agrees closely with the depth of S-wave velocity discontinuities deduced from surface wave observations, and his interpretation did not require any appreciable low P-velocity layer in the upper mantle.

Figure 3 shows the mean P-wave and S-wave velocity structure deduced by BARR and BRUNE and DORMAN, respectively, together

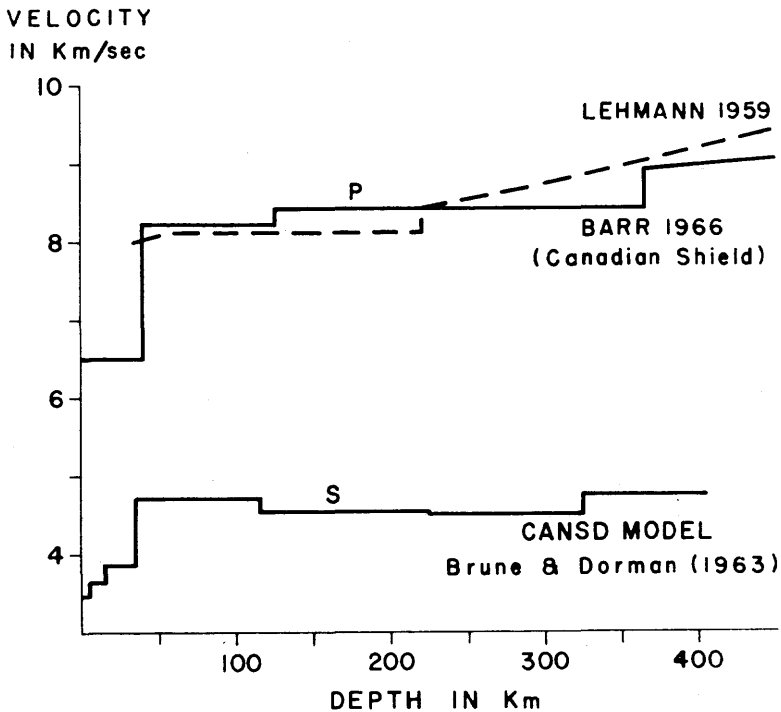


FIG. 3. — Proposed velocity structures in upper mantle, particularly for Canadian Shield.

with an earlier P-wave velocity structure of Lehmann. In his work BARR used all prominent phases which could be read in the first 20 s of the record.

With the availability of a suitable in-house computer, it was considered of interest to examine the signals from some chemical explosions, and in particular to study the travel-time curve to 25° . It was naively believed that from an analysis of time, distance and apparent phase velocity the appropriate branches of the arrivals might more clearly be identified, and the variation of velocity with depth deduced in the average deep apparent layering obtained by others. It is now clear that with the azimuthal complexities revealed in the teleseismic work described above, it is essential to obtain data on $\frac{dT}{d\Delta}$ at shorter ranges corresponding to upper mantle paths in order to carry through the appropriate integrations relating travel time to phase velocity, and to interpret the origin of the teleseismic phase velocity anomalies.

A start on such a major programme of research has now been made and some of the preliminary result to date will be outlined. Figure 4 shows a schematic diagram of 29 Hudson Bay shot locations

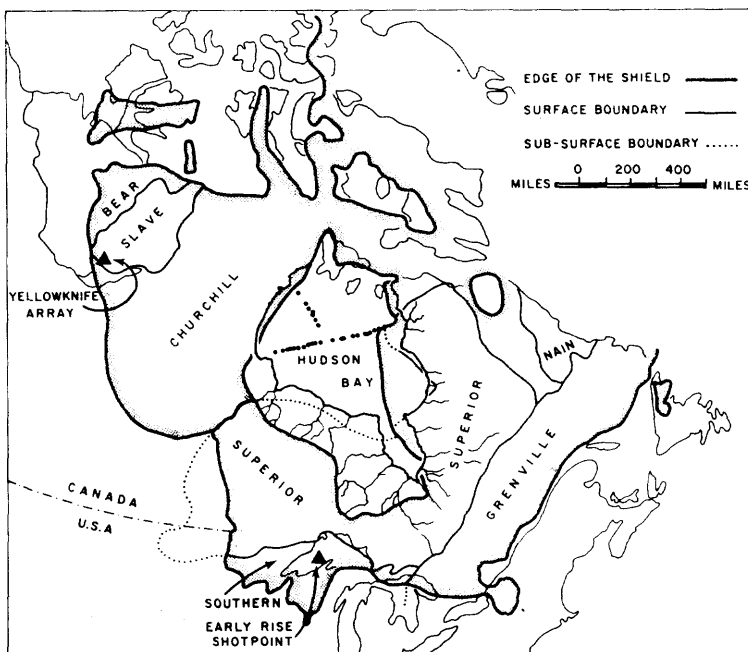


FIG. 4. — Schematic map of YKA, « Early Rise » shot location and processed Hudson Bay shots, together with outline of Precambrian geological provinces in Canada.

used, the " Early Rise " shot point and the Yellowknife seismic array location, together with the Precambrian geological provinces in Canada.

In August 1965, 41 charges, 1800 or 3600 pounds each, were detonated electrically on the seafloor of Hudson Bay for a major crustal refraction programme. The procedures used in the analysis of the Hudson Bay shots will be described in a later more detailed publication. A digital tape file was formed of 29 selected " seen " events. The type-out of the time track served to correlate the sample count within a file to the recorded time. The standard-processing computer programme was used to detect, trigger, rewind and process all digital files. Different weights were used for selected channels of some events, in order to equalize signal amplitude and to eliminate extremely noisy traces. Although this procedure does not obtain the maximum signal-to-noise, it is easy to see that intuitively it is the proper way to optimize vector response. Figure 5

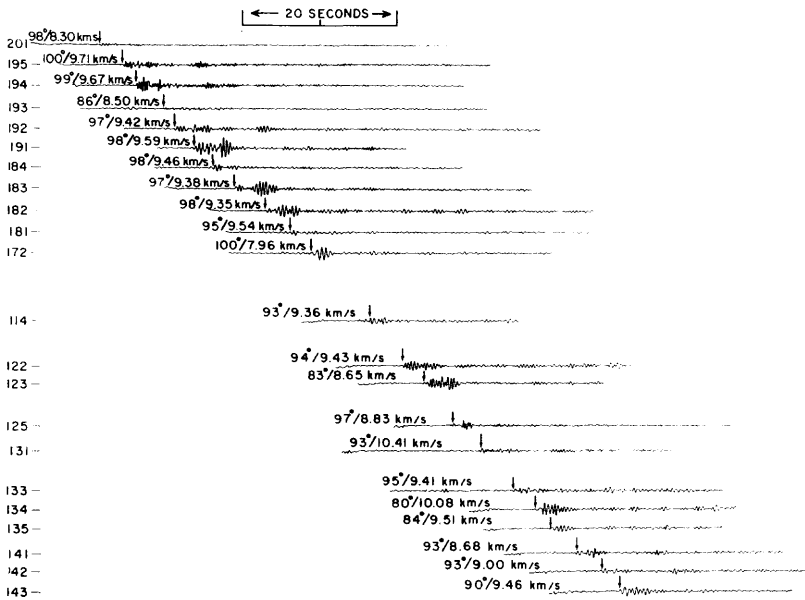


FIG. 5 — Composite of Hudson Bay first arrivals (without shot time corrections) and for red (E-W) line of 22 shots only.

shows a composite of the automatic trigger sumalls for the approximately E-W line (red line) of processed shots in Hudson Bay. In this composite the shot distances have been scaled and the time codes of the traces have been lined up. Small shot time corrections

have thus been ignored in the diagram, though they have been taken into account in the analysis to be described. The velocity and azimuth of the trigger have been noted on each strip as well as the estimated time of arrivals which were based on a visual inspection of all available output traces.

A non-time critical programme was written to output the critical information in the full correlation matrix at predetermined intervals for a 15-20 s initial portion of the arrivals. These outputs were then examined by the authors, and correlated with the actual traces. Figure 6 shows a reduced travel-time curve, with the subtraction of the nominal time terms obtained by HOBSON (1967) for the crustal structure of Hudson Bay. These time terms averaged 3.9 s, and show a variation greater than $\pm \frac{1}{2}$ s between different shot points. The phase velocities represented by segmented slopes on Figure 6 represent the average of different distinct blocks

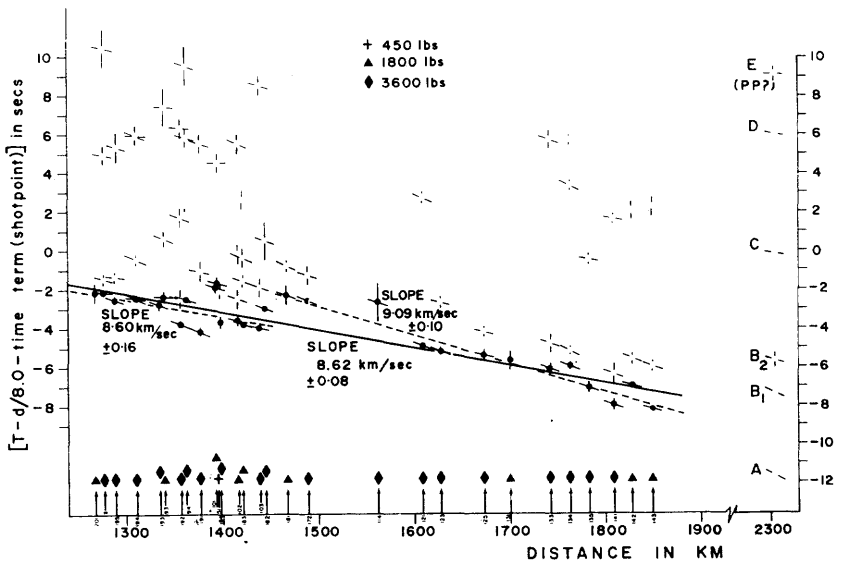


FIG. 6. — Reduced travel-time plot Hudson Bay shots, together with phase-velocity at YKA, estimate of time uncertainty and possible interpretations. Corrected for shot time-terms : the long arrows correspond to the red (E-W) line of shots, the short arrows to the blue (NW-SE) line.

of signals with coherent azimuth within 5° to 10° of the theoretical azimuth from the shot to the array.

The "Early Rise" programme of July 1966 consisted of 38 5-ton shots detonated at a substantially fixed shot point in Lake Superior by American agencies. This experiment was used to develop the

appropriate techniques for stacking array-generated tapes, particularly since, at the time of the "Early Rise" programme, difficulties were experienced on the array with variable tape speed problems.

The standard detection programme operated for teleseismic search detected all the "Early Rise" shots with an average azimuth of 122.8° (theoretical azimuth 124.2°) and an average velocity, corrected for the average tape speed error, of 10.2 km/s. Typical variations were 0.5° in azimuth and 0.1 or 0.2 km/s in velocity.

A digital file was constructed in which 18 of the best "Early Rise" shots were stacked together by digital techniques, and in which continuous corrections were applied for both internal variations of the tape speed and variations from day to day in the offset of the average tape speed from one adopted value. Experiments were performed with various weighting methods, but the final velocity filtering was done on a unit weight composite in which the data were selected for high visual signal-to-noise ratios and a signal-to-noise improvement of a least 20 : 1 was obtained.

Some of the results are briefly described. Figure 7 shows a

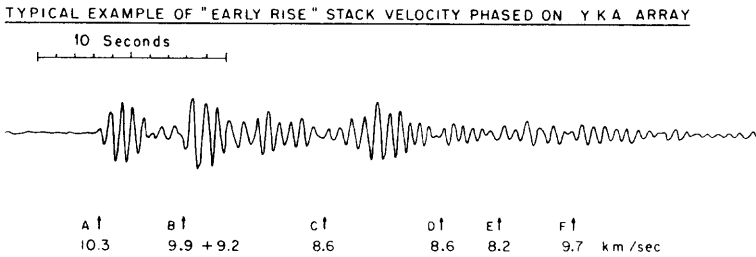


FIG. 7. — Typical velocity-phased « Early Rise » record obtained from one of composite tapes by a free search trigger. The velocities shown are true.

standard automatic trigger determination on the individual stacked seismometers. The small trace does not, of course, optimize the later arrivals. The complexity of the signals can easily be seen. In this example, covering 30 s following the initial P phase, 6 phases can easily be seen. There are shown in a reduced travel-time plot, Figure 6. Data not shown here from the cross-section of correlation indicates that the second arrival B is complex with a signal 1.7 s behind the first, and with a lower phase velocity.

Final interpretation of the data summarised in Figure 6 must await a more detailed study of the second arrivals, and the processing of shots at other ranges. Meanwhile two general interpretations are possible. The first is indicated by the two branches

shown in dashed lines in Figure 6. The first branch has a velocity of 8.60 ± 0.16 km/s : it is regarded as the bottom of a layer extending from the Moho and thus with a known velocity of 8.2 km/s at the top of the layer. Near the bottom of this layer the velocity appears to be substantially constant : the mean phase velocity at Yellowknife is 8.9 ± 0.1 km/s standard deviation in adequate agreement. The scatter of phase velocity values with distance for arrivals on this branch precludes any use of them to study the velocity-depth structure in more detail. The best complete integrations cannot yet be performed but it is clear that the bottom of this layer is greater than 150 km depth. Below this layer a very weak low-velocity layer is required : model calculations suggest that a reduction of velocity by a few percent in a layer of 10 to 20 km only would adequately match the interpreted break. In the second branch the velocity is 9.09 ± 0.10 km/s : again the corresponding phase velocities show no systematic increase with distance and the mean phase velocity is 9.2 ± 0.1 km/s. However, associating this branch with the first "Early Rise " arrival indicates that the velocity must increase with depth from 9.1 to 10 km/s corresponding to the " Early Rise " distance. The time of the A arrival is 3.1 ± 3.4 s late in this model compared to the extrapolated time from the second branch : since the arrival time of "Early Rise " is accurately known, the lower range of possible velocity is preferred, i.e., about 9.0 km/s, in order to obtain agreement. The phase velocities both over the more distant part of the east-west Hudson Bay line and from "Early Rise" appear high, the latter significantly and the former probably not significantly. The appropriate interface under Yellowknife may slope upwards to the northwest. Alternately the difficulty may be with significant differences in P-wave velocity upper mantle structure beneath the Superior and Churchill Geological Provinces.

An alternative, but in our opinion worse, interpretation is indicated by the solid line with slope 8.62 ± 0.08 km/s in Figure 6. The interpretation depends on placing significance in the fact that the phase velocities from all arrivals across Hudson Bay do not show a significant velocity break or systematic variation from 1 290 km to 1 850 km. The first arrivals are therefore all assigned to the same branch. Figure 6 shows a solid straight line which is a least squares fit to 22 red line shots only. A calculation appropriate to the known crustal models in each area gives an estimate of about 100 km as the depth to this marker layer, regarding the upper mantle as horizontally layered in a first approximation. The esti-

mated times require appreciable structure in this surface, and the high average phase velocity at Yellowknife ($9.28 \text{ km/} \pm 0.22$ standard deviation in one observation) requires an appreciable slope upwards to the west in this surface under Yellowknife. The teleseismic observations indicate velocities in approximately the same azimuth which are slower than the theoretical. The source of this discrepancy is not resolved and this interpretation is thus subject to considerable reasonable doubt.

Similarly, this interpretation requires very pronounced local surface structure since a number of the time residuals become quite large. With this interpretation, the "Early Rise" phase velocity data suggest that 2300 km is beyond the cross-over point of a triplicated travel-time curve. The second (slower part) part of the second arrival would naturally be interpreted as an extension of the branch determined by the solid line in Figure 6. Unfortunately, the observed time of arrival of the first high velocity phase (in this interpretation on a steeper branch) agrees with the predicted reduced time within $0.4 \pm 2.3 \text{ s}$. It is thus clear that this interpretation is not consistent across different Precambrian provinces. Furthermore, there is no evidence in Figure 6 for a higher velocity branch corresponding to second arrivals at longer distances.

In any case considerably more data and much closer study of second arrivals and signal character is obviously necessary. To date the variation in phase velocity with distance is puzzling and the explanation is not known. The results do not seem to agree closely with the average travel-time interpretation given by BARR (1967) for standard station visual data from the same shots.

The large amount of information available in the array records is illustrated in Figure 8, which shows a composite covering the first

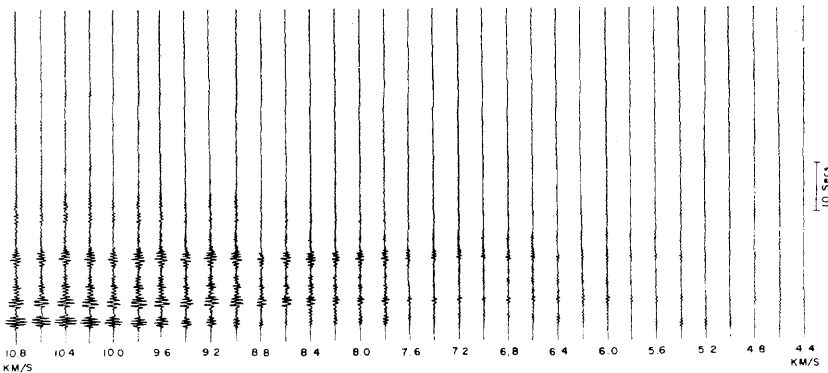


FIG. 8. — Velocity-filtered composite « Early Rise » record for velocities from 10.8 to 4.4 km./s (nominal) for the P arrivals.

few minutes of the P signal from the stacked " Early Rise " shot with different velocity filtering. In this Figure, the velocities shown need reducing by 6.6 % to obtain true velocities. Similary, Figure 9

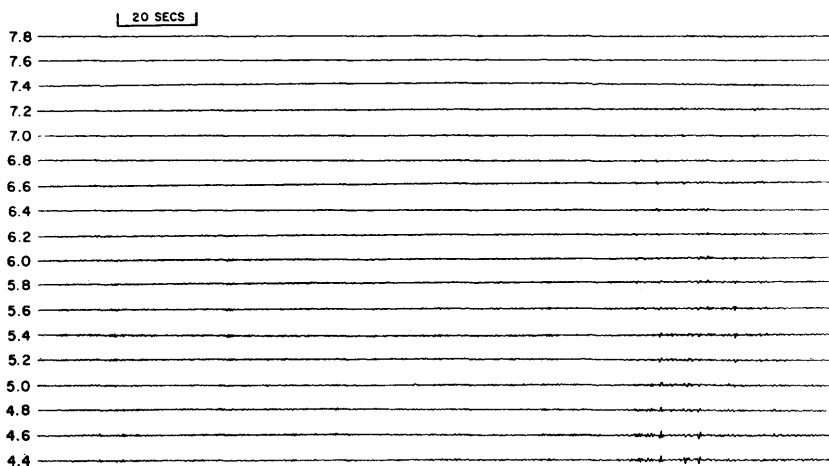


FIG. 9. — Velocity-filtered composite « Early Rise » record for velocities from 7.8 to 4.4 km/s (nominal) for the S and later arrivals.

shows the S arrivals. The first one occurs at 3 mn 32.2 s after P, and is followed by other prominent arrivals, particularly one 13.5 s later. Finally, there is evidence for surface wave arrivals.

Conclusions

A start has been made on an examination of upper mantle structure along different paths using the resolution of a medium aperture array to distinguish and interpret different arrivals. In time the best numerical model will be published, but it seems likely that the situation is complex even within the Precambrian Shield. It is considered essential to clarify this situation in order to interpret structure at greater depths from the observed teleseismic T, $\frac{dT}{d\Delta}$, Δ data. Work is continuing.

REFERENCES

- BARR, K. G., 1967. Upper mantle structure in Canada from seismic observations using chemical explosions. *Can. J. Earth Sci.*, 4, 961-975.
HOBSON, G. D., A. OVERTON, D. N. CLAY and W. THATCHER, 1967. Crustal structure under Hudson Bay, *Can. J. Earth Sci.*, 4, 929-948.

MANCHEE, E. B. and D. H. WEICHERT, 1968. Epicentral uncertainties and detection probabilities from the Yellowknife seismic array data. (In Press, Bull. Seism. Soc. Am.).

WEICHERT, D. H., E. B. MANCHEE and K. WHITHAM, 1967. Digital experiments at twice real-time speed on the capabilities of the Yellowknife seismic array. Geophys. J. of R.A.S., 13, 277-295.

PRELIMINARY RESULTS FROM THE WARRAMUNGA ARRAY

Gordon NEWSTEAD¹, John CLEARY²

1. Introduction

Since October 1965 the Australian National University has been operating a U.K.A.E.A. type array of 20 short period vertical seismometers with a 22 km aperture near Tennant Creek in the Northern Territory of Australia. The name of the station, Warramunga, is taken from that of the aboriginal tribe which used to inhabit the area. Two tapes are recorded at the array, one is sent to the U.K.A.E.A., Blacknest and the other to the A.N.U., Canberra for processing. This paper gives some of the early results of the work at Canberra.

2. Brief description of the array and method of processing results

Tennant Creek is a very quiet site.

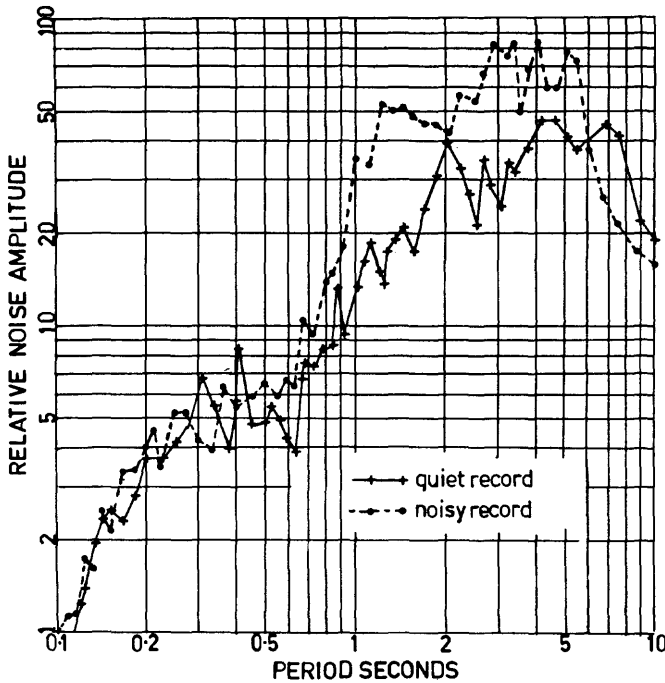


FIG. 1 shows a spectrum of the noise on quiet and noisy days. 100 on the scale corresponds to $10 \text{ m}\mu/\text{s}$ which makes the quiet day ground displacement $1 \text{ m}\mu$ peak to peak at 1 c/s. The gain in a 1 c/s band centred around 1 c/s is 200,000. The difference quiet and noisy days in the long period part spectrum is due to ocean microseisms although Warramunga is hundreds of miles from the nearest point to the sea.

1. Professor of Engineering Physics, A.N.U.

2. Fellow, Department of Geophysics and Geochemistry, A.N.U.

Between June and December 1966 a total of 5 212 events were recorded on the single channel visual monitor, that is approximately 21 per day. Of these only about 25 % were located by the U.S.C.G.S. program. A large proportion of the events were in the circumpacific belt and some local activity has been recorded.

The tape output of the array is processed by a digital computer in Canberra : a paper in the course of publication by Muirhead and Newstead describes the set up used — a few details and some early results are given here. The analogue tapes are played back 'at 12 times real time passed through signal conditioning equipment (filters, etc.) then a multiplex and digitiser into an IBM 360/50 computer where they are temporarily stored on a disc file. The sampling rate preserves frequencies up to 10 c/s and a 16 bit half word is used. Once transferred to the disc file the data can be processed in a variety of ways under program control and can be outputted as alpha-numeric printout, cards or graphs. At present processing of events required for special studies is carried out by delay-sum-correlate method and an edited tape of events only, is produced and preserved.

3. Some preliminary results of the Canberra processing

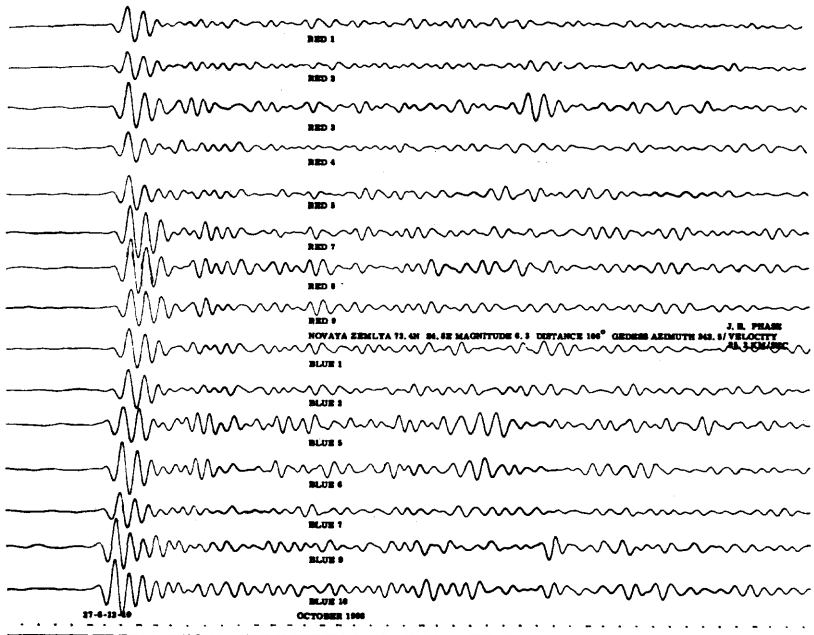


FIG. 2 shows the analogue playout of an underground explosion in Novaya Zemlya. (Magnitude 6.3 distance 103°).

AZIM	VELOCITY IN KILOMETRES PER SECOND																				
	18.00	18.19	18.37	18.50	18.70	18.79	18.99	19.19	19.39	19.59	19.79	19.99	20.19	20.39	20.59	20.79	20.99	21.19	21.39	21.59	21.79
333.0	62	63	64	67	70	75	78	77	78	78	83	81	86	87	87	89	90	90	90	90	90
333.4	62	62	67	70	73	77	77	77	78	78	83	83	86	86	86	89	90	90	90	90	90
333.8	63	65	70	73	76	76	77	77	77	83	83	83	86	86	88	89	90	90	90	90	90
334.3	60	69	71	75	76	76	80	82	82	83	83	84	87	89	89	89	90	91	91	91	90
334.7	66	69	74	74	74	78	81	82	82	85	86	87	88	89	89	91	91	91	91	92	91
335.2	66	69	72	74	78	81	83	85	85	86	86	87	89	89	90	91	91	92	92	92	94
335.6	69	67	72	74	79	81	83	85	85	85	86	87	89	89	88	91	91	92	92	94	94
336.1	68	72	74	74	79	83	85	85	85	85	86	89	89	89	88	91	91	92	94	94	95
336.5	70	76	76	78	84	84	85	85	87	87	87	89	89	91	89	94	94	95	94	95	95
337.0	74	74	78	80	83	83	84	83	87	87	87	89	90	92	94	95	95	95	95	95	95
337.4	74	70	70	80	83	85	86	86	87	87	89	90	93	94	95	94	96	96	95	95	95
337.7	73	78	78	80	83	85	86	85	89	89	89	93	93	95	96	96	96	96	95	95	95
338.3	70	78	78	83	83	85	85	87	88	93	93	94	95	96	96	96	96	96	96	95	94
338.8	79	81	81	81	83	85	87	92	92	94	95	95	95	96	96	96	96	96	95	94	94
339.2	79	81	81	83	85	89	91	91	91	95	95	95	95	95	96	96	96	97	97	94	94
339.7	70	81	83	83	87	87	91	91	95	95	95	95	95	95	95	96	96	97	97	94	94
340.1	77	81	83	87	89	92	93	93	95	95	95	95	95	95	96	96	96	96	97	95	94
340.6	77	86	89	89	91	91	93	93	95	95	95	96	96	96	96	97	97	98	98	95	94
341.0	82	84	89	92	91	91	93	93	95	95	95	96	96	96	97	97	98	98	98	98	95
341.5	84	86	91	92	92	91	93	93	95	96	97	97	98	98	98	98	98	98	98	98	95
341.9	84	87	93	92	92	91	93	93	94	96	97	97	98	98	98	98	98	98	98	98	98
342.3	87	87	90	93	93	93	95	95	96	98	98	99	99	98	98	98	98	98	98	98	97
342.8	86	86	89	93	93	94	94	96	97	98	98	99	99	99	98	98	98	98	98	98	97
343.3	87	86	89	93	93	96	97	97	97	98	98	99	99	99	98	98	98	98	98	97	97
343.7	87	82	90	93	93	96	97	97	97	97	98	99	99	99	98	98	98	98	97	97	97
344.2	86	82	92	93	93	96	97	97	97	97	98	99	99	99	98	97	97	97	97	97	97
344.6	87	82	93	93	93	96	97	97	97	98	99	99	99	99	98	97	97	97	97	97	97
345.1	88	87	93	93	93	95	98	98	98	98	99	99	99	99	98	97	97	97	97	97	97
345.5	87	90	93	93	94	95	97	98	98	98	99	99	99	99	99	98	97	97	96	96	96
346.0	87	91	93	94	94	95	97	98	98	98	99	99	100	99	99	99	99	96	96	96	95
346.4	89	91	94	94	94	95	97	98	98	98	99	99	100	99	99	99	99	96	96	96	95
346.9	90	91	94	94	94	95	97	98	98	98	99	99	99	99	99	99	99	96	96	96	95
347.4	90	90	94	95	95	95	97	98	98	98	99	99	98	98	99	99	99	96	96	96	95
347.9	89	90	91	95	95	95	96	98	99	99	99	99	98	98	99	99	99	98	96	95	95
348.3	90	92	92	95	96	96	96	97	98	99	99	99	98	98	98	98	98	98	98	95	93
348.7	91	92	92	95	96	96	96	97	98	99	99	99	98	98	98	98	98	98	96	93	92
349.1	91	92	93	96	96	96	96	96	97	98	99	99	98	98	98	96	96	96	96	93	90
349.6	92	92	93	96	96	95	95	95	96	97	98	97	97	97	97	97	95	94	94	94	90
350.0	92	93	93	96	96	95	95	95	95	97	97	97	97	95	95	94	94	94	94	94	90
350.5	92	92	92	93	92	95	94	94	94	96	96	95	95	95	95	94	94	94	94	94	92

RELATIVE MAXIMUM POWER =

14443183

NOVAYA ZEMLYA FINE CORRELATION

Fig. 4 shows an expanded version of the last one, around the region of 20 km/s. The velocity steps are now 0.2 km/s and the azimuth steps 0.5 degrees. The greatest correlation is attained at 20.2 kms, 346 degrees and this should be compared with the Gedess value of 25.3 km/s, 342.5°. Differences of this sort are characteristic of array results and arise from inhomogeneity of geological structure under the array. (See next section.)

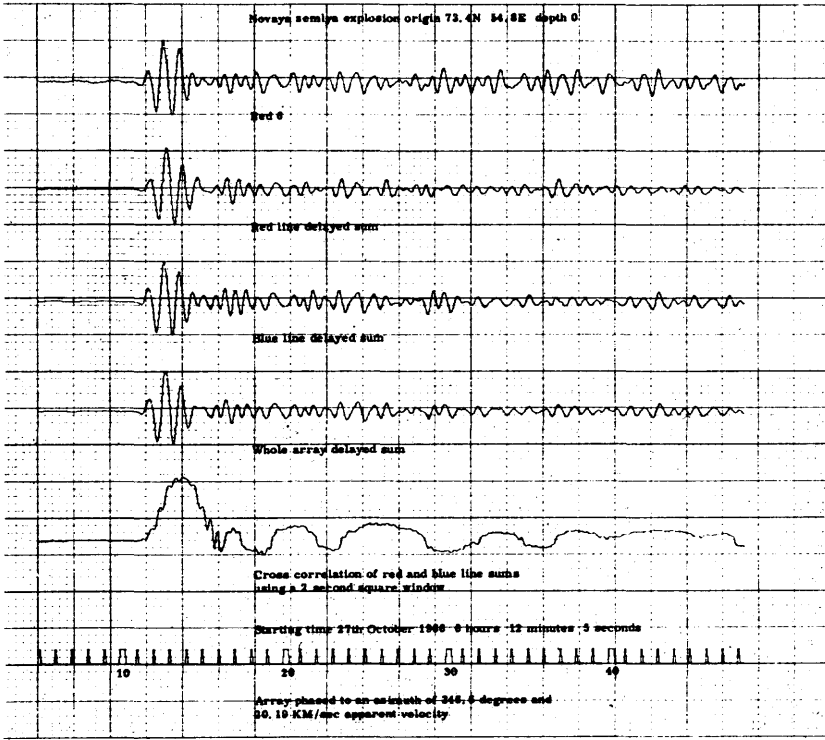


FIG. 5 shows the processed record and correlogram.

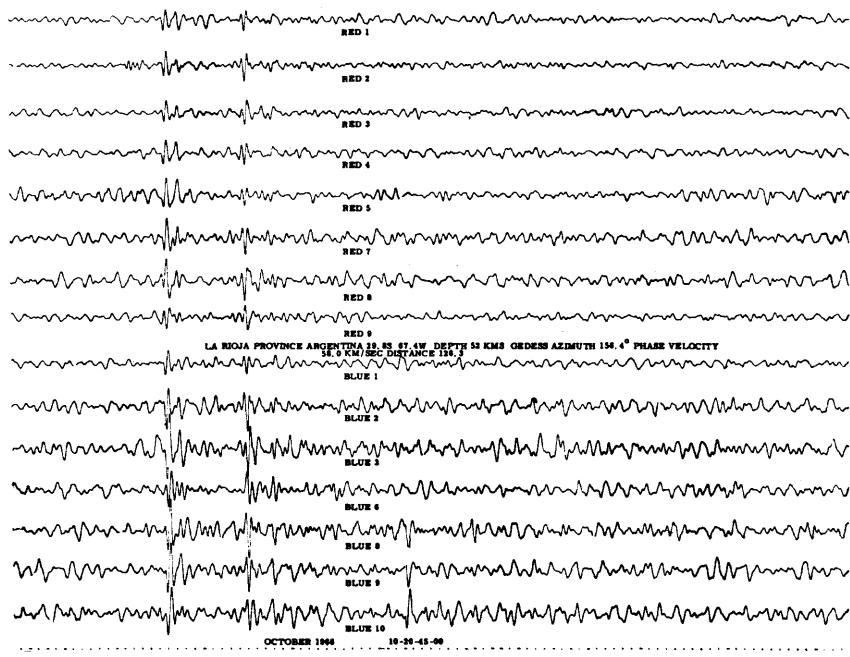


Fig. 6 shows the analogue playout of an Argentine event and Figure 7 the processed record.

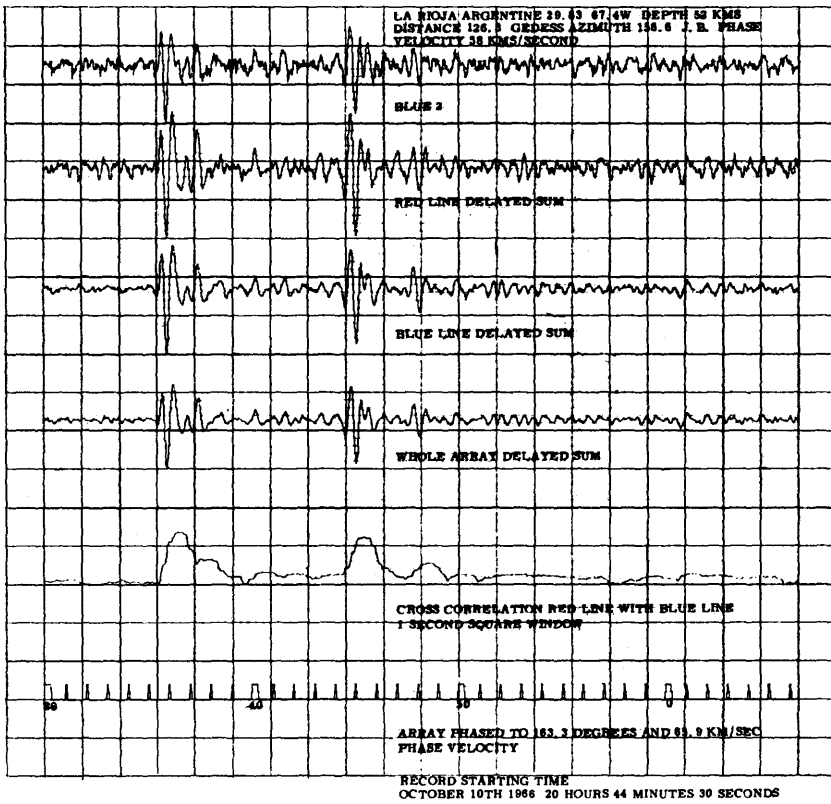


FIG. 7. The usefulness of the correlogram in enhancing the resolution of the extra phase is illustrated here.

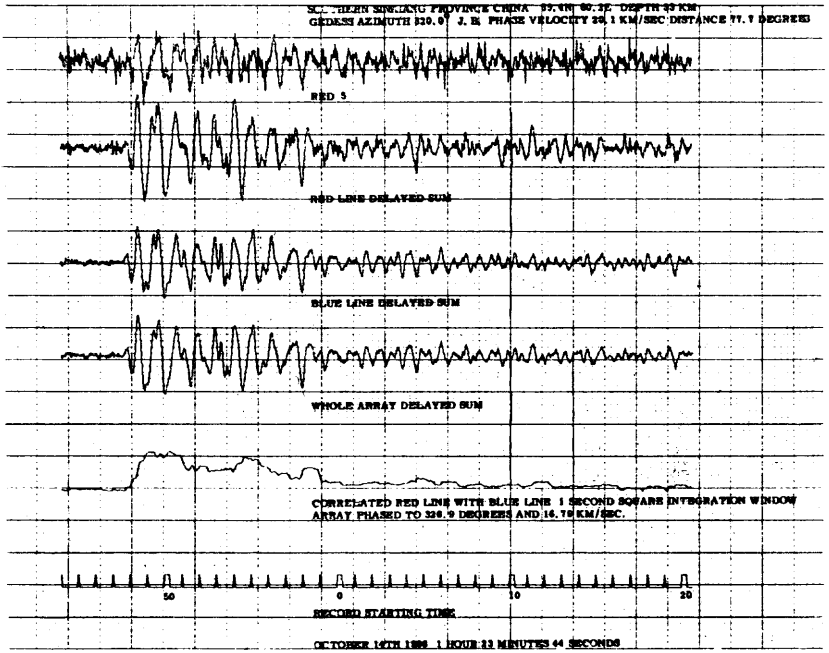


FIG. 8 shows the processed record of a small Chinese earthquake. The increase in resolution produced by the process is evident.

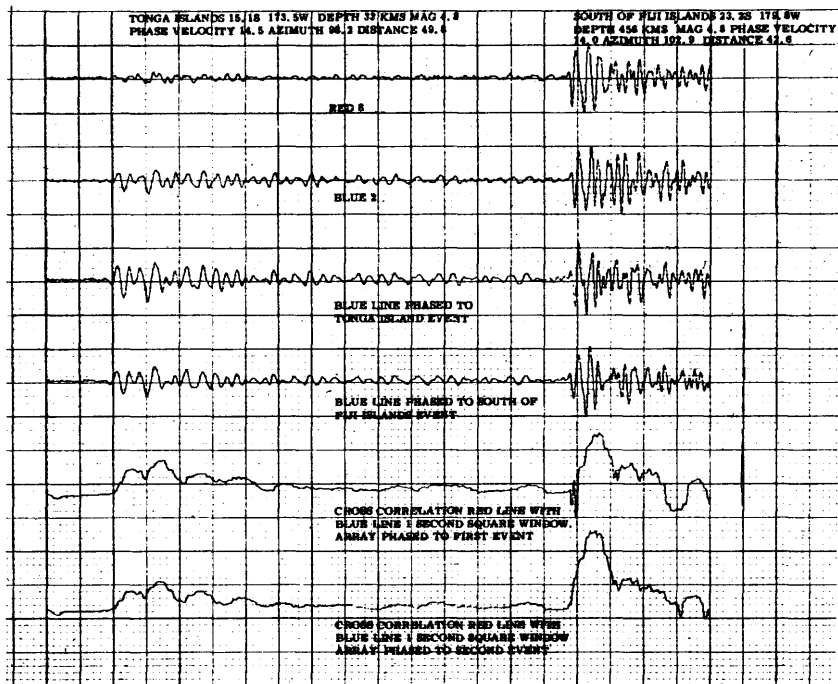


Fig. 9 shows the processed result for two nearby events — Tonga ($\Delta = 49.8^\circ$, azimuth 98.2° J. B. velocity 14.5 km/s) and Fiji ($\Delta 43^\circ$, azimuth 103° J.B. velocity 14.0 km/s). The *lack* of correlation of the Fiji event but *not* the Tongan when tuned to the J.B. phase velocity is evident.

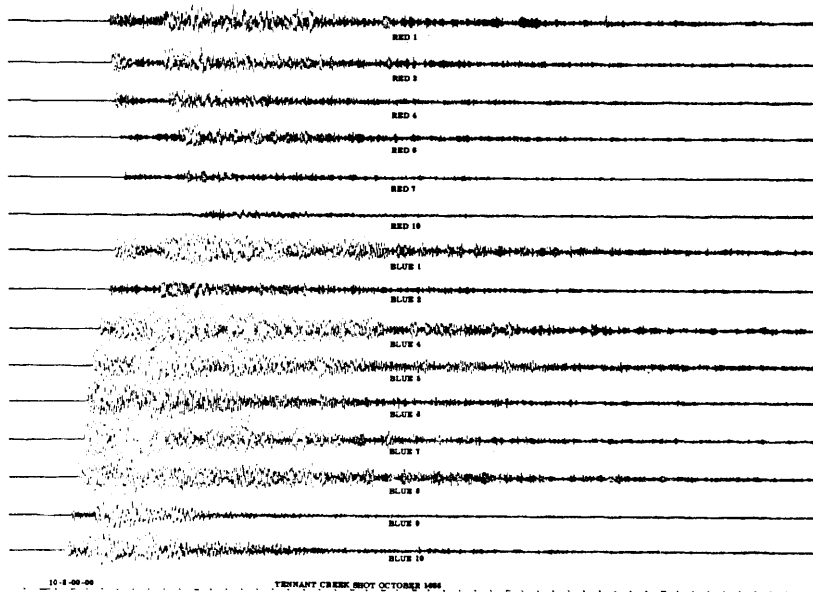


Fig. 10. — Shows the analogue payout of a 1500 pound explosion set off in a disused mine 35 km north of B10. Differences due to local structure can be discerned e.g. B9.

4. Inhomogeneity in macro geological structure

The array is located on granite outcrops on the low Proterozoic Warramunga Geosyncline and it was noticed in early records that there was a substantial difference in the character of the output of some of the seismometers; in particular for certain azimuth there was a comparatively sharp change at B2 in the character of the blue line signals. Cleary and Wright are engaged on a substantial study of this phenomenon with a view to obtaining pit corrections which will be used to calibrate out the effect of major inhomogeneities beneath the array. The success of this programme would increase the usefulness of arrays sited in less favourable geological environments.

In their studies Cleary and Wright use a manual technique of matching waveforms across the array which gives measurements of relative onset times repeatable to 0.01s. Six events were used for this preliminary study — the Longshot explosion, four earthquakes in the Aleutian Islands at distances of 79.4° to 84.7° from WRA and a South African earthquake at a distance of 84.0°. The last event is approximately opposite in azimuth from the array to the Aleutian Islands.

The relative times of arrival at the individual seismometers were measured and compared with the J.B. times on the assumption that the U.S.C.G.S. locations were correct. The residuals on an arbitrary base-line are shown in the next figure (*fig. 11*).

The following features should be noted :

- (i) The trend of the residuals is in the same direction for opposite azimuths indicating that the deviations are caused by the structure dipping to the southwest, rather than by errors in the J.B. tables.
- (ii) The trend is not linear but is roughly symmetrical along both lines with respect to the crossover point of the array. This suggests that the structure consists of a series of monoclinial folds striking northwest.
- (iii) There is a suggestion that the dipping interface rises sharply in the vicinity of the crossover point so that waves travelling to R1, R2 and B2 from the south pass through a structure that is not continuous with that traversed by waves approaching from the north.

Underwood has inferred the presence of a sedimentary structure beneath the array dipping 5° in a direction 200° E of north from the

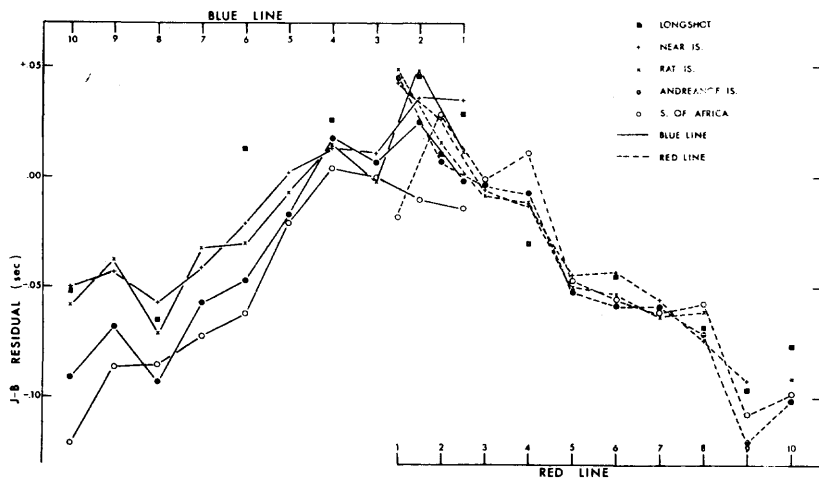


FIGURE 11.

previously mentioned explosion close to the array. Using their teleseismic data Cleary and Wright obtain the following structure : dip angle 6.5° ; dip direction 235° E of N; velocity contrast 0.7. The corrected values of $dT/d\Delta$ using this structure are shown in the figure 12.

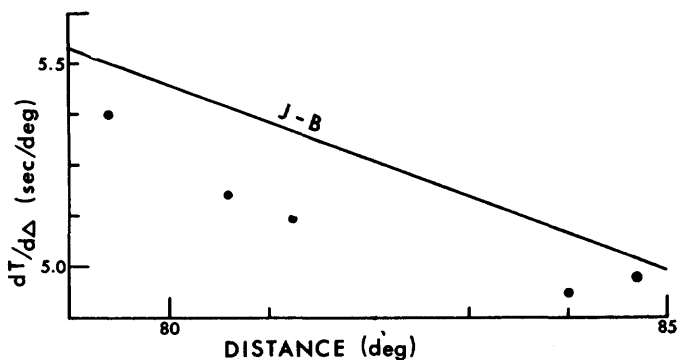


FIGURE 12.

These are still possibly subject to systematic error. The dip angle and direction of the structure are in broad agreement with findings of Underwood mentioned earlier.

5. Conclusion

This paper presents the first results of the processing of the output of the Warramunga seismic array using a digital computer and discusses the structure beneath the array.

LIMITATION GÉOLOGIQUE DANS L'UTILISATION D'UN RÉSEAU DE SISMOGRAPHES

par P. MECHLER et Y. ROCARD
Laboratoire de Physique de l'École Normale Supérieure

Nous avons déjà entendu plusieurs communications relatives à la mesure de $dT/d\Delta$. Leurs auteurs mesuraient, à l'aide d'un réseau de stations, la vitesse apparente des ondes issues d'un séisme lointain. La vitesse apparente ainsi obtenue étant différente de celle que donnent les tables de Jeffreys-Bullen, ils en déduisent une correction à ces tables, correction qui revient à changer légèrement la vitesse des ondes sismiques dans le manteau inférieur. A l'aide de notre propre réseau, nous avons observé des différences similaires dans les temps d'arrivée, mais nous avons essayé de le interpréter exclusivement par des corrections locales, au voisinage de nos stations d'enregistrement.

Entre deux stations voisines, nous mesurons une certaine différence de temps entre les premières arrivées d'une onde, cette différence diffère du temps dT calculé d'un certain écart e que nous voulons expliquer par des différences de structure de la croûte terrestre ou du manteau supérieur en-dessous des stations. Utilisant des stations éloignées de 20 à 30 kilomètres, nous observons couramment des écarts de l'ordre de 0,3 seconde. On peut montrer que l'épaisseur totale de la croûte est le paramètre principal qui doit intervenir dans une explication locale. Le contraste de vitesse est en effet maximum entre la croûte et le manteau, un écart de 0,3 seconde peut être expliqué par des inclinaisons de la discontinuité de Mohorovicic qui sont de l'ordre de 10 à 20°, valeur élevée mais admissible sur de faibles distances, alors que par exemple l'hypothèse d'un gradient horizontal de vitesse, la géométrie des couches ne changeant pas, exigerait une variation de vitesse de l'ordre de 10 %, ce qui est totalement inadmissible entre deux stations aussi proches l'une de l'autre.

Nous avons choisi d'expliquer ces phénomènes par des variations locales de la structure, en effet, nous allons voir que ces écarts sont des fonctions de l'azimut et que, dans la mesure où nous avons pu l'étudier, l'écart de temps dans un azimut donné ne dépend pratiquement pas de la distance. D'autre part, lorsque nous avons des écarts importants variant en fonction de l'azimut, leur valeur

moyenne est voisine de zéro, suggérant ainsi que les tables de Jeffrey's-Bullen sont déjà une très bonne approximation.



RESEAU SISMOLOGIQUE FRANÇAIS

FIG. 1

La figure 1 montre l'implantation de notre réseau en France, constitué de cinq stations principales formées chacune de trois stations reliées par radio, nous allons d'ailleurs très prochainement commencer le regroupement de toutes nos stations sur Paris en profitant des relais hertziens pour implanter de nouveaux sismographes. Nous avons jusqu'à présent surtout étudié les écarts de temps dans les triangles de Normandie, du Morvan et de Provence. Je ne donnerai ici que des résultats pour la Normandie, d'une part, et pour un alignement de huit stations, dans le Tarn-et-Garonne, alignement très temporaire qui nous a permis d'enregistrer une explosion nucléaire algérienne.

La figure 2 montre justement cet ensemble de stations. Nous avons pris soin de les placer sur des séries calcaires des Causses apparemment homogène au point de vue géologique en dessous de ces stations. Si je dis « apparemment homogène » c'est parce que la

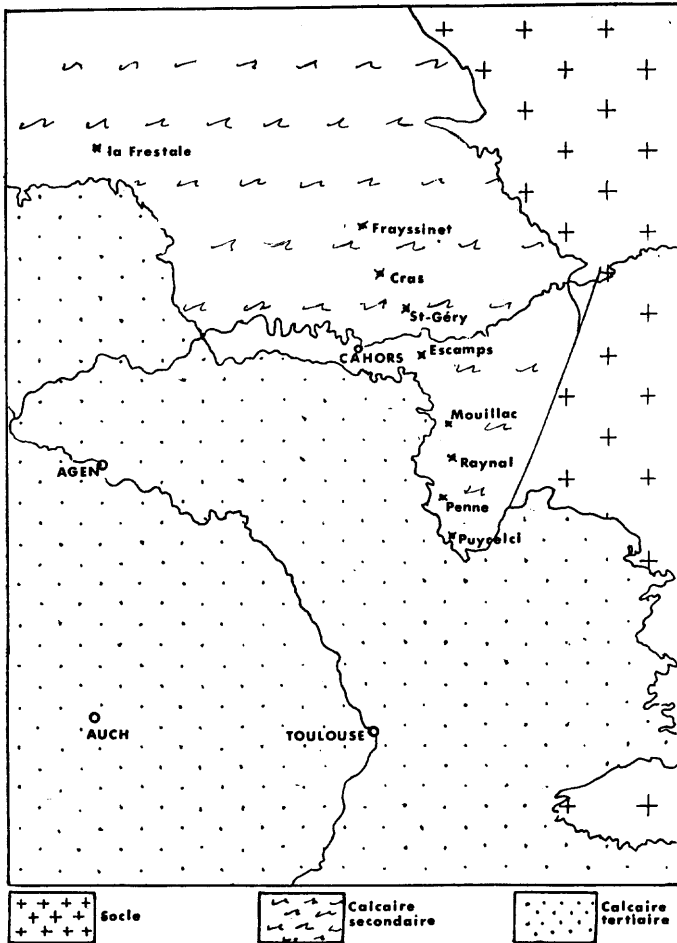


FIG. 2

figure suivante (fig. 3) donne une carte du toit du socle sous les stations, tel qu'il a été déterminé par une prospection aéromagnétique. On observe une cuvette profonde de plus de 3 000 mètres, bordée à l'Est par les affleurements du Massif Central et à l'Ouest par une colline remontant jusqu'à moins de 500 mètres de la surface du sol. Si nous avions la carte complète, il serait facile de voir que nous sommes dans la partie Sud d'une fosse du socle qui borde le Massif Central et est limitée par une ride à l'Ouest.

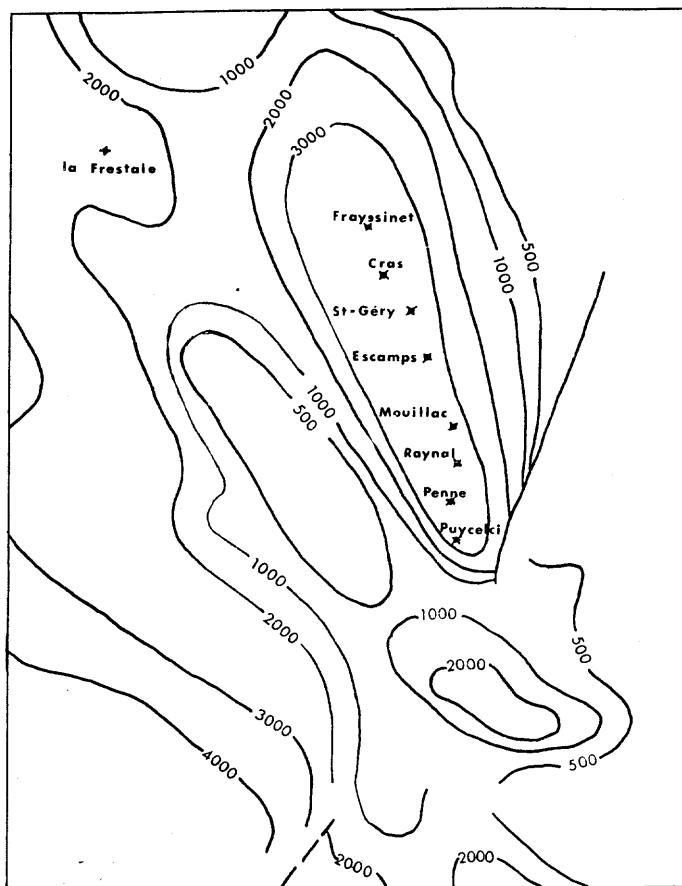


FIG. 3

La figure 4 se rapporte à une explosion nucléaire située à peu près à 2 500 km au Sud dans l'alignement de nos stations. La courbe supérieure représente la variation d'amplitude des signaux enregistrés et la courbe inférieure les écarts de temps. Cette dernière courbe n'est pas complète vers le Sud, nous avons en effet éliminé les trois premiers points pour lesquels le temps n'était pas déterminé de façon suffisamment précise. Pour tous les autres points, nous avons une précision de quelques centièmes de seconde, nous avons en effet une vitesse de déroulement assez grande et nous recevons des signaux horaires; les trois premières stations n'ayant pas reçu de signaux horaires n'ont un temps déterminé qu'à 1 ou 2 dixièmes de seconde, ce qui est insuffisant.

Il est facile de remarquer que ces deux courbes présentent un pic pour la même station d'Escamps et que nous obtenons des

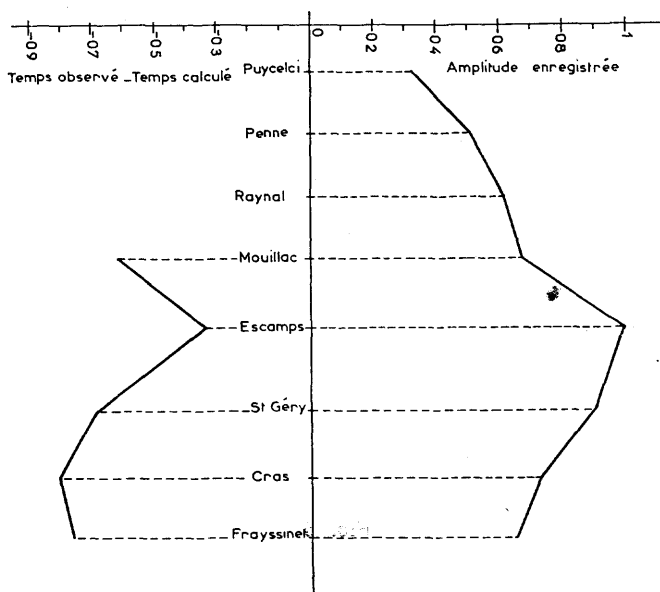


FIG. 4

écarts de temps assez grands, 0,5 seconde entre Escamps et Cras, distants d'environ 25 kilomètres. En tous points, nous avons enregistré à grande vitesse et il y a une excellente corrélation entre les différents signaux.

La figure suivante (fig. 5) représente la structure de la discontinuité de Mohorovicic que nous avons calculée en attribuant, comme nous l'avons dit plus haut, toutes les anomalies à des variations d'épaisseur de la croûte que nous avons supposée homogène. Nous avons aussi représenté le trajet des rayons sismiques; on observe une focalisation au voisinage d'Escamps qui explique au moins de façon qualitative le maximum d'amplitude observé dans cette station.

Dans la figure 6, nous avons tracé d'une part la discontinuité de Mohorovicic, d'autre part le toit du socle. Bien que ce dernier soit très aplati dans le fond de la cuvette, il semble que la partie la plus basse de celle-ci soit à l'aplomb de l'anomalie observée dans le Moho. En tout cas, la régularité dans la variation de cette cuvette ne permet pas d'expliquer les écarts de temps et les variations

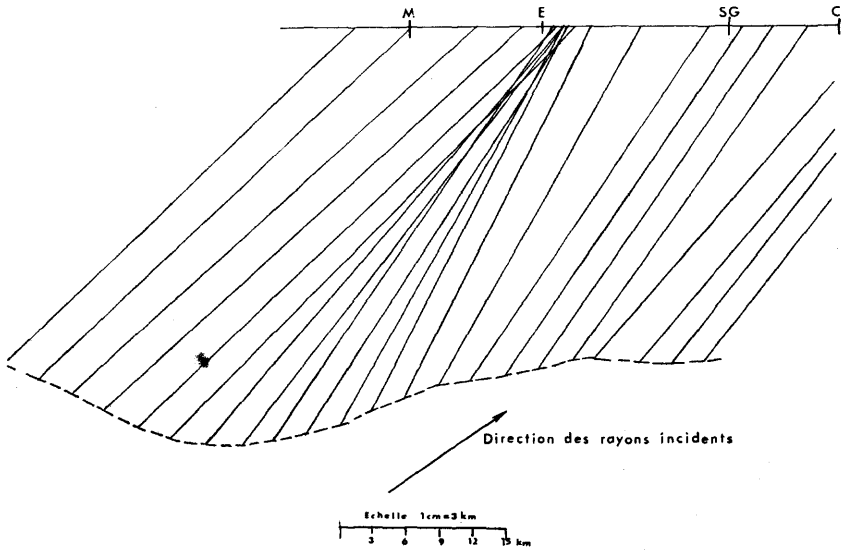


FIG. 5

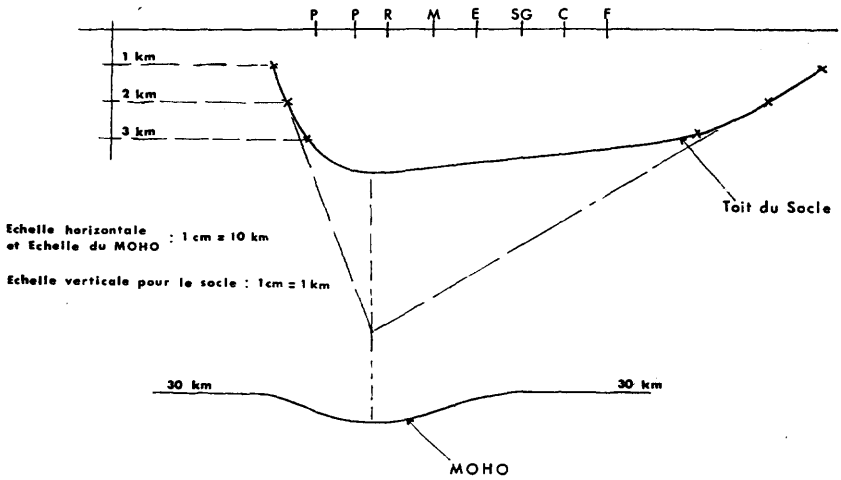


FIG. 6

d'amplitude observés par un phénomène qui se passerait à la limite du socle et des sédiments.

On indiquera également quelques résultats obtenus dans notre station de Normandie. La figure 7 montre les écarts de temps entre

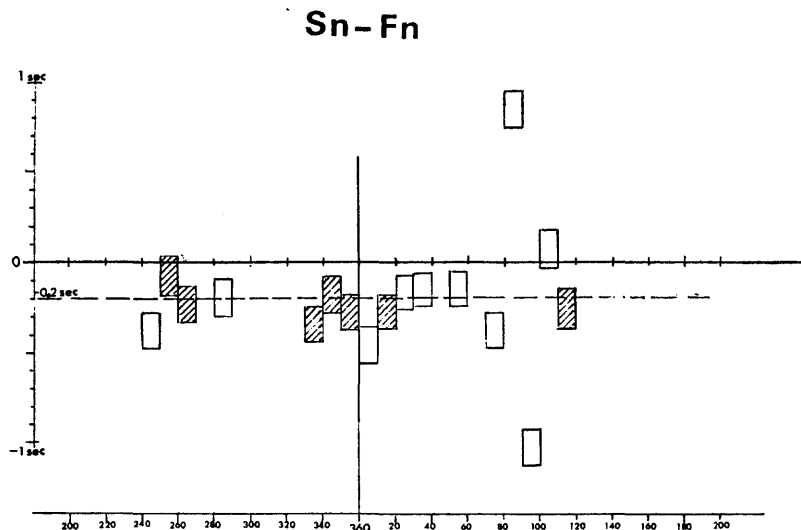


FIG. 7

SN la station la plus à l'Est et FN la station la plus au Nord. Les écarts de temps, moyennés dans la mesure du possible pour des variations d'azimut de 10° , ont été portés en fonction de l'azimut, nous avons des valeurs de -120° à $+120^\circ$. Il y a d'abord deux points aberrants, ces points correspondent à un seul séisme chacun. Pour les autres, nous avons fait des moyennes de plusieurs séismes dans la mesure de nos observations, les rectangles hachurés correspondent à des directions dans lesquelles nous avions des variations de distances supérieures à 1 000 km environ pour les différents séismes. Dans la limite de la précision de nos mesures, il n'y a pas de dépendance de l'écart en fonction de la distance épacentrale.

Pour ces deux stations, nous n'observons pas de variations en fonction de l'azimut, l'écart moyen a une valeur de 0,2 seconde qui peut s'expliquer par un pendage de la discontinuité de Mohorovicic de l'ordre de 10 % ,Moho s'enfoncerait vers l'Ouest, c'est-à-dire sous le Massif Armoricaïn, nos stations étant sur l'extrémité Est de ce Massif). La figure 8 représente, elle, les écarts entre GN, la station la plus à l'Ouest et FN, la plus au Nord. Il y a une incontestable dépendance entre les écarts et l'azimut,

Nous avons été conduit à admettre que la discontinuité de Mohorovicic possède des ondulations de 30 km de longueur d'onde et d'environ 6 km d'amplitude, la direction de ces ondulations est E-O c'est-à-dire dans la parallèle au plissement du Massif Armori-

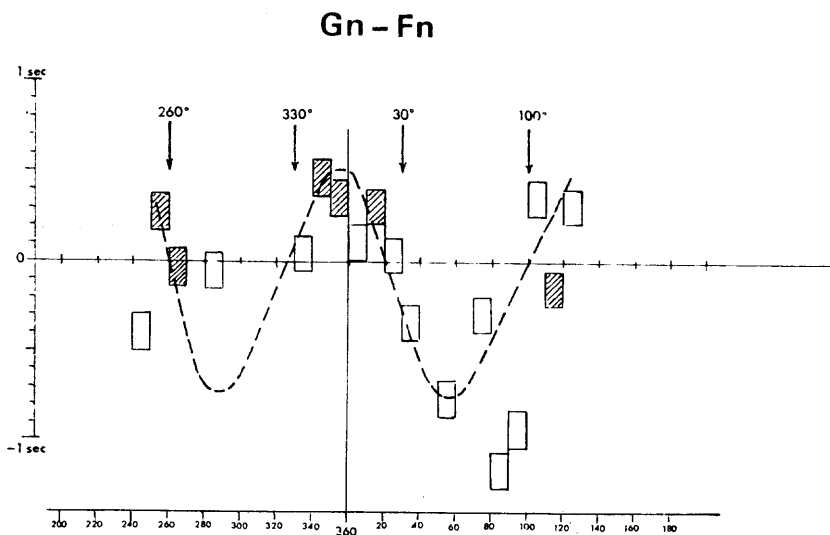


FIG. 8

cain et s'enfonçant vers l'Ouest comme nous l'avons déjà indiqué.

Nous avons pu expliquer les écarts de temps observés par des influences locales, mais cette première approximation n'exclut évidemment pas une influence de $dT/d\Delta$ qui se superposerait à la précédente. Dans les pays comme la France, dans lesquels la géologie est assez tourmentée, l'utilisation d'un réseau nécessite une soigneuse étude locale avant de pouvoir utiliser ce réseau dans des déterminations très précises d'épicentres.

EARTH STRUCTURE AND FOCAL MECHANISM : EVIDENCE FROM THE BERKELEY ARRAY

by Bruce A. BOLT and T. V. McEVILLY
Department of Geology and Geophysics, University of California, Berkeley

ABSTRACT

Since 1960-1961, a telemetry network of seismographic stations has operated in northern California. Initially, vertical-component seismometers at stations in the Coast Ranges which straddle the San Andreas fault were linked; subsequent modification included telemetry from a high-gain station in the Sierra Nevada and the use of horizontal-component instruments. Recording is continuous analogue on film and magnetic tape.

Time control and uniformity of recording over the array have led to greater precision in earthquake location and in correlation between wave trains. The first *coherent* portion of the S waves from teleseisms, recorded at array stations in the Central Ranges, arrives on the order of 3 sec or more *after* the time predicted by the Jeffreys-Bullen tables. Measured wave deviations from great circle paths have reached 10° for P waves and 20° for S waves ($\Delta > 30^\circ$). For P and S, both the deviation from the true bearing and the wave slowness are functions of the azimuth of approach; provisional results suggest that the azimuth anomaly function for S is more complicated than for P. Explanation of the azimuthal anomalies apparently requires variation in structure in the upper mantle along the continental margin.

The array permits the P radiation pattern of small local earthquakes to be analyzed. Fault-plane solutions in the Coast Ranges to the present are consistent with predominately transcurrent right-lateral motion along near-vertical faults; the computed strike of each fault plane is uniformly close to the strike of the main fault-trace in the area. As an example, the polarity diagram for the Bear Valley shock of 1966, April 29, magnitude 3.8, is discussed.

Introduction

An observational program in seismology has been carried out at Berkeley since 1962 using the central California telemetered network of seismographs. Because work on P and pP has previously been published (BOLT, 1965; OTSUKA, 1966 a, b; BOLT and NUTTLI, 1966) this paper deals mainly with the use of the seismonet to investigate the behaviour of S wave-fronts propagating across central California and to study the focal mechanism of small local earthquakes.

One feature of the array needs emphasizing at the outset. Considerable trouble is taken with most arrays to select locations away from the ocean and on a uniform compact, crystalline basement. The University of California array, shown in Figure 1, meets neither of these criteria. Most stations are located in the faulted and seismically active Coast Ranges of central California; from west to east, one encounters three geological provinces : the Coast

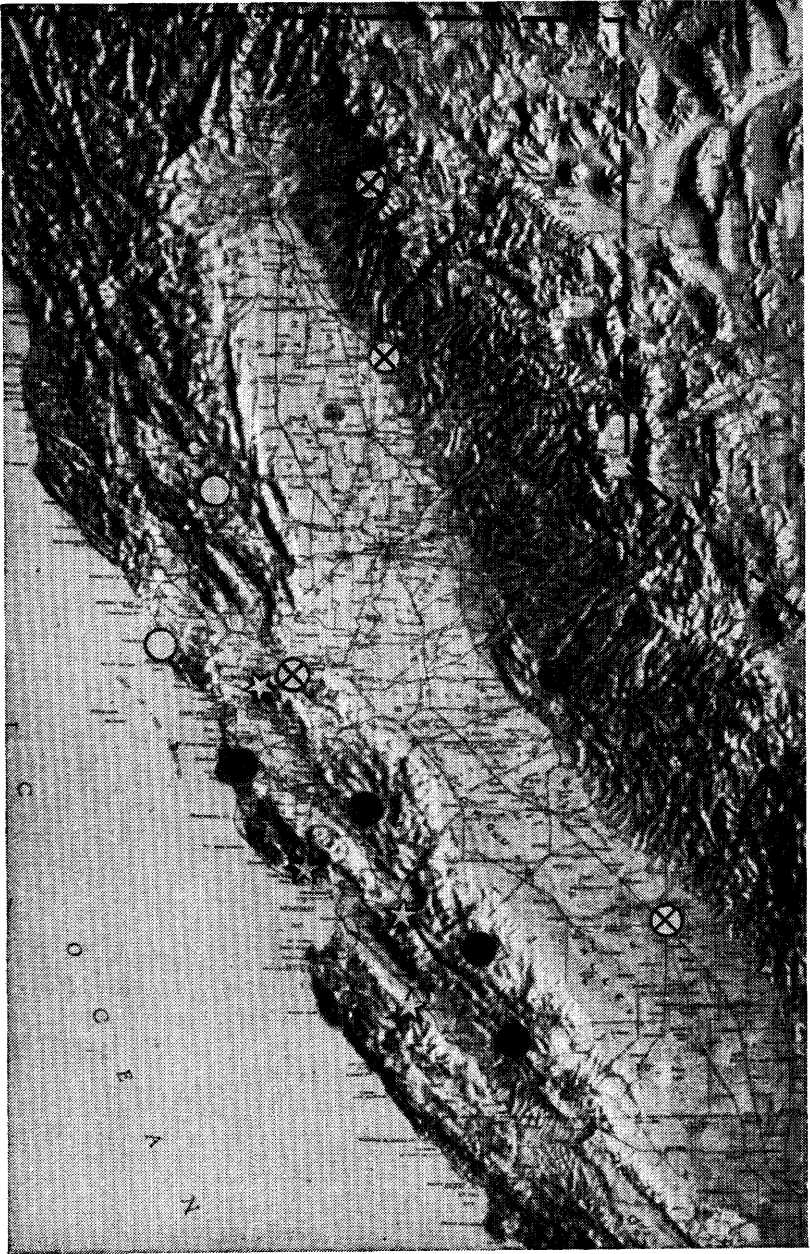


FIG. 1. — The seismonet of the University of California. Telemetry stations are shown as open and full circles and stars; the open circles show the position of the Calistoga (CLS) and Point Reyes (PRC) stations closed in 1965. Ordered strictly from north to south, abbreviations for the telemetry stations are : JAS, BRK, PCC, MHC, GCC, SAO, LLA, PRS, PRI. Non-telemetry stations are shown as crosses.

Ranges (with Franciscan rocks and large granitic masses), the alluvial Central Valley, and the Mesozoic granite batholith of the Sierra Nevada. The average noise level at one cycle per second at Berkeley is 12 millimicrons in the winter and 7 millimicrons in the summer; at Jamestown, in the Sierra, the average level yearly is about one millimicron.

In 1960, VELA UNIFORM funds, under contract with the U.S. Air Force Office of Scientific Research, were made available to establish the central California seismonet. By January 1, 1962, ten stations, were transmitting signals continuously by telemetry to Berkeley. The network straddles the San Andreas fault. The original network (until march, 1965) extended for 320 km along a N 35° W axis and was about 60 km wide; the network apertures, relative to the Vineyard station (now replaced by the nearby San Andreas Geophysical Observatory SAO), were 70 km east and 100 km north.

In 1965, the two northernmost telemetry stations (Calistoga and Point Reyes, shown as open circles in Figure 1) were closed and two additional stations were established, one (Pilarcitos Creek) on the San Francisco peninsula and the other (Jamestown) on the west flank of the Sierra Nevada. The Jamestown station proved to be of the greatest importance for the detection of small earthquakes and for the location of teleseisms by triangulation between array stations. The present configuration has apertures of 60 km east and 80 km north with respect to SAO.

Description and Criticism of the Recording System

The 14-kg Benioff short-period vertical-component seismometer has been used as the main detector. In 1966, 4.6 kg Willmore horizontal-component seismometers, oriented N 45° W, were installed at three stations (Granite Creek, San Andreas Geophysical Observatory and Paraiso). The stations at Berkeley, Mt Hamilton, San Andreas Geophysical Observatory and Jamestown, as well as the non-telemetry stations (shown as crosses in Figure 1), also have a variety of untelemetered seismographs.

From its inception, the array used the familiar photo-tube amplifier and frequency modulation system with the signals being carried over the commercial telephone lines. Carrier frequencies in the band 400 to 2 300 cps are used. The demodulated signals were recorded originally only on a 16-channel developocorder with 16 mm film and on helicorders. In June, 1965, array signals were also

recorded on a 14-channel one-inch FM-tape system at 0.06 inches per second. A playback unit capable of tape speeds up to 60 inches per second is used to transfer selected earthquakes signals in continuous analog form onto library tapes each fortnight.

Although the array was designed for the study of the mechanism of local earthquakes, we have become interested in array recordings of teleseisms and distant underground explosions. Therefore, magnification at most stations has been set at about 70,000 at one cycle per second. (The corresponding Jamestown magnification is 600,000.) This compromise leads to the normal system being overdriven by the larger near-earthquakes. To improve the recording range, several strong-motion channels are recorded in parallel with the unattenuated signal.

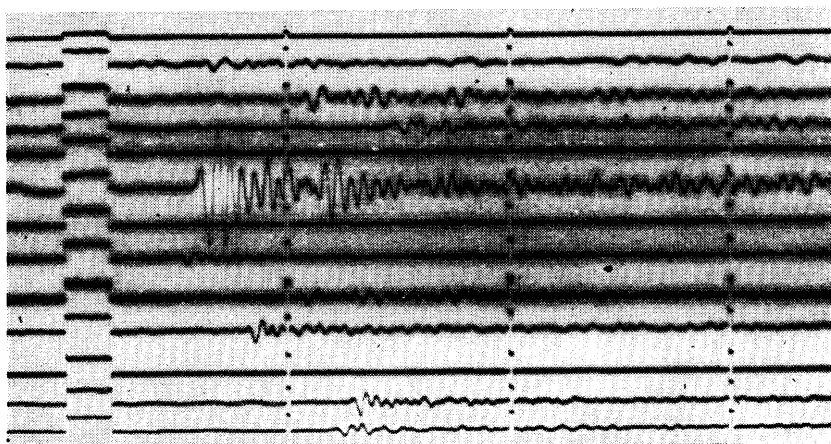


FIG. 2. — Seismic waves recorded on the developocorder of the Berkeley array from the Russian explosion near Semipalatinsk on December 18, 1966. Intervals between time marks are 10 sec. The traces from top to bottom correspond to signals from radio time, PCC, SAO, PRI, PRI (strong motion), JAS, CNC (dead), BRK, SAO (high frequency), MHC, GCC (dead), PRS, LLA.

As an example of teleseismic recording with the present settings, Figure 2 shows the onsets of waves from the explosion in Russia near Semipalatinsk on December 18, 1966 at $04^{\text{h}}57^{\text{m}}57.8^{\text{s}}$. In this case, the array gives, using the Jeffreys-Bullen tables, an epicentral distance from its center of 81° and an azimuth of $N 11^{\circ} W$. Adjustments for lateral refraction of the P waves under the array worked out by OTSUKA (1966a) have been applied. The distance and bearing of SAO from the USCGS epicenter are 92° and $N12^{\circ}W$, respectively. The Richter magnitude calculated at Berkeley is 5.6. It will be noticed that the first onsets are coherent and their polarities are all compressional.

The Jamestown (JAS) recording shows a curious feature which is reminiscent of the " local waves " recorded at the Eskdalemuir array, Scotland (Key, 1967). About 6 seconds after the onset of P, a second group of energetic waves arrives : (PCC and SAO show traces of coherent signals with similar delays). If the source were not a surface explosion, the second onset at JAS would be identified as pP giving a focal depth of 15-25 km. It is suggested that the later phase (" signal-generated noise ") comes from crustal modal vibrations near to the source, or perhaps as Key presumed, from a major nearby topographic irregularity.

After operation for five years, some conclusions on the instrumental side can be made. Initially, there were numerous technical difficulties involving both the telephone system and the recorders. For the last several years, equipment failure has prevented complete recording less than one-half hour per day on the average and each station requires technical service only about once a month. Although the rental of telephone channels requires a considerable budget, the annual operational cost of the 10 telemetry stations is quite comparable to the cost of the 10 conventional University of California stations. (It is also nice to have the telephone company engineers on one's staff !)

On the credit side, the great advantages of the telemetry system are the uniform recording, the continuous signal monitoring and the ease of calibration. With telemetry, only the Berkeley quartz clock is required for all ten network stations.

Several limitations of the original array have recently been partly removed. First, the array geometry is anything but omnidirectional; this leads, in some azimuths, to the lack of relative resolution in the determination of coordinates of teleseisms. Secondly, the limitations arising from the original purely photographic recording have been relaxed by the use of FM tape recording. The tape playback unit is linked to a frequency-filter system with audio and analogue output, and, when the need arises, to an analogue-to-digital converter or to a vectorial summation device. Severe phase shifts introduced by the filters are, however, sometimes difficult to estimate for arrival-time analysis. The third, and most restrictive, drawback is the lack of matched horizontal-component seismometers linked in the array. Further information of the detailed distribution of the focal depths of local earthquakes requires the correct selection of S phases. Similarly, S wave polarizations are needed for further elucidation of focal mechanism of local shocks. Horizontal-component seismographs at Berkeley (BRK), operating

with broad-frequency response on the magnetic-tape system, have recorded S waves which have been used to discriminate between alternative focal mechanism solutions in a local earthquake sequence (McEVILLY and CASADAY, 1967). Because S body waves from teleseisms have relatively little energy for periods less than 3-5 seconds, seismographs with free periods greater than that of the Benioff instrument are needed. The Willmore MK II, set at a free-period of 3 sec, has been found suitable as an array detector of S waves. Examples are given in the next section.

Slowness Anomalies of P and S from Teleseisms

We now consider some aspects of teleseismic observations. Let \mathcal{A} be the azimuth anomaly, defined as the observed azimuth of wave-approach minus the great circle azimuth. Let \mathcal{S} ($= dT/d\Delta$) be the slowness anomaly, defined as the difference between the observed slowness and the slowness calculated from the Jeffreys-Bullen tables (1958).

In a pioneering study, OTSUKA (1966a) showed, using the Berkeley array, that a systematic variation existed in \mathcal{A} and \mathcal{S} for P and pP waves from earthquakes at distances $30^\circ < \Delta < 96^\circ$. (Some intra-array distortion of the wave front was also detected.)

As illustrated in Figure 3, \mathcal{A} and \mathcal{S} are cyclic functions of the bearing to the epicenter. The amplitude of \mathcal{A} is of order 8° with the maximum occurring for waves from earthquakes in southerly and northerly directions, i.e. in South America, Kamchatka, and Alaska; on the other hand, waves from earthquakes in directions to the east and west of the Coast Ranges, such as in the Atlantic Ridge and Southwest Pacific, suffered little deflection in azimuth.

The explanation of the anomalies, favored by OTSUKA (1966 b), was in terms of a structural change in the upper mantle. One model which gave a fit to the observations of \mathcal{A} and \mathcal{S} had an interface beneath the Mohorovičić discontinuity with a strike parallel to the trend of the Coast Ranges and a steep dip of 30° to 40° towards the ocean. The structural model, shown in Figure 4, entails a reversal in P velocity with depth in the mantle and brings the lower velocity material closer to the crust under the Central Valley of California (If the anomalies were ascribed to a sloping Mohorovičić discontinuity alone, an improbably large dip of 15° is necessary (see Figure 3).

As a further step in the investigation of the crustal and upper mantle structure under the array, anomalies \mathcal{A} and \mathcal{S} , for S (and SKS) waves have been measured. In the first stage of the work,

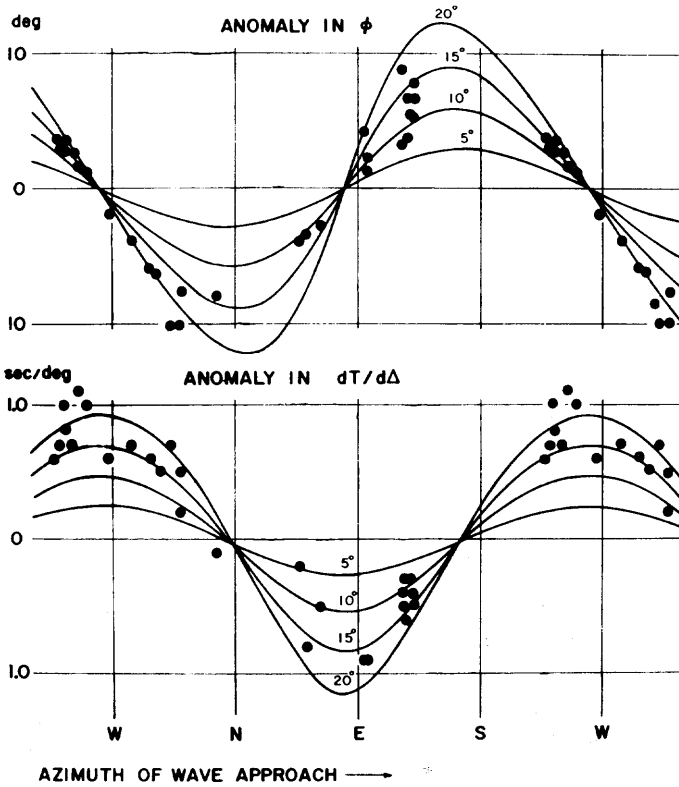


FIG. 3. — Plot against azimuth of measurements made by Otsuka of the azimuth anomaly ϕ and slowness anomaly \mathcal{J} for the original Berkeley network (Central Coast Ranges only). The curves represent theoretical anomalies for a model with a Mohorovičić discontinuity dipping at 5°, 10°, 15° and 20° towards the continent.

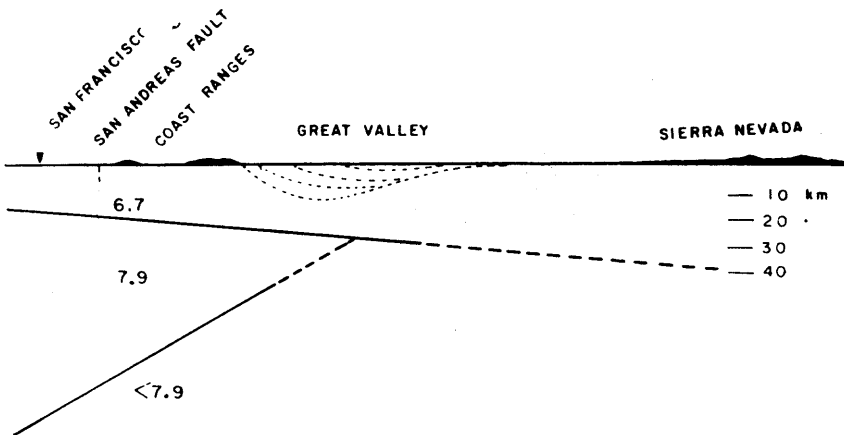


FIG. 4. — Diagram made by Otsuka of the structural model which he favored in explaining the observed anomalies ϕ and \mathcal{J} .

the measurements come from the three stations with horizontal component Willmore instruments, SAO, GCC and PRS. These stations form a tripartite net with base length 97 km and geometrical altitude (to SAO) 23 km. The use of identical recording systems at the three stations permits instrumental phase shifts to be ignored. Additional S recordings are available for comparison from the Berkeley horizontal-component seismographs with free periods of 30 sec; in one or two cases, the S waves were sufficiently energetic to show also on the telemetry developocorder traces from array stations with only Benioff vertical-component instruments.

Only eleven earthquakes, with $30^\circ < \Delta < 100^\circ$, from January to August, 1967, were found to provide adequate S wave-measurements for this first study; these are listed in Table 1. The locations are those given by the USCGS; the magnitudes (M_s) are those calculated at Berkeley.

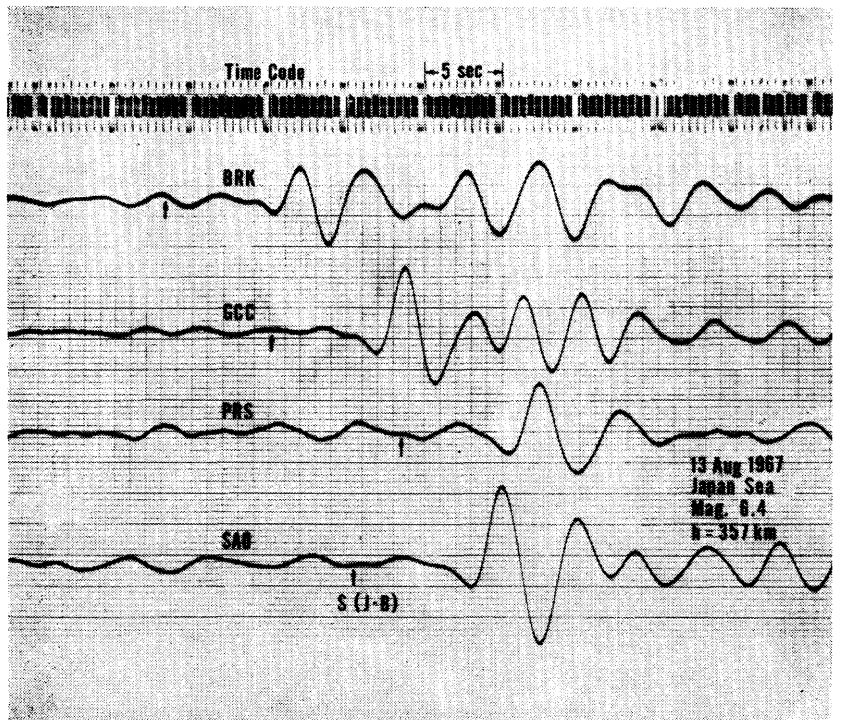


FIG. 5. — Seismic S waves recorded on the magnetic tape system of the Berkeley array from the Japan Sea earthquake of August 13, 1967.

In Figure 5, the quality of the observational material is illustrated by a parallel play-out from the magnetic tapes of the S-wave trains

from the Japan Sea earthquake of August 13, 1967 which is 79° from SAO and has magnitude 6.4. Frequencies above 0.25 cps have been attenuated by low-pass Krohn-Hite filters for each signal. Only the form of the first cycle of S is repeated at each network element; the time interval between the first coherent large peaks can be read to 1/10 sec. The residual against the Jeffreys-Bullen tables for the S onset at SAO, on the adopted epicentral solution, is 5.5 sec; the corresponding P residual at SAO is 2.0 sec (see Table 2).

We do not observe that the degree of coherence in the S wave train at array stations varies strongly between earthquakes from different regions. Indeed, seldom does the S wave coherence between two of the stations BRK, SAO, PCC and PRS continue for more than one to two cycles. The clearest S trains were from the deep-focus earthquakes; signals were particularly clear from the shocks numbered 6, 10, and 11 in Table 1. Our analysis of the 11 earthquakes would support the conclusions of earlier workers that there is a distinct difference between the character of recorded S waves from shallow focus and deep focus earthquakes. Certainly, in the latter case, the signal-to-noise ratio, the sharpness of onset, and marginally, the coherence of the S trains, appears enhanced even for shocks of about the same magnitude. On this point, we were able to detect coherent S signals from the deep-focus earthquake in Argentina ($N^\circ 1$) even though the magnitude was less than 5; unfortunately, this shock is at a distance just beyond the intersection of the S and SKS curves so that we place little reliance on the measured A_s and B_s .

The predominant periods of the coherent S waves between 4 and 7 sec at all four stations. The use of the Willmore instruments ($T_0 = 3$ sec) strongly attenuates waves with periods exceeding 3-4 sec so that significantly longer periods in the recorded waves at SAO, PCC and PRS cannot be expected. However, the BRK recordings, from a system which does not begin attenuation until periods exceed 30 sec, demonstrate that little wave-energy is present above 6 sec, at least for earthquakes with magnitude near 6.5. The observed lack of coherence in S waves with wavelengths of order 20 km between stations of the order of 100 km apart, presumably entails structural differences in the crust under the stations.

There was a striking variation in the form of the early part of the S train between earthquakes; even with array intra-correlation it was often extremely difficult to judge where the S waves first began. Table 2 gives the residuals against the Jeffreys-Bullen

(1958) tables for S (corrected for ellipticity). Most residuals exceed + 3 sec although we always picked the onset *before* the first *clear* coherent peak or trough. For shocks numbered 3, 4, 5 and 8 (all shallow) the residuals are extremely large but we could detect no motion (above the noise) earlier on the records.

BYERLY (1942) drew attention to a smaller movement, which he called *the curtsey*, preceding the main movement of S. In our work we also often found a perceptible downward excursion (ground motion towards the northeast lasting 3-4 sec before the first large excursion of the pendulum (see e. g., the SAO signal in Figure 5). This movement resembles a curtsey but it is of interest that, when the signal to noise ratio is particularly high, additional low-amplitude motion can be detected in the curtsey. For example, with shock 6, the SAO record shows a curtsey but this precursor to the large movements contains a small coherent peak on the BRK, PRS and GCC records.

The measured anomalies, representing empirical functions \mathcal{A}_s and \mathcal{S}_s are shown in Figure 6 for the tripartite network. The anomaly values for the eleven earthquakes used are listed in Table 1. (The error range in the individual estimates of \mathcal{A}_s , from the uncertainty in times, is of order ± 2 degrees.) Of the plotted points, only those from shocks numbered 2, 3, 6, 7, 9, 10, 11 can be considered a uniform set. The measured signal from shock 1 is probably S but may contain SKS components; the first perceptible coherent waves in shock 5 arrive 23 sec after time predicted by the Jeffreys-Bullen tables and may be PS. The waves from shock 8 are undoubtedly SKS.

The reliable points form two groups. The azimuth anomalies for shocks 3, 7 and 11 (N 45° W) are consistent and those for shocks 4, 6, and 9 (E 20° S) agree. The first group shows that azimuth anomalies in S of order 20° can occur as can slowness anomalies of 1 sec/deg.

The curve on Figure 6 represents the curve drawn by OTSUKA for the crustal model with the dipping Mohorovičić discontinuity which gave the best fit to the observed P anomalies. Both P and S wavefronts propagating from northerly foci (Aleutians, Kuriles, Japan, etc.), parallel to the coast of central California, are bent towards the continent. In contrast, although P waves from South American earthquakes (Colombia, Bolivia, etc.) are also deflected towards the continent, the provisional results for S waves (based upon three earthquakes) indicate that S waves are deflected in the opposite sense (at least for the coherent portion of the train

which was measured). The physical condition of the upper mantle under California is evidently such that the portions of the P and S

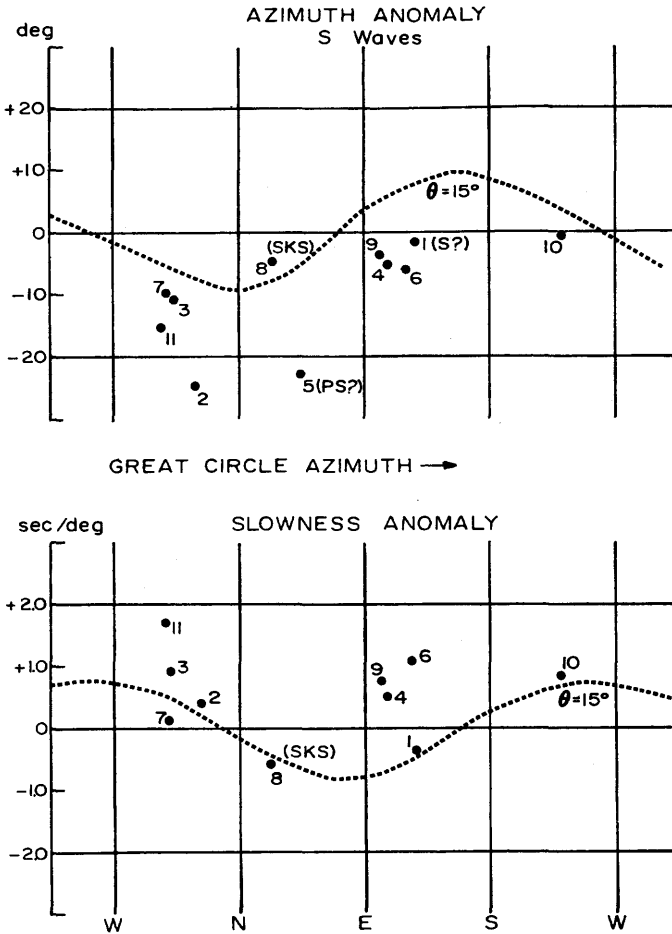


FIG. 6. — Measured anomalies, plotted against azimuth, for S and SKS waves across the triangle SAO, GCC, PRS.

waves which carry the principal energy do not always travel the same ray path.

IBRAHIM and NUTTLI (1967) have recently constructed an average S travel-time table for $3^\circ < \Delta < 65^\circ$ for stations in the United States. For $\Delta > 40^\circ$, their times, based on recordings of long-period waves, are greater than in the Jeffreys-Bullen tables; the differences increase monotonically from 1 sec at $\Delta = 40^\circ$ to 7 sec at $\Delta = 65^\circ$. IBRAHIM and NUTTLI took no account of possible azimuthal variations.

For $\Delta > 30^\circ$, little other recent work has been published on S travel-time tables besides that of KOGAN (1960) and JEFFREYS (1962, 1966). It is noteworthy, in agreement with the conclusions of KOGAN and IBRAHIM and NUTTLI, that for the eleven earthquakes studied here, the readings of S onsets using the array, all gave positive residuals against the Jeffreys-Bullen tables. (Instrumental phase delays are not likely to exceed 1-2 sec at 3 sec period.) Further, the sign of the residual was an invariant of azimuth as exemplified by the most reliable values from shocks 6, 11 and 10. Because the estimates of the slowness anomaly \mathcal{S}_s scatter more than the estimates of \mathcal{A}_s , we are unable at the present to draw any inferences about possible deviations in the $dT/d\Delta$ given by the first differences in the Jeffreys-Bullen tables.

Fault Plane Solutions of Local Earthquakes

The seismonet has greatly increased the effectiveness of studies of local earthquakes. Within the network, virtually all earthquakes in the Coast Ranges with magnitudes greater than 2.5 are now located at the Berkeley Seismographic Station; many smaller magnitude earthquakes are detected but the positions are not determined unless of special interest. Detailed seismicity maps have recently been prepared for central California and the Mendocino Escarpment region for the years 1962, 1963, 1964 and for the first six months of 1965 (BOLT, LOMNITZ and McEVILLY, 1968).

One purpose of the intensive study of local earthquakes is to extend knowledge of earthquake genesis and regional tectonics. To this end, fault-plane solutions have been worked for a considerable number of earthquakes which occurred both singly and in earthquake sequences. Shocks with magnitudes from 5.5 down to about 2.0 have been so studied. The work depends crucially upon the timing accuracy and uniformity of recording of the telemetry network. Even outside the Coast Ranges, the array has proved of importance for first-motion studies. For example, many earthquakes along the Mendocino Escarpment and northwards have a P nodal line which intersects the array so that array measurements constrain this vector closely (e.g. RINEHART, 1964).

As a necessary prerequisite to fault-plane analysis of local shocks, the array measurements have also provided greater precision in hypocentral *location* partly through time control to 1/20 sec and partly through more adequate azimuthal coverage of stations. It has been found (UDIAS, 1965; LOMNITZ and BOLT, 1967) that the

consistency of the polarities of first motions of P is sensitive to the value of the focal depth. This remains the single most difficult focal parameter to measure. One way to improve the precision of depth estimates is to move mobile stations into the epicentral region of the genetic shock. The focal depth of aftershocks can then be determined within a few kilometers using S and P phases recorded by these near stations. On the assumption that the aftershocks occur in the same focal zone, the depth of earlier earthquakes can then be taken as known. Indeed, the array sometimes replaces the assumption by direct evidence. Figure 7 shows the superposition of two film-recordings of separate aftershocks (magnitude $2 \frac{1}{4}$, 18 hours apart) of a sequence which occurred in 1964 near Corralitos which is interior to the array (McEVILLY, 1966). It is clear that the P onset has arrived at identical times at all stations of the array. The conclusion is that the energy in the two earthquakes was released from essentially the same portion of rock at the same focal depth (~ 10 km) in the Earth's crust.

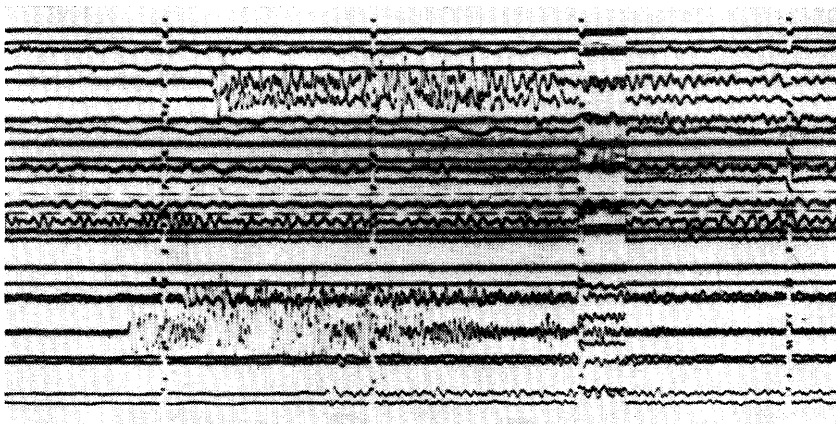


FIG. 7. — Two separate film recordings of waves at array stations from two earthquake aftershocks. The developocorder films have been superimposed so as to align the P arrivals at VIT (fifth and sixth traces from top). Note how closely P onsets at other stations coincide, e.g. the bottom two traces from LLA. The interval between time marks is ten seconds.

Two conclusions can now be drawn with some definiteness from the fault plane work in the Coast Ranges. First, the pattern of compressions and dilatations of P remains constant, with possibly a very few exceptions, throughout an earthquake sequence: the main radiation pattern for the aftershocks is that of the main shock. This rule has now been verified unequivocally using the

array for over six sequences (UDIAS, 1965; McEVILLY, 1966; McEVILLY and CASADAY, 1967; McEVILLY, BAKUN and CASADAY, 1967; BOLT, LOMNITZ and McEVILLY, 1968). Secondly, fault plane diagrams for earthquakes in the Coast Ranges consistently show predominantly righthand strike-slip motion with one plane oriented within a few degrees of the trend of the adjacent main fault trace. The agreement is so close that even *variations* in the strikes of the San Andreas, Hayward or Calaveras faults are reflected in similar variations in the calculated strikes of the fault planes of small shocks on these faults.

As an illustration of the use of the array in fault plane studies of small intra-array shocks, consider the P radiation pattern for a small earthquake of 1966, April 29. The shock, of Richter magnitude 3.8, occurred at 08^h 09^m 27.2 GMT in Bear Valley in the California Coast Ranges. The coordinates of the focus are estimated from P and S times to the array stations as 36° 36' N, 121° 15' W with a focal depth of 2 km. This epicentral position is, formally, 4 km west of the San Andreas fault trace.

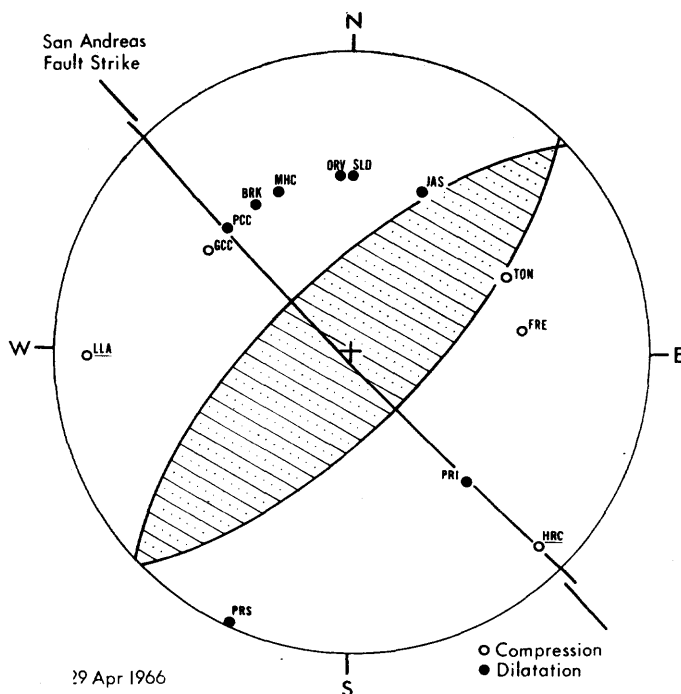


FIG. 8. — P wave polarity diagram for the earthquake of April 29, 1966 in Bear Valley, California. Points on the lower focal hemisphere are projected using an equal area net. The observations would permit the auxiliary nodal line to lie anywhere in the hatched region.

Figure 8 is the projection of the lower hemisphere corresponding to down-going rays at the focus; assuming focal symmetry, the points corresponding to the near stations HRC ($\Delta = 23.5$ km; this station was a temporary one during transition from VIT to SAO) and LLA ($\Delta = 27.6$ km) are projected through the pole from the upper hemisphere. Of the thirteen points shown, only Fresno (FRE), Tonopah (TON), San Luis Dam (SLD) and Oroville (ORV) are not telemetered to Berkeley. The polarities at the array stations define a simple quadrantal pattern, with no exceptions. The developeorder film, for example, clearly shows a dilatation at MHC and a compression at GCC; these stations are on opposite sides of the San Andreas fault and the line between them is about bisected by the extension of the strike of the San Andreas fault at Bear Valley. One focal plane is defined rather precisely by the reversal in polarities at GCC-PCC and at PRI-HRC; this plane is essentially vertical and has a strike ($N47^\circ W$) which is indistinguishable from that of the main fault trace in the region. The auxiliary plane is not closely bounded but the difference in polarity between JAS and FRE is unquestionable. The solution can be interpreted as arising from right-handed transcurrent motion along a predominately vertical fault. The available readings for this shock do not preclude a slight westward dip to the fault, however, and the presence of a minor dip-slip component. The dip-slip could range from normal faulting with the west side down to reverse faulting with the hanging wall on the west.

The most straight-forward explanation of these first motion patterns is right-lateral strain along the San Andreas fault system.

ACKNOWLEDGMENTS

Mr. J. ZANETTI has helped greatly with the data processing. This research was supported by the U.S. Air Force Office of Scientific Research.

TABLE 1
EARTHQUAKES USED IN THE S WAVE ANALYSIS

Date N° (1967)	Region	Lat.	Long.	Mag.	t_0	FD	Δ (SAO)	Az(SAO)	Az res	$dT/d\Delta$ res
					h m s	(km)	(deg)	(deg)	(deg)	(sec)/(deg)
1 Jan. 17	Argentina	27.4S	63.3W	4.8	01-07-54.3	590	84.03	130.6	— 1.5	—0.4
2 Jan. 18	East USSR	56.6N	120.8E	6.5	05-34-32.6	shallow	73.16	329.2	—25.4	+0.4
3 Jan. 28	Aleutians	52.4N	169.5W	6.5	13-52-58.3	47	36.88	310.6	—10.4	+0.9
4 Feb. 9	Colombia	2.9N	74.9W	7.4	15-24-47.2	58	54.44	116.9	— 5.5	+0.5
5 Feb. 13	North Atlantic	52.7N	34.1W	6.7	23-14-19.6	shallow	60.30	44.4	—23.2	—5.4
6 Feb. 15	Bolivia	9.0S	71.3W	7.3	16-11-11.8	597	65.43	123.5	— 5.2	+1.1
7 Mar. 19	Kuriles	45.4N	151.3E	6.0	04-01-36.7	33	63.26	308.0	— 9.3	+0.1
8 July 22	Turkey	40.6N	30.7E	7.2	16-56-53.3	shallow	98.84	21.0	— 4.3	—0.6 (SKS)
9 July 29	Colombia	6.8N	72.9W	6.2	10-24-24.3	158	53.20	111.8	— 4.3	+0.8
10 Aug. 12	Tasman Sea	24.8S	177.6W	6.2	09-39-39	96	80.91	229.9	— 0.9	+0.9
11 Aug. 13	Japan	35.3N	135.7E	6.4	20-06-50	357	78.66	305.6	—15.8	+1.7

TABLE 2

P AND S TRAVEL-TIMES AND RESIDUALS AT SAO

N°	Date (1967)	SAO P		O-C	SAO S		O-C
		Travel-time			Travel-time		
		m	s		m	s	
1	Jan. 17	11	30.8	1.2	21	9.1	3.7
2	Jan. 18	11	32.8	1.8	21	7.2	5.7
3	Jan. 28	7	07.4	2.4	12	55.3	8.9
4	Feb. 9	9	23.8	0.6	17	05.6	9.5
5	Feb. 13	10	09.9	—2.8	18	49.5	23.7
6	Feb. 15	9	46.0	—0.4	17	46.2	0.7
7	Mar. 19	10	29.0	1.1	19	00.1	4.6
8	July 22	13	44.7	1.8	24	28.7	8.0*
9	July 29	9	03.2	—0.5	16	23.9	3.2
10	Aug. 12	12	05.8	0.9	22	06.6	2.4
11	Aug. 13	11	26.8	2.0	20	56.5	5.5

*SKS

REFERENCES

- BOLT (B. A.) 1965, " Gradients of travel-time curves from deep-focus earthquakes ", *Reviews of Geophysics*, 3, 83-98.
- BOLT (B. A.), LOMNITZ (C.) and McEVILLY (T. V.) 1968, " Seismological evidence on the tectonics of central and northern California and the Mendocino Escarpment ", *Bull. Seism. Soc. Am.* (in the press).
- BOLT (B. A.) and NUTTLI (O.) 1966, " P wave residuals as a function of azimuth. 1. Observations ", *J. Geophys. Res.*, 71, 5977-5985.
- IBRAHIM (A. K.) and NUTTLI (O. W.) 1967, " Travel-time curves and upper mantle structure from long period S waves ", *Bull. Seism. Soc. Am.* (in the press).
- JEFFREYS (H.) 1962, " Travel-times for Pacific explosions ", *Geophys. J. R.A.S.*, 7, 212-219.
- JEFFREYS (H.) 1966, " Revision of travel-times ", *Geophys. J. R.A.S.*, 11, 5-12.
- JEFFREYS (H.) and BULLEN (K. E.) 1958, *Seismological Tables*, Brit. Assoc. Adv. Sci., Grey-Milne Trust.
- KEY (F. A.) 1967, " Signal-generated noise recorded at the Eskdalemuir seismometer array station ", *Bull. Seism. Soc. Am.*, 57, 27-38.
- KOGAN (S. D.) 1960, " Travel-times of longitudinal and transverse waves determined from data nuclear explosions, detonated in the Marshall Islands region ", *Bull. Acad. Sci., U.S.S.R., Geophys. Series*, n° 3.
- LOMNITZ (C.) and BOLT (B. A.) 1967, " Evidence on crustal structure in California from the Chase V explosion and the Chico earthquake of May 24, 1966 ", *Bull. Seism. Soc. Am.*, 57, 1093-1114.
- McEVILLY (T. V.) 1966, " The earthquake sequence of November 1964 near Corralitos, California ", *Bull. Seism. Soc. Am.*, 56, 753-773.
- McEVILLY (T. V.) and CASADAY (K. B.) 1967, " The earthquake sequence of September, 1965 near Antioch, California ", *Bull. Seism. Soc. Am.*, 57, 113-124.

- OTSUKA (M.) 1966 a, " Azimuth and slowness anomalies of seismic waves measured on the central California seismographic array. Part I. Observations ", *Bull. Seism. Soc. Am.*, 56, 223-239.
- OTSUKA (M.) 1966 b, " Azimuth and slowness anomalies of seismic waves measured on the central California seismographic array. Part II. Interpretation ", *Bull. Seism. Soc. Am.*, 56, 665-675.
- RINEHART (V. J.) 1964, " Investigation of twelve earthquakes of the Oregon and northern California coasts ", M. S. Thesis, Oregon State University.
- UDIAS (A.) 1965, " A study of the aftershocks and focal mechanism of the Salinas-Watsonville earthquakes of August 31 and September 14, 1963 ", *Bull. Seism. Soc. Am.*, 55, 85-106.

THE USE OF ARRAYS FOR THE INVESTIGATION IN MICROSEISMS

by L. P. VINNIK

Seismometer arrays were used for recording microseisms from the beginning of the century. However, the modern methods of data analysis were introduced in this field only a few years ago. Such methods were described in a few papers published recently in the USSR, USA, and UK. Since 1961 arrays are employed in the study of microseisms at the Institute of the Earth Physics, Moscow. Some records obtained during IGY in 1957-1958 are newly processed by means of the same technique. In our analysis microseisms are treated as random homogeneous field. If it were possible to use sufficiently large and dense seismograph grids for the analysis, it would be not more complicated than the common spectral analysis; but the seismometer arrays actually available often are not good for the purpose and the problem should be solved otherwise.

The detection of comparatively intensive waves may be performed by means of a technique based on the summing of the records of homonymous displacement components with time shifts linearly depending on seismometer cartesian coordinates on plane. Actually mean squares are determined for each array tuning instead of instantaneous values. This method is equivalent to one of the correlation analysis methods. Mean square of the array output can be represented as the sum of a constant term and the variable one depending on array tuning. The variable term can be derived from the cross — correlation functions and represented as the function of horizontal propagation velocities V and propagation azimuths α of the waves to which array is tuned. The variable which is referred to as $Q(V, \alpha)$ is set on a correlation diagram. The diagram construction allows to map (V, α) — plane onto the plane of wave numbers. This way of diagram drawing makes its interpretation easier. It is supposed that the field consists of waves and of irregular component the spectral density of which does not depend on wave numbers; horizontal propagation velocities, propagation azimuths, intensities of waves and intensity of the irregular component should be evaluated. The main difficulties encountered in the interpretation of the correlation diagram are due to the side-pass areas of the array directivity diagram. The case of one wave and of irregular component is the simplest one. The necessary manifestation of this case is the similarity of relieves of the correla-

tion diagram and of the directivity diagram. In order to analyze more complicated cases, the comparison of the diagrams is also necessary.

Tuning of the arrays of horizontal seismometers to the wave with a certain azimuth of propagation can be accompanied by the rotation of seismometer axes at the same direction or perpendicular one, and correlation diagrams which facilitate the separation of SV and SH modes can be made up. In order to separate the elliptically and linearly polarized waves, correlation function of the vertical and radial displacement components at the array output can be computed.

The technique described above is illustrated by the correlation diagrams obtained from the records of the array which operated in E. Kazakhstan (4-6-second microseisms). Seismometers were located as shown on the diagram in figure 1. In figure 2 the corre-

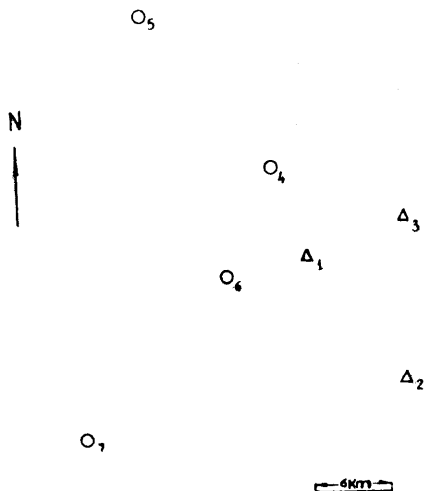


FIG. 1

lation diagram of the vertical component of the seismogram recorded in October 1961 is shown. There is only one wave in this case, its horizontal propagation velocity being of about 20 km/sec. More complicated case of 3 waves is shown in figure 3. One of the detected waves is P-wave with horizontal propagation velocity of about 10 km/sec; the wave with $V \approx 3.5$ km/sec is the fundamental Rayleigh mode; the wave with $V \approx 4$ km/sec is one of the higher Rayleigh modes.

The technique described delivers little information on the weakest waves included in the irregular component although, according to our data, it holds more than a half of full process energy. Therefore

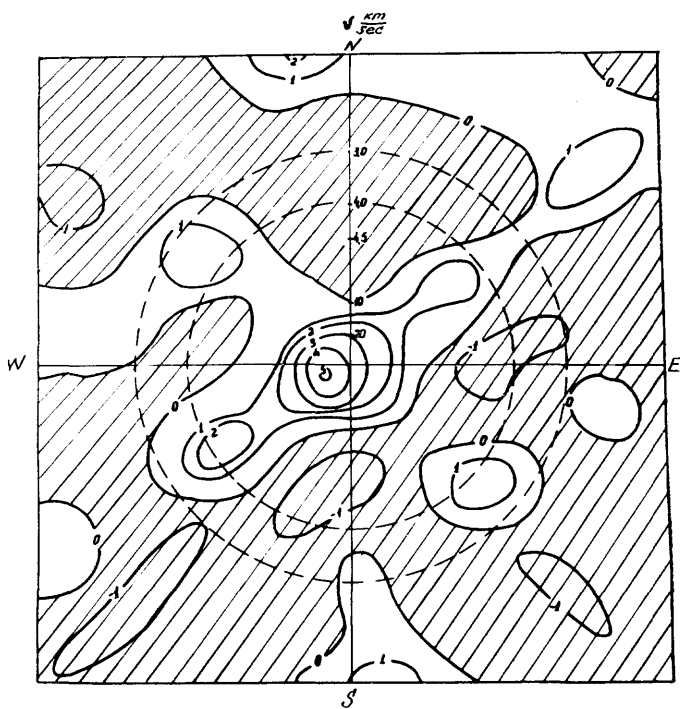


FIG. 2

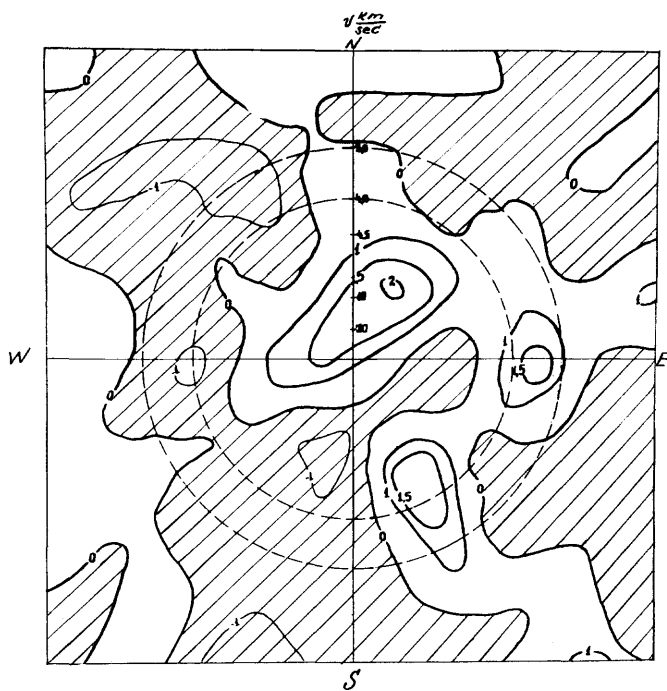


FIG. 3

these methods are complemented by the integral method of analysis. The principle of the integral method can be described as follows. Nearly all of the seismograph grids used in our observations include isosceles rectangular triangles. For each of such triangles 3 cross-spectral estimates were computed. Their real parts were divided by spectral density and the average of 3 normalized estimates referred to as K was computed. The observational values of K are compared with the values computed for a certain model simulated on a high speed computer. The simulated field consists of many weak waves and of 2 comparatively strong ones. All the waves have equal velocities and similar spectrum shapes; their azimuths of propagation are random numbers distributed evenly between 0 and 2π . The standard corridor is constructed in which the value of K obtained from the modelling fall with nearly 90 % probability. The standard corridor of K and the curve of

$$K_0(\zeta) = \frac{2J_0(2\pi\zeta) + J_0(2\sqrt{2}\pi\zeta)}{3}$$

are drawn in the figure 4, J_0 is the *Bessel function* of the first kind of zero order, $\zeta = f\Delta/v$, f — frequency in cps, Δ — triangle cathetus length. In order to analyze the observational data, one may either fix Δ and V and compare standard and observational curves of $K(f)$ or fix V and f and compare curves of $K(\Delta)$. If the values of K obtained from the observations do not fall into the corridor, it is considered the manifestation of the velocity difference between the observed field and the model.

Observational curves of $K(f)$ for one of the triangles are shown in figure 5, for the standard corridor phase velocity of the fundamental Rayleigh mode is taken. The figure shows that the curves lie above the corridor; it indicates the presence of waves with horizontal propagation velocity considerably higher than that taken for the corridor. If one assumes that the field consists of Rayleigh waves and of waves with much higher velocity (20-40 km/sec.), the coherence loss of high-velocity component for the frequency where the coherence of Rayleigh waves diminishes to 0 is negligibly small; the value of K for this frequency may be considered the evaluation of the energy portion of high-velocity component. In the case concerned, this portion is approximately 0,6 of 60 % of full process energy for 1 cps.

Here is the review of the basic conclusions drawn from our data. It is found out the constant presence of P waves in 4-6-second microseisms observed in Middle Asia and Kazakhstan. Their hori-

zonal propagation velocity is 10-20 km/sec, and energy portion lies between 10 % and 40 % of full process energy. Surface waves

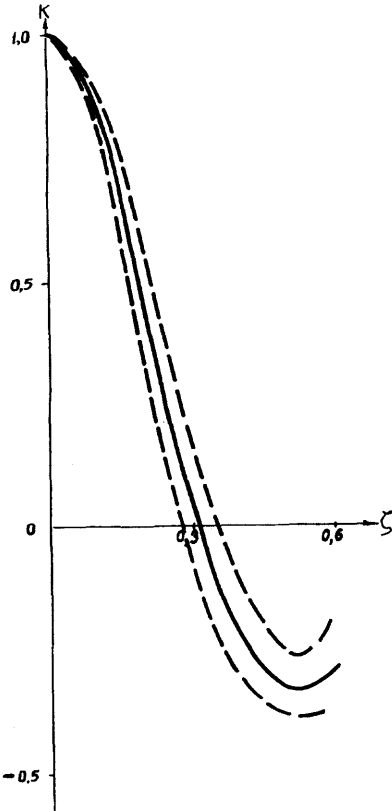


FIG. 4.

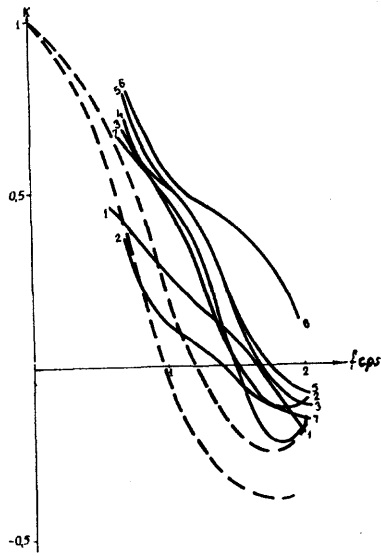


FIG. 5.

sometimes detected in the vertical displacement component are less intensive. They are represented by the fundamental Rayleigh mode and by the higher Rayleigh modes. In the horizontal displacement component Love waves prevail. The total energy portion of all detected waves is, as a rule, less than 50 % of full process energy; irregular component holds the rest. There are significant, of the order of dozens of degrees, differences between the propagation azimuths of different waves in the same seismogram. We believe that P waves in 4-6-second microseisms are mostly ocean-generated. They were not detected by the arrays located in the noisy regions of the USSR. Apparently the prevalence of P waves in the middle of a continent is caused mainly by the surface wave attenuation. It is found out also that the relative intensity of the fundamental

Rayleigh mode and of higher modes is different in quiet and in "stormy" microseisms. In "stormy" microseisms the fundamental mode is considerably more intensive.

When analyzing high frequency microseisms in the quiet region of the USSR (Kazakhstan, Middle Asia) the following conclusion is drawn. In the vicinity of 1 cps waves with horizontal propagation velocity much higher of the Rayleigh wave velocity often prevail. The energy portion of the high velocity component may be close to 60 % or more in 0,5-2 cps frequency band. There are waves with horizontal propagation velocity of about 20 km/sec or more in the high velocity component. In the frequency band 0,5-2 cps either the energy portion of the high velocity component decreases as frequency rises, or prevailing velocity decreases, or both phenomena take place. We believe these waves to be, at least partly, the high frequency components of the P waves detected in 4-6-second microseisms.

For the further study of the nature of microseisms the use of arrays operating simultaneously at a number of locations is highly desirable.

TRAVEL-TIMES OF P IN JAPAN IN THE DISTANCE RANGE OF 0 - 15°

by ZIRO SUZUKI
Geophysical Institute, Tohoku University, Sendai, Japan

INTRODUCTION

Accurate determination of hypocenter has become more and more important to solve many interesting problems in modern seismology, and the exact knowledges of source parameters, of course, should be obtained by means of an adequate standard travel time table. In Japan, the so-called Wadati-Masuda's table has been used as a standard in the routine work of Japan Meteorological Agency (JMA) for a long time. However, recent observations of artificial explosions revealed that the Wadati-Masuda's time for surface origin is far later than the explosion data, at least in the distance range shorter than 400 km. It was also found that this table sometimes has a systematic deviation even from the observation of natural earthquakes. Although some other tables were proposed in 1930-40s, all these Japanese tables have a similar defect to the Wadati-Masuda's.

Under this situation, efforts to revise the standard table is now being made by several authors, and the purpose of the present paper is to review the recent Japanese works on this problem. P times up to 1500 km are exclusively treated in this paper, although some authors discussed S times and the amplitude decay as well.

In general, the recent Japanese studies on travel time curve may be classified into two categories : those based on the observation of natural earthquakes and those based on the explosion data. These two kinds of studies should join at the end, but the combination of the two is not yet completed at the moment. It is convenient, therefore, for the present writer to review these two kinds of approaches separately.

I would like to mention here that the recent development of high speed computer makes these studies possible.

Part I. — Approach from natural earthquake data.

1. Introduction

First we will begin with the studies based on the observation of natural earthquakes. The studies in this direction is essentially to find a travel time curve which fits best to the observed times. An elaborate work was done by the members of Research Group

for Travel Time Curve (RGTTTC), Earthquake Research Institute, Tokyo University, especially by T. USAMI and R. YAMAGUCHI. [1] Data used by them were taken from the report of JMA during 1954-64 when the observation by the JMA network was thought to be most reliable and homogeneous. 46 earthquakes shallower than 80 km were picked up according to the criterion that good readings were available beyond 1 350 km.

2. Various tests

Before computing the final result, they have made exhaustive tests on various points such as what mathematical formula is appropriate to represent the curve, what criterion should be set in the selection of data, how many times of iteration is necessary in the computation to obtain a sufficient convergency and so on. But I have to skip out these tests because of the shortage of time.

3. Computation of standard travel time curve

After these minute tests the authors computed the standard curves for the depths of 0, 20, 40, 60 and 80 km. The distance up to 1 500 km is separated into two ranges of 0-170 km and 150-1 500 km and somewhat different procedures are adopted for the two ranges, mainly because not so many data for shorter distance range are available under the same criterion as that for longer range.

For the range of 150-1 500 km, the procedure is as follows :

- 1) The cubic formula without a quadratic term is adopted.
- 2) A preliminary curve for each individual shock is calculated based on the source parameters determined by JMA.
- 3) Several curves having a similar feature are averaged.
- 4) Source parameters of each shock are revised using thus averaged curve.
- 5) The curve for individual shock is re-determined by means of the new parameters.
- 6) These curves are averaged.

For the range of 0-170 km :

- 1) A cubic formula with a quadratic term is adopted, except for the depth of 80 km.
- 2) Several local shocks are added to the data.
- 3) The source parameters are determined based on the data beyond 150 km and on the standard curve obtained in the above stage.

4) The curve for the distance less than 170 km is then calculated.

An example of thus obtained curves for short range is seen in Fig. 1.

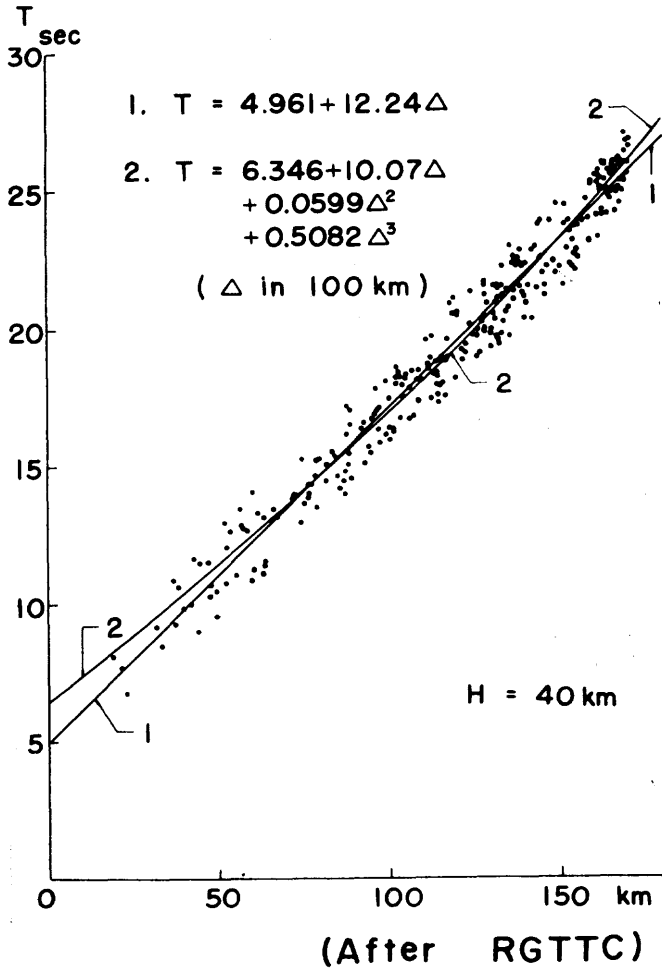


FIG. 1

Connecting the curves for two ranges, the first approximation of the standard travel time curve is constructed. The authors call this curve α -approximation.

The discrepancy between this α -approximation and the observed values is thought to be the sum of station correction, term due to erroneous location of epicenter and also error of the α -approxima-

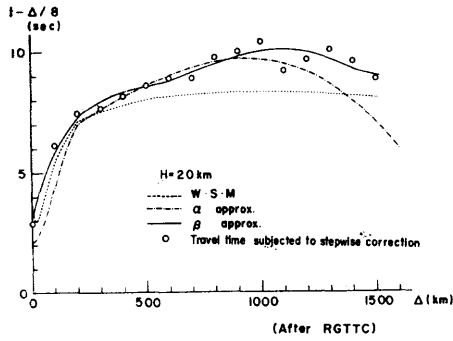


FIG. 2

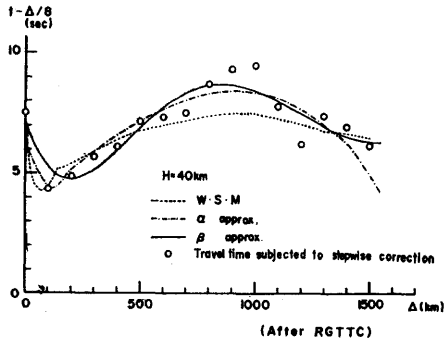


FIG. 3

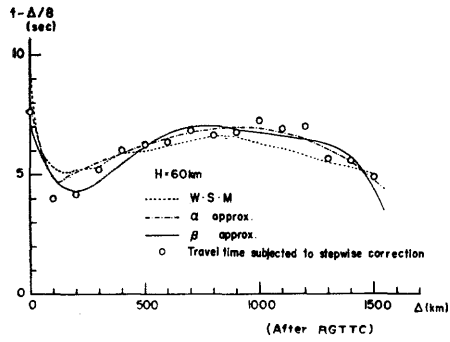


FIG. 4

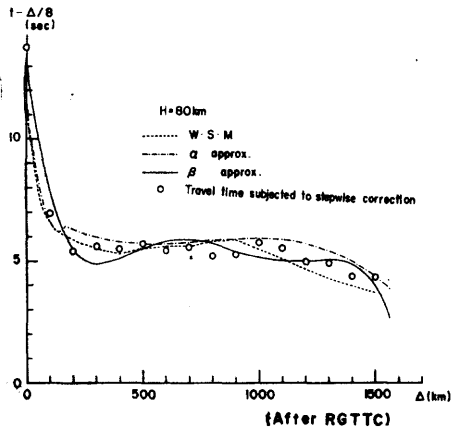


FIG. 5

tion itself. These errors, therefore, are simultaneously calculated by the method of least squares and the final curve, that is the β -approximation, is obtained. The results are shown in Fig. 2, 3, 4 and 5. Fig. 2 shows the α - and β -approximation curves for the depth of 20 km. Fig. 3 is the similar figure for $H = 40$ km. Figs. 4 and 5 are those for $H = 60$ and 80 km respectively.

The difference between the β -approximation curve and the Wadati-Masuda's is synthetically seen in the next figure. (Fig. 6.)

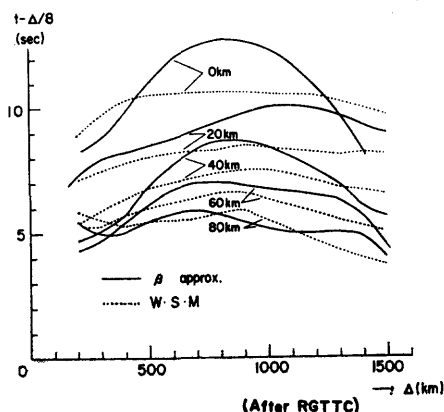


FIG. 6

The maximum difference for the depths deeper than 40 km is less than 2 seconds but it reaches more than 2 seconds for shallower depth around the distance of 800-1100 km.

The curve for the surface origin, however, is not compatible with the explosion data even after these tedious adjustments, as will be seen in Fig. 7. This figure shows that even the solution for natural earthquakes (chain line) and α -approximation (dotted line) are systematically later than the observation of explosions by the Research Group for Explosion Seismology (RGES) by about 2 seconds. To avoid this defect they tentatively adopted the compromise that the times of α -approximation for the distance larger than 170 km are reduced by 0.9 seconds and are connected with the least square solution of explosion data for shorter distance.

It is the present writer's opinion that the discrepancy between natural and artificial earthquake data may be due to the inaccurate estimation of depth of hypocenter and origin time for natural earthquakes. Although the members of RGTTC made an elaborate examination of horizontal location of epicenter, they adopted the

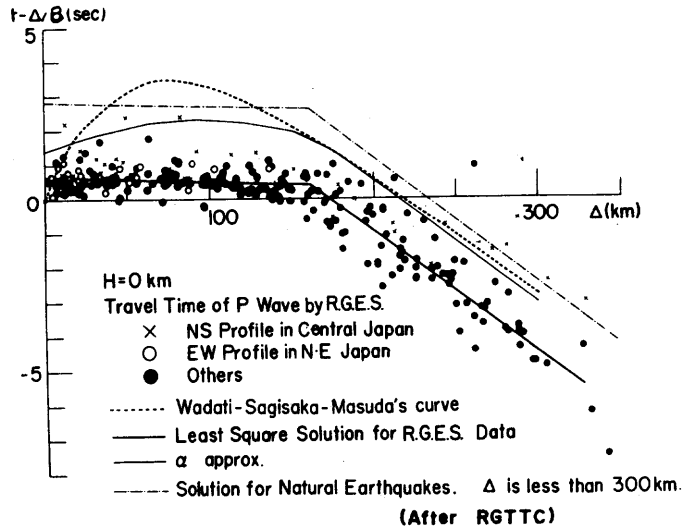


FIG. 7

depth determined by JMA so as to fit the Wadati-Masuda's time table. Since the W-M time has a systematic delay for surface origin those for deeper depth may have a similar defect and the depth estimated from the times may be erroneous. The members of RGTTC are now trying to examine the consistency of their curves for various depths through the velocity distribution in order to correct their results.

5. On station correction

I would like to make a brief comment here about the station corrections of the Japanese stations. Since the standard travel time curve is obtained, we can discuss the time terms of stations and their dependency on the location of hypocenter, irrespective of the remained problem on the estimation of depth of hypocenter. The studies of the kind were carried out by S. ICHIKAWA [2] of JMA and the members of RGTTC. ICHIKAWA used the Wadati-Masuda's table as a standard and discussed the residual times from it. The residuals depend on epicentral distance and the locations of both hypocenter and station. The relation between epicentral distance and the variance of observed times from the standard curve is seen in Fig. 8. This figure indicates that the variance is approximately 2 sec^2 at the distance less than 200 km and it

increases with distance up to about 6 sec^2 around the distance of 1500 km.

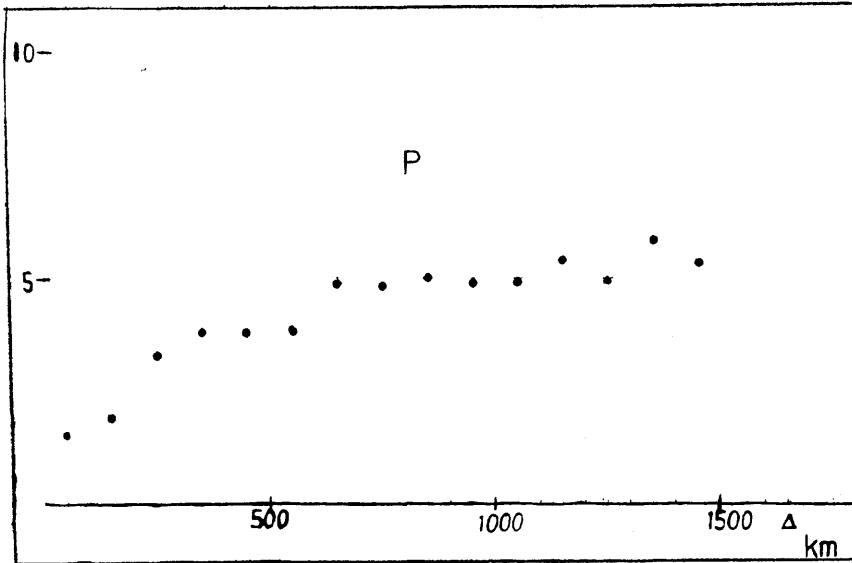


FIG. 8. — Variances of P travel times observations as a function of epicentral distance. (After Ichikawa.)

Fig. 9 shows the relation between residual times and the locations of epicenter and station. The geographical distribution of residuals changes in a complicated way according to the change of epicenter, which is shown by the hatched area in the figure. However, it may be said that the Pacific coast of Hokkaido and northeastern Japan usually shows an earlier arrival than the standard. This tendency is also the case of study by RGTTTC.

Part II. — Approach from the explosion data.

1. Introduction

The second way of construction of a standard time table is in the direction of approach from the explosion seismological observations. This kind of studies was made by the present writer. [3] Since 1953 the Research Group for Explosion Seismology, Japan has carried out the observations of many explosions in various parts of Japan. Fig. 10 shows the locations of shot points and measuring lines of which the data were used for this study. The regions of Tohoku and Kinki, which will be discussed separately in some

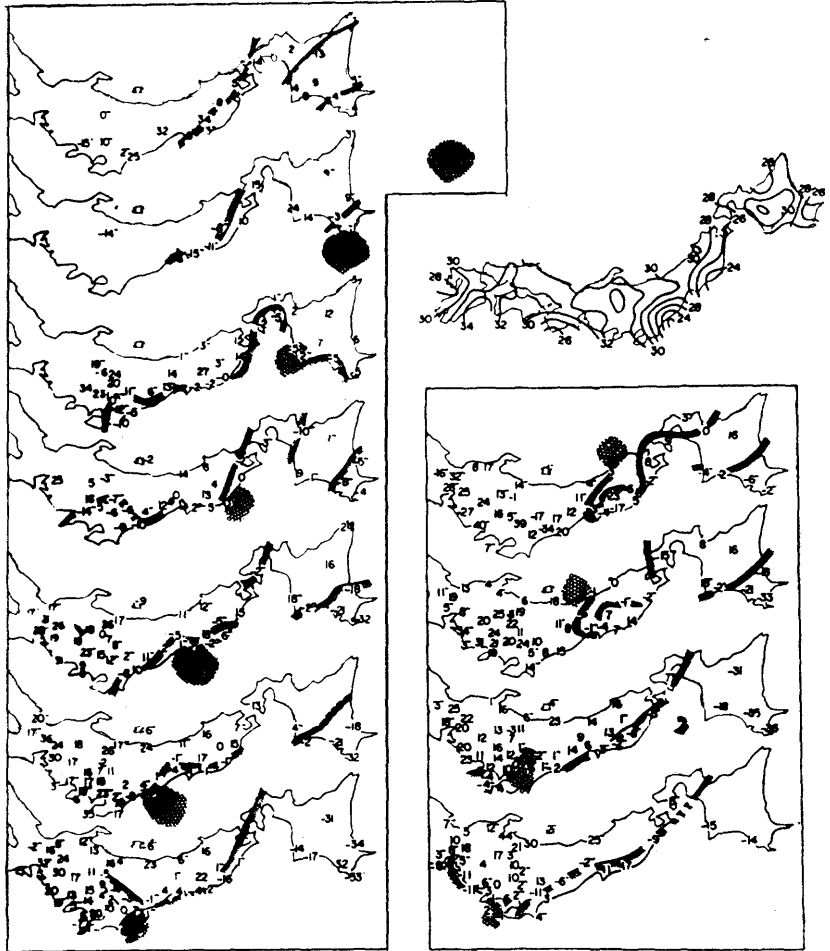


FIG. 9. — Geographical distribution of mean P travel time residuals (in .10 sec) for earthquakes occurring in various zones, and map showing the thickness of crust (in km) given by H Kanamori. The hatched area show epicentral zone. (After Ichikawa.)

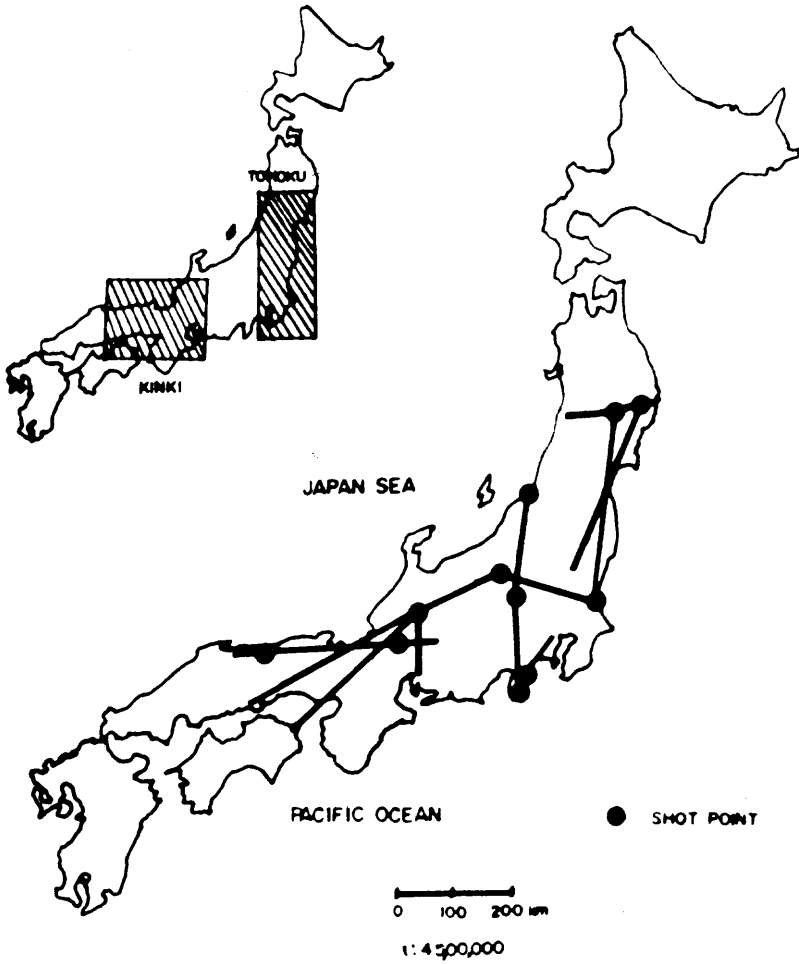


FIG. 10

cases of later discussions, are also indicated in the map. The results of observations are seen in Fig. 11 en bloc. Full circles (●) and crosses (x) are the observations in Tohoku and Kinki regions respectively. Open circles are the data in other regions. This figure demonstrates many important facts for the study of travel time curve.

- 1) The Wadati-Masuda's curve is far late in comparison with the observations, as already mentioned.
- 2) The Jeffreys-Bullen table is better but still has a systematic delay.

3) A regional difference is clearly seen especially for Tohoku and Kinki regions.

This suggests that the usage of regional standard table may give a better result.

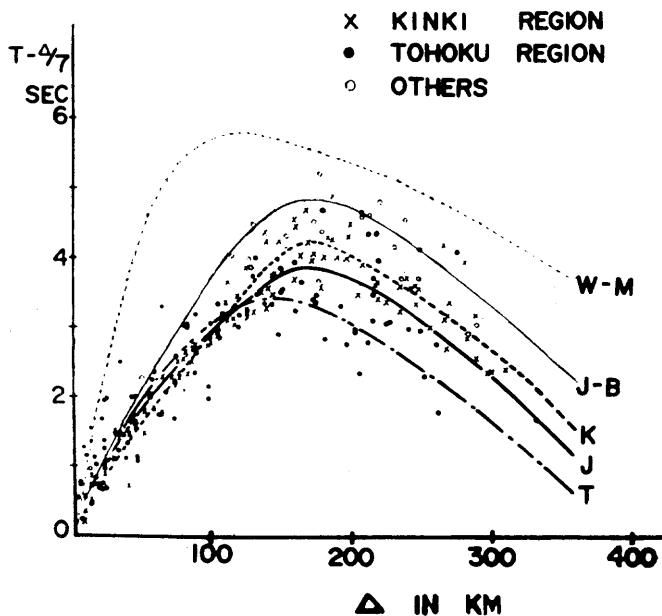


FIG. 11

4) When the whole Japan is taken as one block, the scatter of observed times is of the order of ± 1.5 seconds, and even if the regional standard curve is adopted, still the scatter of the order of ± 0.5 seconds should remain.

Since the accuracy of explosion data is extremely high for both epicentral distance and travel time, this scatter should not be attributed to the observational error but it implies that the deviation from the standard curve of this order is expected for natural earthquake data, whatever standard may be used. This fact gives us a key to solve the problem.

2. Basis of the method used

The main difficulty on the construction of standard table from explosion data lies on the following points : The selection of models of underground structure is more or less arbitrary in many cases. A flat layered model fits to the data as well as a

continuous velocity distribution within the limit of scatter. Or, even when the structure is determined, the obtained structure is sometimes too complicated to calculate a simple standard time. However, it is justified by many trials that this difficulty can be avoided if several tenth of second is permitted as a limit of accuracy. An example will be seen in Fig. 12. This figure shows three

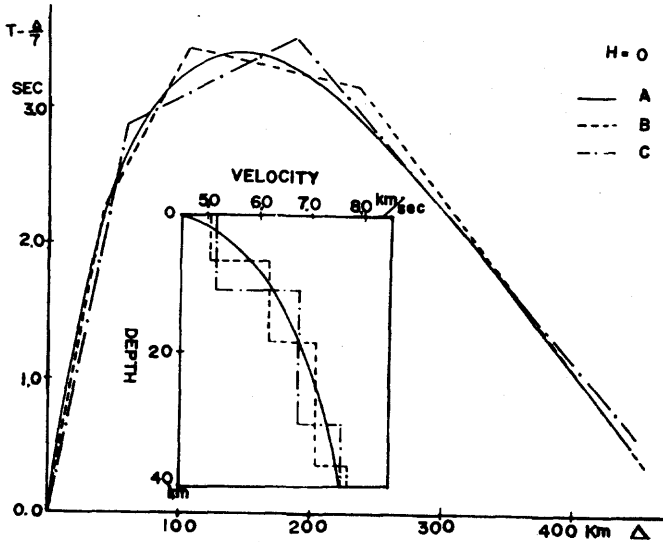


FIG. 12

curves which are close to each other within the limit of 0.2 seconds for surface origin. Of course, each (full, dotted and chain) line corresponds to a quite different structure shown in the figure. However, the times for the depth of 5 Km based on these different structures are close to each other within the limit of the same order of magnitude, as seen in Fig. 13. Fig. 14 is also the case for $H = 20$ Km. These examples show that we can calculate a sufficiently accurate standard time even if the structure adopted is only provisional.

3. Results

Under this basis the travel times are calculated, assuming a continuous velocity distribution tentatively. The results are seen in Figs. 15 and 16. Fig. 15 is the result for the depth of 5 Km. Full line shows the curve when all Japan is taken as a whole. In this case, the scatter of actual data within approximately 1.5 seconds

should be permitted. The dotted and chain lines are the times for Kinki and Tohoku regions repectively. This figure implies the

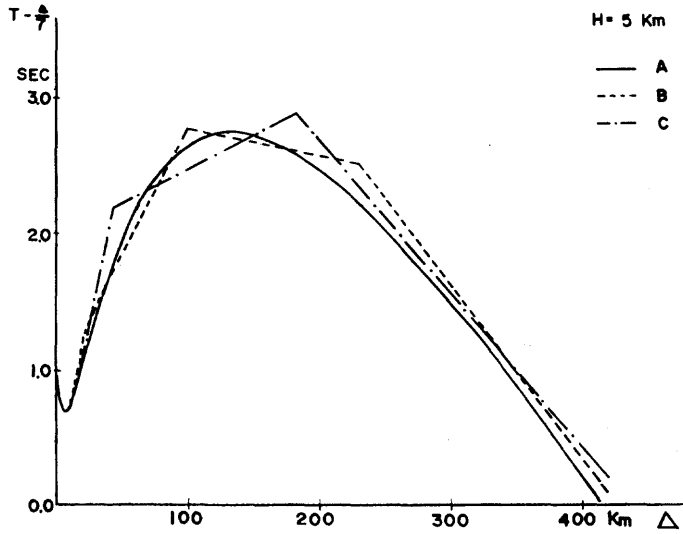


FIG. 13

regional difference is of the order of 1 second. In these cases, the scatter permitted is approximately 0.5 seconds. Fig. 16 shows a

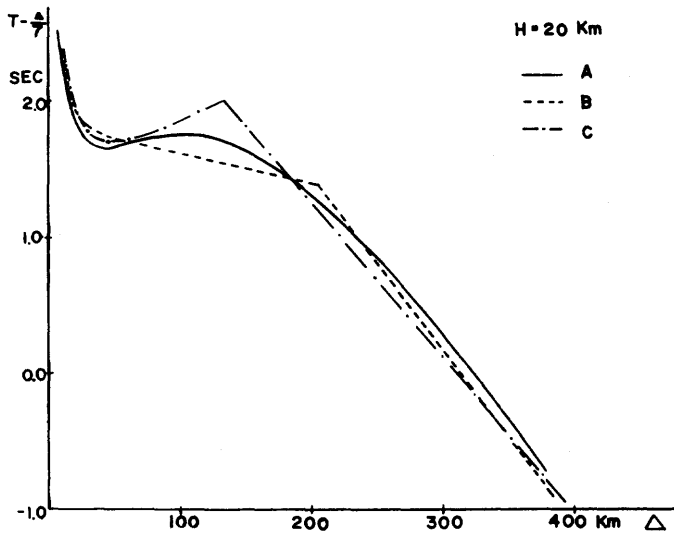


FIG. 14

similar result for the depth of 30 Km. The regional difference decreases down to 0.5 seconds.

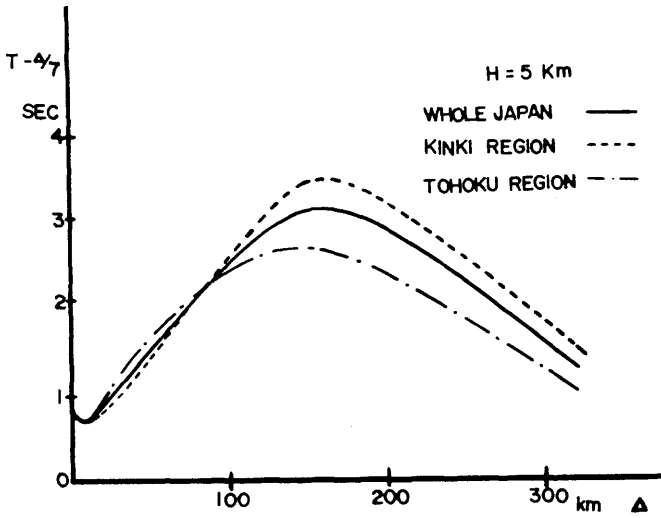


FIG. 15

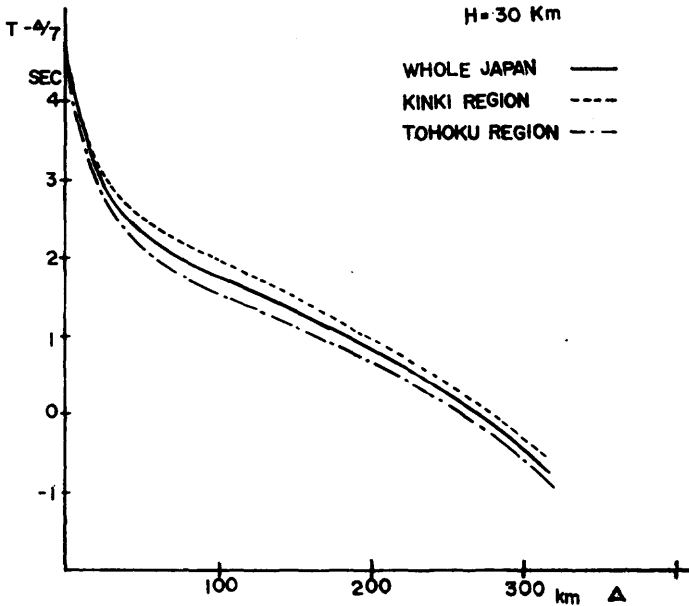


FIG. 16

4. Problems remained

The problems left are to extend the result to longer distance. The explosion data are usually limited within the distance of 350 Km so that the combination of explosion results to those from natural earthquakes is necessary to solve this problem. The study in this direction is now under the way from both sides of natural and artificial earthquakes. Although there still remains some barriers to come over, the present writer believes the complete standard travel time curve for Japan or various regions in Japan will be established in a very near future.

REFERENCES

- [1] Research Group for Travel Time Curve; Will be published on the Bulletin of the Earthquake Research Institute, Tokyo University, Vol. 45, n° 2 (1967).
- [2] M. ICHIKAWA; Technical Report of the Japan Meteorological Agency, n° 55 (1967) (in Japanese).
- [3] Z. SUZUKI; Not yet published.

P AND S TIMES IN JAPAN

by E. P. ARNOLD

RÉSUMÉ

Les variations maintenant bien établies dans le manteau supérieur rendent l'emploi de moyennes mondiales insuffisantes pour les durées de propagation séismologiques. J'ai effectué une révision sur une base régionale.

D'habitude les tables de durées sont construites d'après des données de tremblements de terre qui ont leur foyer dans les couches supérieures mais, ceci fait, il est difficile de tenir compte de la profondeur du foyer et de pourvoir aux classes critiques de distance. Dans cette étude j'ai surmonté ces difficultés en utilisant des tremblements à foyer profond, avec l'avantage supplémentaire de séries d'observations extrêmement consistantes.

Sur un groupement de 103 tremblements de terre japonais, 31 convenaient à l'établissement de corrections aux durées de propagation des P. Dans la table résultante il fallait remplacer la discontinuité à 20° , du moins au Japon, par une forte courbure aux environs de 15° . Il n'y avait aucune évidence pour justifier une couche à basse vitesse. J'ai construit une nouvelle table des S d'après des séries d'observations d'une consistance exceptionnelle tirées de 18 séismes que j'avais relocalisés d'après les nouvelles tables des P. La discontinuité à 20° disparut et il n'y avait pas de signes d'une couche à basse vitesse. Les tables P et S, qu'on trouvera plus loin, sont fonction de la profondeur du foyer et de la distance.

Pour les deux tables il fallait trouver les temps de parcours à travers les couches supérieures en les déduisant d'observations pP-P et sS-S. J'ai noté une grande variation dans ces durées pour les différentes parties du Japon. J'ai adopté comme typiques les durées pour le Hondo du Sud.

On discute également les avantages de l'étude des durées de propagation sur une base régionale plutôt que générale.

Introduction

The Jeffreys-Bullen Seismological Tables [1] of 1940 were the last in a long series of attempts to provide a general set of travel-times that could be compared with any earthquake and not be wrong by more than two or three seconds. Most of the previous tables had very serious errors sometimes amounting to as much as 20 or 30 seconds [2]. Owing to the poor geographical distribution of both seismic observatories and earthquakes, these tables were not, as is commonly supposed, as much a world average as they were a composite, a patchwork quilt. Small Japanese shocks supplied times to about 10° ; European data were used for intermediate distances and North American and some European epicentres were used to extend both the P — and S — times to the core shadow.

Despite the inadequacies of the J.-B. Tables, they have remained the world standard for over 27 years testifying to the accuracy of Prof. JEFFREYS'S 1939 statement [3] : « The present P, S, PKP and SKS tables [this refers to what eventually became known as the J.B. Tables] all rest now on observational material through their entire course; it would be impossible to alter any of them to give better agreement with one old or new set of observations without making agreement worse with another. Though we have apparently reached the stage where further improvement is impossible for all earthquakes, since small departures from independence of the errors are beginning to reveal themselves, further development is unlikely to lead to the substitution of any single set of tables for the present ones. It is more likely to lead to the introduction of minor corrections, not always of the same sign, that can be applied to the present tables in specified circumstances. »

One should notice from this statement that even while the tables were being constructed anomalies had begun to appear and soon after their publication, definite evidence of regional characteristics was established [4, 5]. By regional characteristics I mean differences in upper-mantle velocities at the base of the superficial layers and differences in velocity-depth function to about 200 km. There is also some reason to suspect that there are regional variations at very great depths indeed. These characteristics have been much discussed of late and it is unnecessary to cite details here.

The problem, however, is that once regional characteristics are recognized, a procedure for constructing tables that account for the differences needs to be found. Prof. BOLT, in an earlier paper in this symposium, has outlined the general procedure which involves finding regional corrections to a general set of travel-time tables along with adjustments for both stations and sources which depend on relative geographical locations. Such a general solution could contain tens of thousands of unknowns and would require a prodigious effort. Some simplifications, therefore, must be made and two methods present themselves. One is that used by Professors HERRIN and HALES whose papers also appear in this issue. Briefly their method was to ignore both source corrections, or adjustments, and observations under 20° and then to calculate station corrections, as a function of azimuth, and adjustments to a general set of tables for distances beyond 20° .

The other, the method that was used here, is simply to restrict the source region and construct a set of tables for *all* distance ranges. This has the advantage over the first method that we

can use deep-focus earthquakes in the solution. Later, corrections for most stations can be easily added because, beyond the source area, stations can be considered to be at the same distance and azimuth from all epicentres and a constant will suffice. For the stations within the source area, station corrections can be functions of both distance and azimuth without severely increasing the number of adjustable parameters in the solution. Source corrections are then found by comparing shallow — and deep — focus shocks. The values of these parameters can then be refined by repeating the process until no further changes take place.

This study, then, is the first step in developing a truly regional set of travel-times. The Japanese region was selected for three reasons; the great density of near seismic stations, the existence of preliminary travel-times [6] and a relatively large number of earthquakes with foci below the superficial layers. This last reason is particularly important since these shocks, which I shall loosely call “deep-focus”, have special properties. It is much easier to determine the depth of focus with precision than in the case of shallow shocks, and, in general, deep-focus quakes have better series of S-observations. As will be appreciated later, the use of deep-focus shocks make it possible to compensate for the lack of observations in critical distance ranges. In addition, if there is a general low-velocity layer in this region, shocks with foci in the layer will be more sensitive to this anomaly.

Corrections to P

The method used to find corrections to the P-table from deep-focus shocks is an adaptation of one due to S. ΜΟΗΟΡΟΝΙΩΤΗΣ; its principles are as follows : In Figure 1, supposing a focus at F, there will be two rays, FP and FP', one which descends and one which ascends from the focus, both having the same $dt/d\Delta$. Then the corrections to each can be added to form corrections to the ray PP' both points being on the surface separated by the distance $\Delta = \Delta_1 + \Delta_2$.

If there are m earthquakes and n ranges of $p = dt/d\Delta$ which have been selected such that dt/dh does not vary much in a given range, then the equations of condition have the form

$$2 \delta t_{rs} + \zeta_s = \bar{t}_{rs} \pm \sigma_{rs} \quad \left\{ \begin{array}{l} r = 1, \dots, m \\ s = 1, \dots, n \end{array} \right. , \quad (1)$$

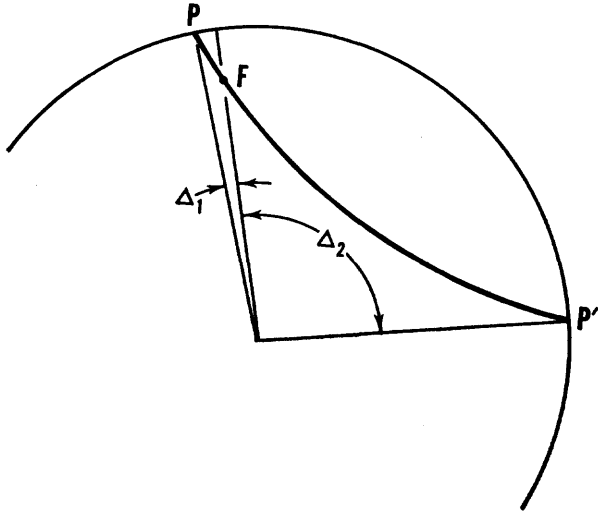


FIG. 1

where δt_{or} is the correction to origin time of the r^{th} quake and ζ_s is the s^{th} correction to the tables. Also

$$\xi_{rs} = \frac{\sum_i W_{irs} \xi_{irs}}{\sum_i W_{irs}} + \frac{\sum_j W_{jrs} \xi_{jrs}}{\sum_j W_{jrs}} \quad (2)$$

$$W_{rs} = \sigma_{rs}^{-1} = \frac{\sum_j W_{jrs} \sum_i W_{irs}}{\left(\sum_i W_{irs} + \sum_j W_{jrs} \right)} \quad (3)$$

$$W_{krs}^{-1} = 1 + \mu \exp \left\{ -h^2 (\xi_{krs} - \alpha)^2 \right\}$$

where ξ_{irs} is the i^{th} residual in the s^{th} range of the r^{th} quake and i takes on values corresponding to observations of ascending rays and j descending ones.

These equations neglect corrections to epicentres but these will be cleared out on successive iterations; corrections to depths of focus cancel.

About 100 earthquakes, taken mostly from the International Seismological Summary, were deemed suitable for finding corrections to the 1954 P-times. These were all relocated using the method of uniform reduction [8] with the 1954 Tables. So as to obviate introducing systematic errors in corrections due to errors in focal locations, the following criteria were used to eliminate shocks with doubtful determinations of focal parameters: (1) the uncertainty in depth of focus was to be less than .001R; in time of origin less than 1'; and in epicentre less than 0°.1. Additionally

(2), it was required that there would be observations in the range of distance $0^\circ \leq \Delta \leq 15^\circ$ in at least three quadrants and (3) that there would be at least one observation nearer to the epicentre than the inflexion. Condition (3) ensures that the epicentral determination depends, at least partially, on comparison of near and far observations and not totally on comparison of observations in the ranges $20^\circ \leq \Delta \leq 45^\circ$ and $60^\circ \leq \Delta \leq 95^\circ$ as often happens. Of the 100 originally selected shocks, 33 survived these tests and are listed in Table 1.

TABLE I. — Earthquakes used for finding corrections to P.

Epicentral Index		Origin	Time	Epicentre		Depth (R)	
				Latitude °N	Longitude °E		
d	h	m					
6	1940 Jul	14	15	31	36.0	140.0	.002
7	1940 Nov	18	12	47	33.9	135.4	.003
8	1941 Mar	15	19	07	40.6	139.7	.024
17	1949 Aug	17	18	34	42.8	145.7	.008
27	1952 Apr	15	05	59	41.9	142.9	.004
28	1952 Apr	28	10	54	41.9	142.8	.005
30	1952 Jun	03	13	21	42.2	143.3	.006
31	1952 Oct	26	08	41	34.5	137.7	.043
36	1952 Nov	02	01	42	36.3	140.7	.004
38	1953 Feb	16	00	07	42.4	142.9	.011
40	1953 Apr	29	20	21	42.2	143.1	.005
41	1953 May	10	19	49	36.2	140.9	.003
42	1953 May	17	22	12	34.6	139.7	.014
43	1953 May	26	01	43	41.8	142.9	.002
44	1953 Jul	22	12	52	41.7	143.9	.002
45	1953 Aug	27	22	16	43.2	142.7	.023
61	1953 Dec	20	00	21	39.6	136.9	.047
63	1953 Dec	21	17	36	41.6	142.2	.005
64	1954 Jan	17	11	46	36.1	140.0	.005
66	1954 Feb	24	17	28	36.0	140.0	.004
67	1954 Feb	24	20	45	26.9	140.3	.074
69	1954 Mar	26	04	35	41.2	142.3	.004
70	1954 Apr	04	23	14	41.8	142.8	.004
71	1954 Apr	16	10	30	42.4	143.0	.006
72	1954 Apr	17	12	10	41.7	141.1	.014
74	1954 Jun	05	13	14	36.0	139.9	.004
75	1954 Jun	06	21	58	32.3	140.4	.012
78	1954 Aug	28	10	01	36.6	141.2	.002
80	1954 Sep	27	16	38	42.5	142.5	.004
82	1954 Nov	19	05	56	40.9	132.1	.080
83	1955 Jan	17	02	21	35.5	140.3	.005
89	1955 May	31	14	44	42.0	141.4	.012
95	1955 Jul	24	11	02	35.7	140.6	.005

JEFFREYS'S 1954 Tables are most accurate in the range $0^\circ \leq \Delta \leq 15^\circ$ and there is reason to suspect that at large distances there is a systematic error due to faulty allowances for depth. Also, since these tables were compiled, much new equipment has been installed in various observatories and as a consequence there has been an increase in station reliabilities generally and particularly in those of India and Central Asia. For these reasons, it was thought necessary to fix the depth at the estimate given by the first relocation, then solve for a new estimate of origin time and epicentre using only observations up to 15° . This requires that the standard errors in origin time and depth of focus be increased to account for the decreased number of observations. If, from the first solution the standard error in epicentre is σ_1 from the second is σ_2 and the effect on depth of shifting the epicentre by σ_2 is τ_h , then the required increase in the uncertainty in depth is

$$\sigma_h^{**} = \frac{\tau_h^2}{\sigma_2^2} \left(\sigma_2^2 - \sigma_1^2 \right) \quad (4)$$

A similar relation exists for origin time and τ in both cases is found by re-solving the normal equations from the first solution after altering the roots by an amount corresponding to the increased uncertainties in epicentre.

The mean shifts in epicentre were $- .^\circ 02 \pm .^\circ 006$ in latitude and $+ .^\circ 05 \pm .^\circ 007$ in longitude or about $^\circ 054$ in an east-south-easterly direction. χ^2 was 68.3 on 60 degrees of freedom which is well within the usual limits of $\nu \pm \sqrt{(2\nu)}$ where ν is the number of degrees of freedom. On close inspection, there appeared to be no correlation between the shifts and epicentral positions. This result tends to confirm the hypothesis that there is a systematic error in the times to European and Central Asian stations.

After the second relocation, all but two of the epicentres in Table 1 were found satisfactory. The two were numbers 17 and 66 which were dropped because the uncertainties in their epicentres were greater than $0^\circ.1$. For the remaining 31 earthquakes, the standard deviation of one observation, σ , was $1^\circ.51$ on 4 086 observations and the uniform reduction constant, μ , was 0.048. Table 2 gives the frequencies of P-residuals.

Equations of condition given by (1) were found using ranges of $p = dt/d\Delta$ shown in Table 3; the group or range number is arbitrary and is used for identification. Normal equations were formed in the usual way, the left sides yielding a matrix of dimension 41 and

rank 40. The normal equations are therefore ambiguous and can only be solved in terms of one of the unknowns; the correction to group 2 was taken to be zero. The equations were solved by successive elimination on an electronic computing machine; the roots are given in Table 3 along with their standard errors.

It should be noted that the corrections are quite well behaved and are, in fact, smoother than they have any right to be. The standard errors are considerably better than those for the 1954 tables, especially at moderate and large distances. Tables 4 gives individual

TABLE 2. — Frequencies of P. residuals.

Residual	≤ -10	-9	-8	-7	-6	-5	-4	-3	-2	-1	
Number	55	12	7	19	19	41	76	151	411	734	
Residual	0	1	2	3	4	5	6	7	8	9	≥ 10
Number	887	750	374	150	83	56	42	26	37	25	131

TABLE 3. — Roots of the normal equations for P — Corrections to P

Number Group	P (s/1°)	Surface Δ (degrees)	Correction (sec)	σ (sec)
1	14.34	0	.076	±.76
2	— 13.94	— 8	.000	.17
3	— 13.72	— 10	.133	.27
4	— 13.45	— 12	.323	.33
5	— 13.12	— 14	.321	.49
6	— 12.70	— 16	.858	.66
7	— 11.84	— 18	1.764	.61
8	— 8.81	— 30	1.660	.40
9	— 6.51	— 65	.872	.34
10	— 4.48	— 95	.553	.38

Corrections to Times of Origin

Epicentre Index	2 x Correction to t_0 (sec)	σ_{t_0} (sec)	Epicentre Index	2 x Correction to t_0 (sec)	σ_{t_0} (sec)
44	— .20	± .70	83	.22	± .41
78	— .35	.47	64	.55	.45
43	.11	.56	30	— .14	.55
6	— .27	.52	71	.26	.53
41	— .28	.42	38	.03	.77
7	.52	.46	75	.08	.50
70	.24	.48	89	.31	.46
27	.33	.50	42	.54	.53
74	— .02	.39	72	— .58	.67
69	— .23	.51	45	.89	.53
80	— .23	.54	8	.94	.70
36	— .74	.61	31	.62	.40
28	— .03	.51	61	.60	.58
95	.46	.36	66	— .20	.43
63	.02	.55	82	1.40	.57
40	.19	.52			

contributions to χ^2 which is 90 on 94 degrees of freedom, very close to expectation.

If there is a low-velocity layer beneath Japan, one would expect some anomalies to appear. If, for instance, the layer begins at the Mohorovičić discontinuity with a velocity decreasing steadily to a depth of .02R as GUTENBERG [9] has it, then χ^2 for the groups for which the ray leaves the focus nearly horizontally should be larger in the aggregate than the rest. In Table 4 these contributions are underlined and the earthquakes are arranged in order of depth of focus, the shallowest at the top. As can be seen they are not abnormal, if anything they are somewhat smaller than expected. Others [10] expect that if such a layer exists it will be between .03R and .05R. Since there is little information in this range, no conclusions can be drawn.

The 1954 times are, in general, complementary to the present ones and since they are based on independent data, they may be combined with the present ones to increase accuracy. They ought to differ by a constant plus an allowance for the upper layers satisfying equations of condition of the form

$$\xi = a + .5 \sqrt{(400 - p^2)} b \quad (5)$$

where p is $dt/d\Delta$ for the mean Δ in each group and ξ is the observed difference between the the two tabular points. Using the relation $a' = a + 6.9b$, the solutions are $a' = -.16$ and $b = -.40$. χ^2 is 8.2 on 8 degrees of freedom thus confirming the hypothesis that the two tables were consistent. Calculated values of (5) were added to the 1954 Times and means of the two sets of times were found; they are given in Table 5. From now on, these combined tables will be referred to as the 1965 Japanese P-Times.

The ambiguity can be resolved by using observations of pP -P intervals. The trial tables will yield good estimates of depth of focus below the MOHORovičić discontinuity; pP -P intervals will provide estimates of depth measured from the surface. Since these are both estimates of the same quantity, the difference must be accounted for by a correction to the time through the upper layers.

For a set of pP -P intervals consistent with a corresponding set of P-times, the equation of condition for each pP -P observation will have the form

$$\left. \frac{\partial t}{\partial h} \right|_{pP-P} \delta h = (O - C)_{pP-P} \quad (6)$$

TABLE 4. —
DISTRIBUTION OF χ^2 FOR CORRECTIONS TO P

GROUP	1	2	3	4	5	6	7	8	9	10
EPICENTRE										
78	<u>.08</u>	1.02	1.22					.71	2.73	
44	<u>.14</u>	.02			.99					
43		.17	3.10						.30	
6		.03	.22						0.00	.85
7		3.26	.02	.23				4.27	3.97	
41		.40	.06				.02	.01	.26	1.29
74		.24	1.91	.27			1.50	.26	.41	.00
66		.20	.60						1.77	1.13
70		.17	.09	.25	.52					.01
69		.14	1.37	1.22	.16					
80		.14		.02	0.00					.38
36		.03	.05						.63	
27		0.00	.33	2.01	0.00					.24
95		1.37	2.23	.51		.41		.01		
83		<u>.33</u>	2.04	.05					.56	
64		<u>.51</u>	.01						1.90	
63		<u>.76</u>	1.84	4.23	1.93	.01		.03		
40		<u>.62</u>	1.08	0.00				.61		.14
28		<u>.01</u>	1.04	.15		3.62				
30		<u>.22</u>	.04	.35				.69		.18
71		<u>.21</u>	.01	.23	.09				.91	.99
38			<u>.01</u>	.02					.16	
75			<u>.44</u>	2.49	1.58					
89			<u>1.08</u>	.03	.02	.12		1.54	.01	.58
42				1.05			.31	.82	.01	1.15
72				.08					.02	.61
45					<u>.31</u>	.01	1.50	.13	.07	.91
8					<u>.08</u>	.79			.74	
31							<u>.38</u>	.16	.47	.31
61							<u>.35</u>	.18	.02	
82								<u>0.00</u>	0.00	

χ^2 is 89.9 on 94 degrees of freedom

TABLE 5. —
COMBINING THE 1954 AND 1965 P-TIMES

Δ	Mean	t_{1954}	wt	t_{1965}	wt	t_{1965}	wt	t_{1965}	t_{1965}
(deg)	(sec)	(sec)		(raw)		(sec)		- t_{1954}	- t_{1940}
				(sec)					
3	49.5	6.7	49.435	1.7	49.359	8.4	-0.152	-	4
7	106.2	6.7	106.222	52.1	106.201	58.8	-0.021	-	.1
9	134.0	6.7	133.913	13.7	133.929	20.4	-0.177	-	3
11	161.5	6.7	161.220	9.2	161.186	15.9	-0.357	-	5
13	188.4	6.7	188.112	4.2	188.043	10.9	-0.390	-	5
15	214.7	6.7	213.820	2.2	214.121	8.9	-0.557	-	6
17	240.0	6	238.236	2.8	239.030	8.8	-0.970	-	1.4
23	306.2	1	304.548	6.3	304.648	7.3	-1.560	-	2.3
48	520.7	2	519.851	8.7	519.785	10.7	-0.938	-	2.7
83	747.3	4	746.706	6.9	746.452	10.9	-0.807	-	1.7

were δh is the correction to the depth of focus and the right side is the pP -P residual taken at the depth determined from P alone. The correction in the time from focus to epicentre, δt , that will make $\delta h = 0$ is

$$\delta t = t_P - t_{pP-P} = t_P - \left(t_P + \frac{\partial t}{\partial h} \Big|_{\substack{\Delta=0 \\ pP-P}} \delta h \right) \quad (7)$$

or simply

$$2 \delta t = \frac{\partial t}{\partial h} \Big|_{\substack{\Delta=0 \\ P}} \delta h \quad (8)$$

after recognizing that at $\Delta = 0$, dt/dh for P is just half that for pP -P because the latter must travel twice through the upper layers.

Tables of pP -P, consistent with the 1954 Times, were calculated, but since they will be of no further use they are not presented. Of the 31 earthquakes, numbers 31, 42, 43, 61, 63, 69, 72, 74, 78, 82, 83, 95, 27, 28, 70 and 40 had good series of pP -P observations. Equations of condition (7) were formed for these earthquakes, δh was found for each by uniform reduction and finally an estimate of $2\delta t$ from (8) was found. σ is $1'.51$ on 466 observations and μ is 0.10 . For comparison, JEFFREYS [11] obtained $\sigma = 1'.83$ and $\mu = 0.065$. A possible reflexion from the MOHOROVIĆIĆ discontinuity

did not appear to be present. Table 6 gives the frequencies of the residuals.

χ^2 on the combined estimate of all the δt was greater than 80 on 17 degrees of freedom, indicating a systematic error which turned out to be a distinct geographical division. The epicentres divided into two groups, one in the region of Tokyo the other at the southern tip of Hokkaido. A summary of the results for the first group is given as Table 7. There are two components for the standard error in δt ; one is derived from the uncertainty in depth from *pP-P* intervals, the other from the *P*-solution including the additional uncertainty due to limiting the range of observations to the first 15°. For Southern Honshu, then, $\delta t = -.44 \pm .13$

TABLE 6. —

Distribution of *pP-P* Residuals

Residual	≤-10	-9	-8	-7	-6	-5	-4	-3	-2	-1	0	1	2	3	4	5	6	7	8	9	≥10
Number	20	1	4	3	10	11	12	17	33	66	95	84	37	16	9	9	6	5	3	5	20

TABLE 7. — Correction to time through upper layers from *pP-P* intervals.

Epicentre	δt (s)	σ (s)	(O-E) (s)	χ^2
31	.43 ± .13 = ± .19	.19	-.01	0.00
42	.37 ± .30 = ± .47	.47	-.07	.23
43	.85 ± .22 = ± .79	.79	+.41	.28
61	-.02 ± .28 = ± .39	.39	-.46	1.40
63	.40 ± .53 = ± .63	.63	-.04	.05
69	.48 ± .62 = ± .65	.65	+.04	.05
72	.09 ± .47 = ± .66	.66	-.35	.27
74	-.01 ± .49 = ± .75	.75	-.45	.36
78	.28 ± .64 = ± .69	.69	-.16	.04
82	.91 ± .38 = ± .41	.41	+.47	1.30
83	.28 ± .48 = ± .59	.59	-.16	.09
95	1.31 ± .45 = ± .57	.57	+.87	2.37
				<hr/> 6.44

and χ^2 is 6.44 on 11 degrees of freedom which confirms the hypothesis of geographical separation. The four earthquakes with epicentres in Hokkaido are similarly summarised in Table 8. δt was $1'.89 \pm '.23$ and $\chi^2 = 0.8$ on 3 degrees of freedom which, although it appears to be small, is within the usual limits. In any case, one expects large variations in χ^2 on few degrees of freedom. The reference time for the 1954 tables was 5'.00; the time for one vertical traverse of the upper layers in Honshu is then $5'.44 \pm '.13$

which corresponds to a thickness of $30.19 \pm .76$ km if one assumes 5.55 km/sec for the velocity of Pg. Similar figures for Hokkaido are $6^{\circ}.89 \pm ^{\circ}.23$ and 38.24 ± 1.3 km.

TABLE 8. — Corrections to time through upper layers from pP-P intervals. (Hokkaido)

Epicentre Number	δt (sec)	Weight	(O-C) (sec)	χ^2
27	1.68	5.6	— .2	.2
28	1.69	5.2	— .2	.2
40	2.21	4.3	+ .3	.4
70	2.10	3.5	+ .1	.0
				.8

The figure for Southern Honshu was thought to be more widely applicable and was adopted as standard for the final tables.

In the range $0^{\circ} \leq \Delta \leq 15^{\circ}$ the cubic

$$t = (6.517 \pm .090) + (14.343 \pm .091)\Delta - (2.26 \times 10^{-3} \pm 3.0 \times 10^{-4})\Delta^3 \quad (9)$$

is the least squares solution. These six data contribute 0.7 to χ^2 on three degrees of freedom; again within the normal range of expectations.

A useful formula for stripping thin layers is

$$t = t_1 + (2t_1/p_0) \sqrt{(p_0^2 - p^2)} \quad (10)$$

where t_1 is the travel-time from the base of a thin layer to the corresponding point at a given distance, t is the travel-time for the same distance with the layer added. The layer has velocity, p_0 , which is expressed in seconds per degree, $p = dt/d\Delta$ or the parameter of the ray and t_1 is time of one vertical traverse of the overlying layer.

Using (10) the P_n intercept is $7^{\circ}.582 \pm ^{\circ}.18$ so that (9) can now be written as

$$t = (7.582 \pm .18) + (14.343 \pm .091)\Delta - (2.26 \times 10^{-3} \pm 3.0 \times 10^{-4})\Delta^3 \quad (11)$$

The linear term gives a P_n velocity of $7.73 \pm .05$ km/sec which is consistent with previous determinations for Japan.

The corrections at distances greater than 15° also need smoothing. This was done in two ways. First, instead of taking the correction at the mean distance of the group it was taken, except for $\Delta = 17^{\circ}$, at the 1/4 and 3/4 points of the ranges each with half the weight [12]. Secondly, a quarter of the second difference was added to each tabular value. Table 9 gives the smoothed corrections. The range $15^{\circ} \leq \Delta \leq 30^{\circ}$ was still not very smooth so a point at 30° of $369^{\circ}.33$, weight 3.6 was interpolated by divided differences

TABLE 9. — Smoothing corrections to P at large distances.

Δ °	Correction (sec)	δ	δ^2	Smoothed Correction (sec)
17	— .970	— .590		— 1.068
21	— 1.560	— .0	+ .590	— 1.413
27	— 1.560	+ .622	+ .622	— 1.405
40	— .938	— .0	— .622	— 1.093
55	— .938	.0	+ .131	— .906
72	— .807	+ .131	— .131	— .839
88	— .807	.0		— .785
95				— .761

and a cubic was fitted to the data in this range. The result was

$$t = -55.31 + 23.97 \Delta - .475 \Delta^2 + 4.94 \times 10^{-3} \Delta^3 \quad (12)$$

χ^2 was 16.7 on 16 degrees of freedom using the original data for comparison.

In the range $30^\circ < \Delta \leq 95^\circ$ the corrections were interpolated by divided differences, added to the 1954 Tables and the whole of the resulting table subjected to smoothing by the subtraction of a twelfth of the fourth differences. Actually, this last smoothing changed the times by less than $.1$ but the derivatives were made somewhat smoother, a necessity when finding a velocity distribution.

(11) and (12) intersect at $\Delta = 15^\circ.8$; it would be more accurate to say they osculate at this point as $dt/d\Delta$ matches to within $.01/1^\circ$. Since χ^2 on both ranges is acceptable there is no reason to maintain the hypothesis of a discontinuity in the neighbourhood of 20° ; a strong curvature at $15^\circ.8$ is used instead.

The next step was to compute a complete set of tables for foci at varying depths. This process is well known in principle and can be found in any standard work [13] on the subject. Implementation of the method, however, varies a good deal and therefore a brief description of the procedure will be given.

The upper layer was first stripped off using (10) resulting in a (t, Δ) relation for points on the MOHROVIČIĆ discontinuity. Derivatives for each tabular point were found using a Newton-Stirling formula with third differences. Abel's equation is then integrated using Gregory's method with third forward and backward differences except for the singularity at the deepest point of the ray, where a special integration procedure [14] was used. The resulting velocity-depth relation was in unequal intervals; a table with intervals of $.005$ earth's radius was obtained by interpolating with third divided differences.

The velocity distribution was then integrated over paths of constant $dt/d\Delta$ for various focal depths. One-half the effect of upper layer was then added and the resulting tables interpolated by a special divided difference formula [15] for use when derivatives are given.

Times for depths in steps of $.01R$ from the Mohorovičić discontinuity to $.12R$ were calculated for Δ in increments of 1° . Because there are few stations reporting Japanese earthquakes beyond 95° , the tables are limited to that distance. A special table is also given for use in cases where both depth and distance are small; times are given for $.005R$ intervals in depth and $.1$ steps in distance from the Moho to $.030R$ and Δ from 0° to 5° . A complete set of tables will be found, along with a velocity distribution, at the end of the paper.

It is often very useful in the study of earthquakes to know the parameters of the inflexion point; these are given in the form of a graph in Figure 2.

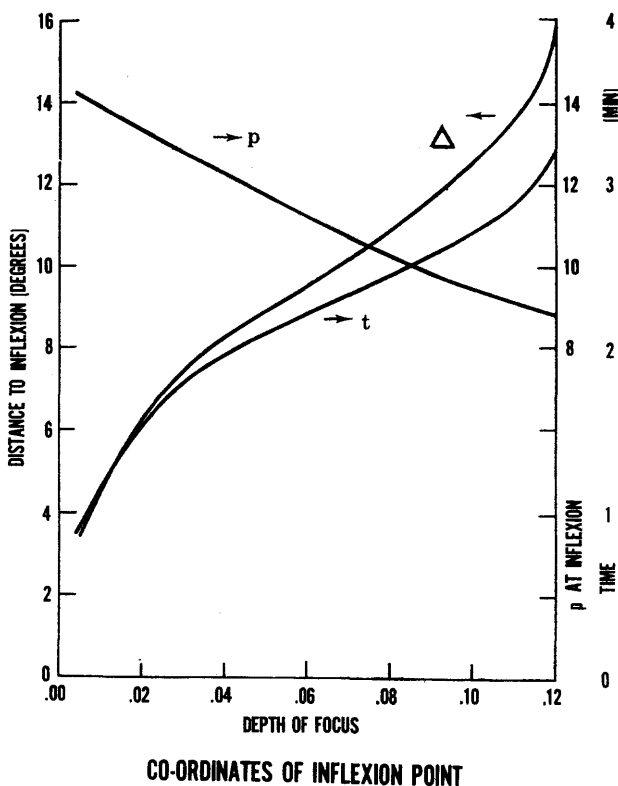


FIG. 2

Corrections to S

Normal Japanese earthquakes have perhaps the poorest series of S observations of any region, especially at short range so that the use of deep-focus quakes for the revision of the S-table is definitely indicated.

Of the 100 earthquakes, 41 appeared at first to have good observations of S. However, after these were relocated using the 1965 P-tables, four of them failed to converge on a solution and four more apparently had foci in the upper layers. Residuals against the 1940 Jeffreys-Bullen tables of S-times were found for the rest. The standard deviation of one S-observation was 2^s.68 on 2868 observations for which μ was 0.14. Table 10 gives the frequencies

TABLE 10. — Frequencies of S-residuals.

Residual Number	≤ -20	-19	-18	-17	-16	-15	-14	-13	-12	-11	
	88	5	5	12	7	6	14	14	10	14	
Residual Number	-10	-9	-8	-7	-6	-5	-4	-3	-2	-1	
	30	42	43	89	102	146	227	269	270	306	
Residual Number	0	1	2	3	4	5	6	7	8	9	10
	284	271	205	144	112	79	49	39	25	28	21
Residual Number	11	12	13	14	15	16	17	18	19	≥ 20	
	21	21	11	12	6	10	8	9	6	92	

of S-residuals. The location parameter of the mode, which corresponds to the mean Z-correction was —^s.57. A list of earthquakes used to find corrections to S is given in Table 11.

Two methods for finding corrections to S were used; the first is very much like that for P. The observations in each quake were divided into groups according to the ray parameter, p , which is given sufficiently well by the 1940 tables; the ranges of p are shown in Table 12. Weighted means for ascending and descending rays were found separately then added for groups with the same p to form a set of partial corrections between points on the surface. For S, however, we already had an estimate of origin time from P and it was unnecessary to allow for it; combining the partial corrections for all quakes in the usual way yielded the desired corrections to S directly. Since origin time from P was taken as

TABLE 11. --- Earthquakes used for finding corrections to S.

Epicentral Index	Origin	Time	Epicentre		Depth (R)
			Latitude °N	Longitude °E	
1	1936 Nov.	d h m 12 20 04	45.4	148.5	.013
4	1939 Apr.	21 04 09	47.7	139.8	.077
13	1943 Nov.	17 14 57	33.0	137.9	.049
16	1949 Mar.	19 18 19	31.4	130.4	.020
21	1951 Jul.	11 18 21	28.2	139.6	.073
23	1952 Mar.	05 15 54	41.9	145.1	.002
27	1952 Apr.	15 05 59	41.9	142.8	.003
31	1952 Oct.	26 08 41	34.5	137.6	.043
40	1953 Apr.	29 20 21	42.3	143.0	.004
45	1953 Aug.	27 22 16	43.2	142.6	.021
47	1953 Oct.	27 03 40	42.7	145.4	.003
48	1953 Nov.	25 17 48	34.0	141.5	.002
60	1953 Dec.	07 14 11	38.8	142.2	.001
76	1954 Jun.	10 22 37	29.2	139.6	.059
77	1954 Jul.	09 18 28	41.0	138.5	.036
82	1954 Nov.	19 05 56	40.9	132.0	.080
83	1955 Jan.	17 02 21	35.6	140.3	.006
88	1955 May.	30 12 31	24.2	142.5	.085
94	1955 Jun.	23 08 39	37.4	141.4	.004
95	1955 Jul.	24 11 02	35.7	140.5	.003
96	1955 Aug.	30 17 35	27.9	139.3	.080
98	1956 Jan.	06 22 25	38.5	142.3	.001
102	1956 Feb.	18 07 34	30.1	138.2	.071

TABLE 12. --- Ranges of $dt/d\Delta$ for S.

Number	Mean Δ	$dt/d\Delta$
1	3.0	25.436 —25.140
2	7.5	—24.763
3	10.5	—24.240
4	13.5	—23.567
5	16.5	—22.744
6	20	—19.067
7	23	—17.217
8	30	—15.517
9	45	—13.400
10	65	—11.108
11	85	-- 8.633

standard, the resulting corrections were absolute and did not strictly require an extra datum as did the P-corrections. As it turned out, however, the time of vertical travel through the upper layers

obtained in this way was so poorly determined that it had to be augmented by an independent estimate derived from sS-S observations.

At this point each earthquake was examined for any abnormalities. Two shocks had poorer series of S than at first appeared; four more had unaccountably large mean residuals (probably from poor depth determinations); and eight others would have only contributed information to one group thereby making comparisons between groups in a single earthquake impossible. All these were eliminated from the solution leaving a total of eighteen.

These data were combined in the manner described. On the first trial, groups 6 and 7 in Table 12 were taken as a single group; χ^2 was found to be 65.2 on 45 degrees of freedom which indicated that some variation had not been accounted for; the combined group 6 and 7 contributed 39.1 on 12 degrees of freedom. After this group was divided, a second trial was made which yielded the corrections shown in Table 11 for which χ^2 was 42.9 on 51 degrees of freedom, an acceptable figure justifying the hypothesis of no Z-phenomenon. Contributions to χ^2 are given in Table 13. The weights in the range $0 \leq \Delta \leq 17^\circ$ are rather small and the corrections are not very smooth.

Several quakes at depths less than .005R were available to yield results by a second method. For a limited range of depth and for small distances one can assume that the correction to an ascending ray will be a constant. The observations were grouped by distance and the equations of condition

$$\delta t_{or} + \zeta_s = \bar{\xi}_{rs} \pm \sigma_{rs} \quad \left. \begin{array}{l} r = 1, 2 \dots m \\ s = 1, 2 \dots n \end{array} \right\} \quad (13)$$

were formed, the symbols being the same as in the section on P. Prof. JEFFREYS performed the calculation on data supplied by me. The results are shown in Tables 14 and 15 where the weights are given in terms of $\sigma = 2^\circ.68$ instead of 1° as given elsewhere in this paper. χ^2 is then 19.6 on 19 degrees of freedom, a highly satisfactory figure.

The cubic

$$t = (11.60 \pm .9) + (25.32 \pm .2)\Delta - (.0031 \pm 0008)(\Delta - .5)^3 \quad (14)$$

is a least squares fit to the data in the first five ranges, *i. e.*, up to $16^\circ.5$. χ^2 was 5.6 on 2 *d. f.* From (10) and (14) the time for a vertical traverse of the upper layers for S is $9^\circ.18 \pm ^\circ.72$ or weight 1.9.

TABLE 13. —

CONTRIBUTIONS TO χ^2 FOR S-CORRECTIONS

		GROUP										
		1	2	3	4	5	6	7	8	9	10	11
	60	.8		.2								
	76						1.1	1.4	0.0			
	77						0.0			0.0		
	82							.3	0.0	.1		
E	88							.6	1.3			
P	45				1.0	0.0	.8	0.0	.4		0.0	
I	40	.2	.2	.2			0.0				.4	
C	4							6	0.0	.2		
E	13						0.0			0.0	0.0	0.0
N	16				5.2	0.0						
T	21						0.0	.3				2.4
R	27	.6		0.0	.2					0.0		
E	31						0.0		.2	.3	0.0	.8
	94	.2		1.6								
	96							4.2	.1			1.5
	95	2.6		2.6	0.0	.8	.2	.7		0.0		
	98	.2	.2									
	102						.1	4.3	0.0	1.6		

χ^2 is 42.9 on 51 degrees of freedom

TABLE 14. — Corrections to S by Direct Method.

Δ (deg)	Corrections to Tables		Corrections to Origin Time		
	Correc- tion (sec)	Weight	Quake	Correc- tion (sec)	Weight
0-3	0.0	87	1	+ .7	23
3-5	+2	34	23	—1.2	29
5-9	+1	49	40	+ .1	29
9-12	+3	18	47	— .6	28
12-14	—3	4	48	.0	55
14-16	—1	2	60	+ .5	49
16-18	+7	2	83	— .1	50

TABLE 15. — Contributions to χ^2 (Direct Method)

Quake	Δ	0-3	3-5	5-9	9-12	12-14	14-16	16-18
1		1.2	5.7	.2	14.4	1.3	.6	
23		6.5	2.2	6.1	.6		.4	
40		1.9	3.4	.3	.2	1.6		8.1
47		5.0	13.7	13.0	1.5			8.1
48		.1	.8	9.3	5.0			
60		13.3	.7	12.3	2.4			
83		.3	.1	.4				

As in the case of P, an estimate of t_s can be found from observations of sS-S intervals. Unfortunately no routine observations of sS were available at the time of this study but Prof. ROTHE and his staff at the Bureau Central International de Séismologie kindly supplied me with readings of sS for a number of earthquakes of which four gave accurate results.

Using the same method as that for pP-P intervals, δt_s was $-.14 \pm .24$ for the three earthquakes in Southern Honshu. The other, in Hokkaido, yielded a correction to t_s of $+2'.16 \pm '.27$ which tends to confirm the suggestion of a thicker crust in Hokkaido. The standard was $9'.2$ so t_s is $9'.06 \pm '.24$. χ^2 was 1.8 on 2 d. f. Combining the two estimates of t_s does not alter the sS-S figure and, from (10), the S-intercept, t_s , is $11'.46 \pm '.3$.

The times from the second, or direct, method, t_b , are relative to $t_s = 10'.7$ so $.76$ had to be added to them; the time from the first, or matching, technique, t_m , are relative to $t_s = 11'.6$ so $.14$ had to be subtracted from them. They were then combined in the usual way to obtain the 1965 Times. It was found that for the first 17°, the cubic

$t_{1965} = (11.46 \pm .3) + (25.39 \pm .09)\Delta - (.0033 \pm .00044)(\Delta - .5)^3$ (15)
gave the best fit. χ^2 from the original observations was 36.3 on 41 degrees of freedom, a normal value.

The same procedure as was used in smoothing the P-corrections was adopted for S. In the range, $17^\circ \leq \Delta \leq 33^\circ$, the cubic.

$$t = -150.2 + 47.51 \Delta - .953 \Delta^2 + 9.35 \times 10^{-3} \Delta^3 \quad (16)$$

was found to give the best fit yielding a χ^2 of 17.7 on 25 d. f. (15) and (16) intersect at $16^\circ.9$ with nearly equal slopes as was the case for P. This point is, however, $1^\circ.1$ more distant than for P but does not lead to impossible values for Poisson's ratio. By way of comparison, the 20° discontinuity was $1^\circ.4$ further on for S than for P in the 1940 tables.

For distances greater than 33° , the corrections were again taken at the quarter and three-quarter points and the resulting table subjected to second difference smoothing as shown in Table 16. It should be noted that throughout the smoothing process, no correction was changed by an amount more than one-half its standard error.

TABLE 16. — Smoothing Distant Corrections.

Δ	Correction	Differences		Smoothed Corrections	Differences	
(deg)	(sec)	1st	2nd	(sec)	1st	2nd
22	-1.45	0		-1.66	+ .54	
24	-1.45	+1.25	+1.25	-1.14	+ .63	+ .09
27	- .20	0	-1.25	- .51	+ .03	- .60
33	- .20	-1.11	-1.11	- .48	- .55	- .58
40	-1.31	0	+1.11	-1.03	- .19	+ .36
50	-1.31	+ .38	+ .38	-1.22	+ .19	+ .38
60	- .93	0	- .38	-1.03	- .01	- .20
70	- .93	- .44	- .44	-1.04	- .22	- .21
80	-1.37	0	+ .44	-1.26	- .03	+ .19
90	-1.37			-1.29	- .01	+ .02
95				-1.30		

The procedure for adapting these tables to different depths of focus was identical with that used for the 1965 P-Tables and finished S-Tables with the same tabular intervals as for P are given at the end of this paper as is the S-velocity distribution.

Comments

Perhaps the most important conclusion to be drawn from this study is the suggestion that regional differences are not confined to the upper-mantle and crust but extend deep into the mantle. This is shown by Figure 3 which gives corrections to the 1940 P-times obtained from, in addition to this work, one regional and two general studies of P-times. The means of each of these sets of corrections are unimportant since they only reflect assumptions concerning the crust. It should be noted, though, that in the distance range $20^\circ \leq \Delta \leq 45^\circ$, the 1965 Japanese times and the Herrin 1966 times have almost identical shapes. Comparison at lesser distances is not valid because the 1966 Herrin times are arbitrary in this range as indicated by the dashed line. At distances greater than 45° , however, there is a marked difference. The

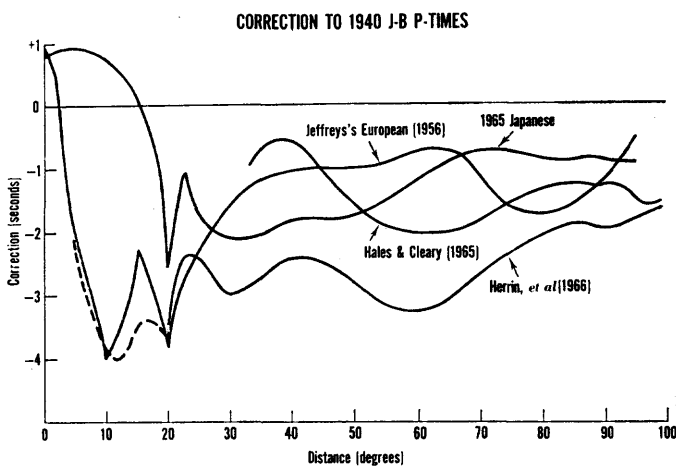


FIG. 3

Herrin corrections show a pronounced dip at about 60° which does not appear in the 1965 Japanese corrections. Herrin's dip is supported by Cleary and Hales's study but does not appear in the 1956 Jeffrey's European corrections. Since there is no reason to believe that any of these studies are not genuine, the only conclusion to be drawn is that there are regional differences in the mantle to a depth of nearly 2,000 kilometers. No check can be made using S-times as there are no other recent studies available.

The standard errors in the corrections, especially for S, are

larger than desirable but these will improve with the introduction of new data as the project continues.

Acknowledgments

The author wishes to acknowledge with gratitude the help, encouragement and inspiration so freely given him by Prof. Sir Harold JEFFREYS. He thanks the U. S. National Science Foundation and National Aeronautics and Space Administration for financial help and Lamont Geological Observatory and B. P. Refinery (Kent) Ltd. for the use of their facilities.

REFERENCES

- [1] JEFFREYS, Harold and BULLEN, K. E., *Seismological Tables*, British Association, London, (1940).
- [2] Cf. The Z. T. Tables, Bull. British Ass. Seism. Ctee., May, 1917.
- [3] JEFFREYS, Harold, M.N.R.A.S. geophys. Suppl., 4 (1939) p. 507.
- [4] JEFFREYS, Harold, M.N.R.A.S. geophys. Suppl., 5 (1947) p. 99.
- [5] WILLMORE, P. L., Phil. Trans. A, 242 p. 123.
- [6] JEFFREYS, Harold, M.N.R.A.S. geophys. Suppl., 6 (1954) pp. 557-65.
- [7] GUTENBERG, B., Bull. seism. Soc. Amer., 43 (1953) p. 223.
- [8] JEFFREYS, Harold, *Theory of Probability*, 3rd Edition, O.U.P. (1961) pp. 214-216.
- [9] GUTENBERG, B., *loc. cite*.
- [10] JEFFREYS, Harold, Private communication, 1962.
- [11] JEFFREYS, Harold, M.N.R.A.S. geophys. Suppl., 4 (1939) p. 424.
- [12] JEFFREYS, Harold, *Theory of Probability*, *loc. cite*, p. 223.
- [13] eg. BULLEN, K. E., *Intro. to Seismology*, C.U.P. (1963) p. 119 *et seq.*
- [14] JEFFREYS, Harold and JEFFREYS, B. S., *Mathematical Physics*, C.U.P. (1956) p. 289.
- [15] JEFFREYS, Harold, Private communication, 1965.

Geophysics Research Group,
U.S. Coast and Geodetic Survey,
Rockville, Maryland, U.S.A.

VELOCITIES OF P AND S IN JAPAN

r/R	α	β	r/R	α	β
	km/sec	km/sec		km/sec	km/sec
1.000	7.730	4.362	.765	12.079	6.649
.995	7.833	4.410	.760	12.121	6.667
.990	7.938	4.460	.755	12.163	6.684
.985	8.046	4.510	.750	12.206	6.701
.980	8.156	4.561	.745	12.249	6.717
.975	8.268	4.613	.740	12.291	6.734
.970	8.383	4.667	.735	12.334	6.750
.965	8.503	4.721	.730	12.376	6.766
.960	8.637	4.779	.725	12.417	6.782
.955	8.786	4.845	.720	12.458	6.798
.950	8.944	4.920	.715	12.499	6.812
.945	9.106	5.001	.710	12.540	6.827
.940	9.270	5.082	.705	12.581	6.844
.935	9.438	5.166	.700	12.621	6.861
.930	9.606	5.252	.695	12.662	6.879
.925	9.775	5.340	.690	12.703	6.895
.920	9.942	5.429	.685	12.744	6.911
.915	10.108	5.519	.680	12.785	6.926
.910	10.272	5.608	.675	12.825	6.941
.905	10.431	5.697	.670	12.865	6.956
.900	10.586	5.786	.665	12.905	6.970
.895	10.735	5.873	.660	12.946	6.985
.890	10.875	5.958	.655	12.986	7.001
.885	11.006	6.041	.650	13.027	7.016
.880	11.085	6.120	.645	13.067	7.030
.875	11.151	6.195	.640	13.106	7.044
.870	11.211	6.264	.635	13.146	7.058
.865	11.272	6.273	.630	13.185	7.073
.860	11.327	6.294	.625	13.224	7.089
.855	11.380	6.319	.620	13.262	7.104
.850	11.434	6.345	.615	13.300	7.120
.845	11.486	6.373	.610	13.337	7.136
.840	11.533	6.400	.605	13.374	7.153
.835	11.577	6.425	.600	13.410	7.169
.830	11.619	6.448	.595	13.445	7.185
.825	11.661	6.470	.590	13.480	7.201
.820	11.702	6.491	.585	13.514	7.218
.815	11.744	6.512	.580	13.546	7.235
.810	11.787	6.531	.575	13.577	7.252
.805	11.829	6.548	.570	13.605	7.269
.800	11.870	6.567	.565	13.629	7.283
.795	11.912	6.584	.560	13.653	7.296
.790	11.954	6.600	.555	13.676	7.310
.785	11.996	6.615	.550	13.700	7.327
.770	12.037	6.631	.545	13.724	7.348

TIMES OF P IN JAPAN

Δ	Depth $h =$						
	Surface	.00	.01	.02	.03	.04	.05
°	s	s	s	s	s	s	s
0	7.582	5.440	13.537	21.421	29.093	36.542	43.761
1	21.923	18.119	20.542	25.973	32.377	39.081	45.817
2	36.250	32.431	33.264	36.256	40.635	45.818	51.398
3	50.550	46.718	46.848	48.508	51.403	55.153	59.510
4	64.810	60.966	60.618	61.443	63.281	65.916	69.181
5	79.015	75.161	74.433	74.627	75.698	77.455	79.806
6	93.152	89.286	88.213	87.922	88.364	89.420	90.976
7	107.209	103.329	101.915	101.232	101.144	101.603	102.478
8	121.170	117.274	115.567	114.485	113.945	113.916	114.172
9	135.024	131.108	129.125	127.683	126.743	126.229	125.945
10	148.755	144.814	142.548	140.771	139.447	138.499	137.686
11	162.351	158.380	155.839	153.755	152.077	150.662	149.370
12	175.798	171.789	168.977	166.592	164.546	162.636	160.936
13	189.082	185.028	181.956	179.271	176.818	174.425	172.334
14	202.191	198.081	194.746	191.726	188.820	186.013	183.548
15	215.110	210.935	207.310	203.867	200.541	197.383	194.559
16	227.808	223.618	219.533	215.617	211.958	208.493	205.349
17	240.125	235.829	231.243	227.057	223.082	219.344	215.907
18	251.995	247.606	242.706	238.196	233.925	229.928	226.248
19	263.448	258.978	253.793	249.018	244.499	240.247	236.348
20	274.514	269.971	264.540	259.536	254.804	250.345	246.231
21	285.221	280.616	274.971	269.773	264.851	260.216	255.918
22	295.600	290.940	285.108	279.753	274.654	269.857	265.410
23	305.679	300.972	294.992	289.476	284.244	279.313	274.729
24	315.490	310.741	304.624	298.987	293.640	288.589	283.902
25	325.061	320.277	314.053	308.308	302.859	297.717	292.924
26	334.423	329.609	323.296	317.460	311.922	306.698	301.843
27	343.605	338.766	332.373	326.466	320.866	315.597	310.701
28	352.630	347.770	341.325	335.378	329.740	324.437	319.513
29	361.539	356.665	350.202	344.224	338.560	333.235	328.299
30	370.388	365.508	359.023	353.026	347.347	342.027	337.096
31	379.216	374.333	367.810	361.815	356.142	350.799	345.815
32	388.008	383.121	376.605	370.594	364.881	359.483	354.449
33	396.750	391.856	385.346	379.285	373.530	368.097	363.035
34	405.438	400.537	393.994	387.902	382.126	376.666	371.574
35	414.074	409.165	402.588	396.477	390.674	385.173	380.039
36	422.647	417.730	411.137	404.992	399.148	393.618	388.453
37	431.159	426.234	419.614	413.440	407.566	402.018	396.823
38	439.615	434.683	428.033	421.838	415.944	410.361	405.121
39	448.014	443.075	436.403	430.178	424.249	418.632	413.348
40	456.349	451.402	444.701	438.447	432.481	426.825	421.513
41	464.615	459.659	452.930	446.642	440.649	434.966	429.631
42	472.815	467.851	461.096	454.784	448.764	443.058	437.690
43	480.954	475.983	469.204	462.873	456.829	451.093	445.693
44	489.037	484.059	477.259	470.903	464.839	459.071	453.649
45	497.065	492.080	485.260	478.878	472.791	466.995	461.544
46	505.040	500.050	493.204	486.801	480.689	474.863	469.377
47	512.959	507.962	501.097	494.669	488.525	482.668	477.148
48	520.817	515.812	508.920	502.468	496.292	490.407	484.853
49	528.609	523.596	516.678	510.195	503.993	498.077	492.491
50	536.332	531.312	524.371	517.855	511.626	505.678	500.056

TIMES OF P IN JAPAN

Δ	Depth $h =$						
	.06	.07	.08	.09	.10	.11	.12
°	s	s	s	s	s	s	s
0	50.727	57.449	63.940	70.217	76.300	82.211	87.983
1	52.424	58.928	65.164	71.334	77.307	83.120	88.827
2	57.137	62.917	68.666	74.364	79.988	85.517	90.993
3	64.201	69.104	74.112	79.176	84.243	89.310	94.399
4	72.871	76.866	81.075	85.431	89.890	94.415	99.003
5	82.584	85.724	89.164	92.797	96.606	100.552	104.627
6	92.972	95.342	98.020	100.984	104.149	107.510	111.052
7	103.779	105.446	107.448	109.744	112.308	115.106	118.122
8	114.829	115.867	117.242	118.940	120.928	123.173	125.694
9	126.030	126.478	127.275	128.419	129.865	131.607	133.638
10	137.261	137.200	137.461	138.079	139.028	140.297	141.881
11	148.462	147.907	147.718	147.857	148.331	149.148	150.328
12	159.593	158.582	157.947	157.673	157.725	158.120	158.916
13	170.596	169.185	168.142	167.461	167.140	167.171	167.588
14	181.436	179.662	178.265	177.214	176.532	176.231	176.322
15	192.088	189.993	188.267	186.900	185.895	185.264	185.101
16	202.569	200.153	198.139	196.475	195.205	194.283	193.903
17	212.851	210.168	207.860	205.946	204.423	203.278	202.692
18	222.930	220.006	217.448	215.297	213.556	212.211	211.478
19	232.828	229.659	226.900	224.543	222.592	221.078	220.251
20	242.508	239.161	236.216	233.682	231.547	229.911	229.001
21	252.008	248.506	245.401	242.700	240.440	238.718	237.713
22	261.354	257.700	254.457	251.629	249.283	247.511	246.374
23	270.546	266.760	263.404	260.499	258.089	256.299	255.003
24	279.601	275.711	272.286	269.322	266.878	265.035	263.600
25	288.548	284.595	281.114	278.113	275.667	273.698	272.164
26	297.422	293.425	289.906	286.911	284.394	282.308	280.685
27	306.241	302.219	298.694	295.670	293.043	290.880	289.155
28	315.027	311.012	307.455	304.332	301.641	299.407	297.582
29	323.822	319.775	316.134	312.932	310.201	307.881	305.970
30	332.570	328.449	324.750	321.503	318.698	316.308	314.313
31	341.229	337.060	333.323	330.019	327.133	324.691	322.609
32	349.827	345.628	341.840	338.472	335.532	333.017	331.055
33	358.378	354.136	350.295	346.878	343.886	341.278	339.188
34	366.870	362.582	358.701	355.238	352.173	349.480	346.841
35	375.305	370.982	367.058	363.535	360.397	357.632	355.237
36	383.692	379.326	375.352	371.763	368.564	365.741	363.279
37	392.015	387.603	383.570	379.928	376.682	373.805	371.274
38	400.269	395.805	391.726	388.047	384.751	381.820	379.222
39	408.455	403.950	399.842	396.114	392.770	389.781	387.121
40	416.588	412.049	407.903	404.129	400.733	397.692	394.967
41	424.670	420.097	415.909	412.090	408.648	405.551	402.755
42	432.701	428.093	423.861	420.005	416.514	413.352	410.490
43	440.673	436.034	431.763	427.867	424.315	421.094	418.164
44	448.593	443.916	439.606	435.660	432.052	428.774	425.776
45	456.462	451.738	447.385	443.392	439.730	436.390	433.326
46	464.259	459.500	455.100	451.053	447.342	443.944	440.812
47	471.993	467.197	462.748	458.655	454.888	451.430	448.233
48	479.659	474.823	470.333	466.190	462.368	458.848	455.590
49	487.257	482.382	477.846	473.650	469.775	466.201	462.881
50	494.784	489.869	485.285	481.044	477.120	473.484	470.109

TIMES OF P IN JAPAN

△	Depth $h =$						
	Surface	.00	.01	.02	.03	.04	.05
°	s	s	s	s	s	s	s
51	543.985	538.956	531.989	525.446	519.187	513.208	507.549
52	551.565	546.529	539.533	532.967	526.672	520.665	514.974
53	559.073	554.028	547.008	540.410	534.091	528.046	522.322
54	566.507	561.455	554.409	547.783	541.433	535.355	529.599
55	573.866	568.805	561.735	555.082	548.699	542.590	536.798
56	581.149	576.080	568.979	562.297	555.885	549.744	543.917
57	588.355	583.277	576.148	569.439	562.993	556.821	550.965
58	595.481	590.396	583.238	576.498	570.029	563.826	557.931
59	602.528	597.435	590.253	583.486	576.982	570.748	564.813
60	609.492	604.390	597.180	590.384	583.844	577.579	571.618
61	616.370	611.260	604.020	597.194	590.635	584.334	578.339
62	623.165	618.046	610.782	603.932	597.342	591.012	584.983
63	629.878	624.751	617.460	610.585	603.967	597.611	591.554
64	636.512	631.377	624.060	617.162	610.517	604.135	598.048
65	643.067	637.925	630.587	623.661	616.992	610.587	604.466
66	649.546	644.397	637.037	630.087	623.394	616.953	610.808
67	655.946	650.790	643.407	636.432	629.708	623.249	617.077
68	662.267	657.104	649.695	642.696	635.950	629.465	623.261
69	668.508	663.337	655.907	648.889	642.110	635.592	629.363
70	674.666	669.488	662.035	654.990	648.194	641.647	635.392
71	680.743	675.558	668.087	661.016	654.190	647.619	641.338
72	686.739	681.547	674.052	666.959	660.110	653.519	647.209
73	692.656	687.457	679.939	672.822	665.955	659.340	653.003
74	698.494	693.289	685.750	678.615	671.724	665.080	658.722
75	704.252	699.040	691.481	684.322	677.410	670.742	664.351
76	709.927	704.709	697.126	689.948	683.010	676.317	669.908
77	715.523	710.298	702.696	695.498	688.540	681.831	675.393
78	721.041	715.810	708.189	700.971	693.993	687.261	680.807
79	726.485	721.248	713.607	706.373	699.374	692.619	686.143
80	731.853	726.610	718.954	711.696	704.681	697.911	691.409
81	737.147	731.899	724.223	716.951	709.914	703.126	696.606
82	742.369	737.116	729.426	722.133	715.081	708.274	701.738
83	747.522	742.264	734.560	727.255	720.182	713.358	706.805
84	752.608	747.345	739.628	732.307	725.219	718.377	711.804
85	757.627	752.359	744.627	737.288	730.186	723.325	716.738
86	762.580	757.308	749.558	742.205	735.093	728.218	721.614
87	767.471	762.195	754.433	747.071	739.940	733.052	726.433
88	772.304	767.024	759.252	751.874	744.734	737.833	731.200
89	777.084	771.800	764.017	756.631	749.476	742.565	735.921
90	781.816	776.530	768.735	761.340	754.180	747.260	740.603
91	786.507	781.217	773.416	766.009	758.843	751.911	745.248
92	791.153	785.860	778.051	770.638	763.457	756.513	749.856
93	795.751	790.456	782.631	775.227	768.022	761.066	754.427
94	800.301	795.002	787.147	779.776	772.538	765.570	
95	804.803	799.499					

TIMES OF P IN JAPAN

△	Depth $h =$						
	.06	.07	.08	.09	.10	.11	.12
°	s	s	s	s	s	s	s
51	502.239	497.281	492.663	488.372	484.395	480.701	477.261
52	509.626	504.627	499.963	495.626	491.595	487.849	484.340
53	516.942	511.900	507.192	502.806	498.725	494.921	491.354
54	524.181	519.100	514.345	509.914	505.777	501.921	498.303
55	531.344	526.221	521.425	516.943	512.764	508.850	505.161
56	538.423	533.266	528.429	523.906	519.670	515.695	511.957
57	545.434	540.238	535.356	530.778	526.493	522.474	518.678
58	552.364	547.124	542.199	537.576	533.244	529.177	525.326
59	559.211	553.930	548.969	544.304	539.923	535.803	531.900
60	565.981	560.662	555.656	550.949	546.527	542.360	538.413
61	572.669	567.313	562.272	557.527	553.062	548.847	544.852
62	579.279	573.893	568.817	564.031	559.523	555.261	551.221
63	585.816	580.398	575.286	570.457	565.906	561.606	557.514
64	592.281	586.827	581.674	576.812	572.221	567.874	563.738
65	598.668	593.183	587.995	583.096	578.462	574.074	569.886
66	604.980	599.461	594.240	589.298	584.625	580.191	575.962
67	611.214	605.662	600.401	595.425	590.715	586.236	581.963
68	617.365	611.782	606.489	601.479	596.724	592.209	587.888
69	623.444	617.823	612.497	607.452	602.656	598.101	593.744
70	629.439	623.787	618.430	613.438	608.519	603.930	599.529
71	635.359	629.677	624.287	619.171	614.314	609.681	605.239
72	641.203	635.495	630.076	624.924	620.026	615.351	610.873
73	646.969	641.234	635.777	630.595	625.657	620.949	616.433
74	642.659	646.889	641.404	636.186	631.218	626.479	621.928
75	658.262	652.464	646.955	641.711	636.710	631.935	627.350
76	663.797	657.978	652.436	647.161	642.132	637.322	632.700
77	669.258	663.410	657.842	652.539	647.480	642.639	637.988
78	674.645	668.772	663.180	657.848	652.762	647.887	643.204
79	679.960	674.062	668.445	663.090	657.973	653.072	648.358
80	685.203	679.289	673.643	668.260	663.118	658.191	653.449
81	690.381	684.441	678.773	673.369	668.201	663.249	658.478
82	695.493	689.530	683.843	678.414	673.222	668.240	663.442
83	700.541	694.556	688.848	683.394	678.174	673.169	668.346
84	705.520	699.516	693.785	688.309	683.069	678.045	673.197
85	710.435	704.414	698.666	693.171	687.913	682.864	677.997
86	715.294	709.258	703.490	697.979	692.699	687.632	682.746
87	720.100	714.048	708.264	702.736	697.440	692.358	687.456
88	724.853	718.789	712.990	707.449	702.138	697.043	692.126
89	729.564	723.489	717.678	712.122	706.800	701.688	696.750
90	734.236	728.148	722.323	716.754	711.417	706.293	701.328
91	738.864	732.760	726.924	721.345	715.989	710.858	705.860
92	743.448	737.325	731.481	725.895	720.516	715.383	710.346
93	747.988	741.843	735.994				

TIMES OF P FOR SMALL DEPTHS AND DISTANCES

Δ	Depth $h =$						
	.000	.005	.010	.015	.020	.025	.030
0.0	5.440	9.515	13.537	17.506	21.421	25.283	29.093
.1	5.790	9.605	13.595	17.530	21.482	25.317	29.141
.2	6.661	9.937	13.867	17.708	21.638	25.433	29.255
.3	8.093	10.569	14.278	18.065	21.883	25.633	29.433
.4	9.526	11.433	14.845	18.493	22.212	25.918	29.672
.5	10.958	12.473	15.546	19.031	22.640	26.289	29.970
.6	12.390	13.617	16.387	19.669	23.158	26.724	30.324
.7	13.823	14.847	17.319	20.408	23.759	27.227	30.750
.8	15.255	16.106	18.324	21.220	24.425	27.795	31.237
.9	16.687	17.415	19.413	22.103	25.168	28.424	31.786
1.0	18.119	18.745	20.542	23.057	25.973	29.109	32.377
1.1	19.551	20.090	21.712	24.062	26.824	29.857	33.029
1.2	20.983	21.450	22.919	25.109	27.735	30.648	33.722
1.3	22.414	22.824	24.164	26.189	28.695	31.480	34.465
1.4	23.846	24.200	25.424	27.320	29.685	32.354	35.242
1.5	25.277	25.580	26.699	28.460	30.715	33.280	36.063
1.6	26.708	26.965	27.984	29.639	31.766	34.226	36.912
1.7	28.139	28.353	29.301	30.838	32.848	35.210	37.796
1.8	29.570	29.743	30.606	32.057	33.963	36.218	38.721
1.9	31.001	31.134	31.935	33.292	35.105	37.257	39.644
2.0	32.431	32.526	33.264	34.533	36.256	38.315	40.635
2.1	33.861	33.921	34.611	35.798	37.420	39.393	41.630
2.2	35.291	35.317	35.961	37.071	38.605	40.489	42.648
2.3	36.721	36.714	37.310	38.352	39.811	41.605	43.691
2.4	38.150	38.113	38.664	39.633	41.014	42.739	44.749
2.5	39.579	39.513	40.022	40.943	42.249	43.893	45.824
2.6	41.007	40.914	41.383	42.237	43.489	45.065	46.913
2.7	42.436	42.317	42.747	43.539	44.728	46.223	48.017
2.8	43.864	43.720	44.113	44.865	45.982	47.415	49.134
2.9	45.291	45.124	45.480	46.185	47.236	48.611	50.263
3.0	46.718	46.530	46.848	47.504	48.508	49.808	51.403
3.1	48.145	47.936	48.218	48.827	49.777	51.030	52.554
3.2	49.572	49.342	49.590	50.161	51.057	52.249	53.713
3.3	50.998	50.749	50.964	51.501	52.343	53.479	54.881
3.4	52.423	52.157	52.339	52.839	53.636	54.714	56.055
3.5	53.848	53.565	53.716	54.176	54.928	55.957	57.235
3.6	55.273	54.974	55.095	55.515	56.217	57.205	58.429
3.7	56.697	56.382	56.474	56.857	57.515	58.452	59.634
3.8	58.121	57.791	57.855	58.201	58.819	59.707	60.837
3.9	59.544	59.200	59.236	59.546	60.129	60.978	62.060
4.0	60.966	60.608	60.618	60.894	61.443	62.245	63.281
4.1	62.389	62.017	62.001	62.241	62.754	63.514	64.498
4.2	63.810	63.425	63.384	63.590	64.065	64.787	65.724
4.3	65.231	64.834	64.765	64.940	65.376	66.060	66.959
4.4	66.651	66.241	66.147	66.291	66.691	67.336	68.198
4.5	68.071	67.648	67.528	67.642	68.009	68.617	69.440
4.6	69.490	69.055	68.909	68.994	69.330	69.904	70.684
4.7	70.909	70.461	70.291	70.347	70.653	71.192	71.930
4.8	72.327	71.866	71.672	71.701	71.977	72.480	73.182
4.9	73.744	73.270	73.053	73.055	73.301	73.769	74.438
5.0	75.161	74.674	74.433	74.409	74.627	75.060	75.698

TIMES OF S IN JAPAN

Δ	Depth $h =$						
	Surface	0.00	0.01	0.02	0.03	0.04	0.05
°	s	s	s	s	s	s	s
0	(11.460)	(9.06)	23.428	37.492	51.240	64.661	77.745
1	36.849	31.070	35.591	45.457	57.038	69.166	81.417
2	62.228	56.432	58.102	63.614	71.661	81.134	91.360
3	87.578	81.762	82.219	85.393	90.752	97.782	105.875
4	112.877	107.039	106.693	108.427	111.971	117.007	123.187
5	138.107	132.242	131.253	131.939	134.169	137.667	142.264
6	163.247	157.353	155.794	155.656	156.826	159.091	162.387
7	188.278	182.352	180.295	179.462	179.733	180.963	183.119
8	213.179	207.219	204.703	203.219	202.740	203.129	204.243
9	237.931	231.934	228.935	226.889	225.732	225.432	225.605
10	262.513	256.476	253.064	250.453	248.674	247.704	246.985
11	286.906	280.824	276.987	273.888	271.497	269.885	268.304
12	311.090	304.961	300.709	297.088	294.172	291.877	289.495
13	335.045	328.865	324.188	320.119	316.726	313.566	310.453
14	358.751	352.517	347.435	342.910	338.906	334.925	331.135
15	382.188	375.895	370.416	365.436	360.726	355.934	351.508
16	405.336	398.981	393.109	387.571	381.953	376.568	371.482
17	428.176	421.753	415.401	408.984	402.743	396.735	391.072
18	450.986	444.428	436.862	429.823	423.005	416.426	410.188
19	472.854	466.042	457.799	450.123	442.702	435.587	428.871
20	493.884	486.865	478.012	469.792	461.864	454.283	447.098
21	514.129	506.932	497.563	488.853	480.489	472.489	464.930
22	533.648	526.294	516.461	507.358	498.611	490.255	482.339
23	552.496	545.007	534.800	525.341	516.254	507.573	499.351
24	570.729	563.123	552.592	542.822	533.456	524.495	516.001
25	588.403	580.696	569.895	559.865	550.239	541.039	532.309
26	605.575	597.781	586.745	576.498	566.652	557.236	548.318
27	622.301	614.432	603.200	592.760	582.724	573.152	564.082
28	638.635	630.704	619.309	608.711	598.545	588.827	579.608
29	654.638	646.656	635.139	624.403	614.116	604.307	595.091
30	670.287	662.300	650.710	639.886	629.600	619.809	610.574
31	685.776	677.752	666.190	655.388	645.091	635.280	626.020
32	701.163	693.097	681.678	670.863	660.545	650.708	641.417
33	716.516	708.439	697.131	686.296	675.949	666.081	656.751
34	731.884	723.815	712.533	701.674	691.290	681.384	672.011
35	747.278	739.215	727.874	716.983	706.556	696.606	687.148
36	762.650	754.601	743.139	732.209	721.704	711.679	702.185
37	777.956	769.900	758.282	747.280	736.739	726.692	717.178
38	793.196	785.100	773.317	762.291	751.732	741.668	732.156
39	808.302	800.192	788.311	777.269	766.713	756.610	747.004
40	823.306	815.181	803.298	792.219	781.581	771.380	761.697
41	838.197	830.055	818.153	806.987	796.283	786.029	776.287
42	852.963	844.804	832.840	821.637	810.869	800.570	790.766
43	867.605	859.428	847.417	836.173	825.352	815.009	805.158
44	882.133	873.941	861.891	850.600	839.752	829.358	819.466
45	896.557	888.351	876.280	864.947	854.064	843.610	833.672
46	910.890	902.672	890.578	879.194	868.261	857.766	847.776
47	925.129	916.898	904.764	893.342	882.365	871.830	861.781
48	939.273	931.029	918.852	907.401	896.374	885.790	875.691
49	953.311	945.052	932.843	921.348	910.279	899.651	889.508

TIMES OF S IN JAPAN

△	Depth $h =$						
	0.06	0.07	0.08	0.09	0.10	0.11	0.12
0	90.430	102.709	114.587	126.083	137.218	148.020	158.523
1	93.546	105.396	116.880	128.215	139.028	149.661	159.997
2	101.897	112.527	123.096	133.638	143.875	153.999	163.897
3	114.575	123.653	132.914	142.249	151.589	160.876	170.107
4	130.158	137.642	145.478	153.578	161.802	170.120	178.495
5	147.639	153.617	160.102	166.908	173.985	181.253	188.685
6	166.389	171.013	176.147	181.721	187.673	193.896	200.360
7	185.915	189.328	193.254	197.667	202.493	207.699	213.210
8	205.931	208.240	211.073	214.405	218.191	222.383	226.977
9	226.266	227.535	229.350	231.681	234.492	237.745	241.416
10	246.769	247.078	247.924	249.307	251.202	253.586	256.418
11	267.243	266.700	266.677	267.170	268.196	269.745	271.776
12	287.645	286.282	285.430	285.148	285.375	286.132	287.407
13	307.880	305.760	304.136	303.094	302.611	302.661	303.213
14	327.826	325.025	322.724	320.984	319.811	319.204	319.131
15	347.511	344.016	341.096	338.747	336.947	335.710	335.048
16	366.873	362.756	359.232	356.290	353.960	352.153	350.938
17	385.834	381.186	377.122	373.630	370.766	368.483	366.783
18	404.458	399.278	394.712	390.757	387.391	384.622	382.545
19	422.674	417.043	412.010	407.620	403.816	400.624	398.139
20	440.495	434.453	429.032	424.220	420.015	416.491	413.637
21	457.917	451.527	445.741	440.562	436.010	432.189	429.113
22	474.987	468.231	462.148	456.643	451.848	447.707	444.594
23	491.701	484.650	478.247	472.539	467.473	463.175	460.044
24	508.094	500.787	494.141	488.208	482.933	478.660	475.453
25	524.163	516.671	509.827	503.650	498.424	494.113	490.812
26	540.011	532.321	525.300	519.128	513.886	509.523	506.110
27	555.611	547.797	540.799	534.595	529.309	524.879	521.340
28	571.079	563.297	556.273	550.031	544.681	540.170	536.446
29	586.570	578.766	571.710	565.423	559.991	555.384	551.476
30	602.029	594.194	587.095	580.755	575.229	570.456	566.470
31	617.443	609.567	602.418	596.015	590.346	585.471	581.460
32	632.800	624.873	617.664	611.151	605.380	600.441	596.387
33	648.086	640.101	632.775	626.191	620.369	615.391	611.154
34	663.279	655.183	647.803	641.183	635.339	630.223	625.801
35	678.337	670.201	662.791	656.152	650.208	644.930	640.351
36	693.343	685.180	677.771	671.014	664.935	659.534	654.825
37	708.321	700.142	692.614	685.732	679.550	674.041	669.225
38	723.239	714.949	707.304	700.349	694.057	688.459	683.549
39	737.995	729.622	721.893	714.851	708.474	702.797	697.778
40	752.628	744.184	736.383	729.260	722.820	717.046	711.920
41	767.150	758.643	750.783	743.595	737.073	731.206	725.983
42	781.573	773.017	765.096	757.840	751.232	745.283	739.952
43	795.913	787.300	779.320	771.989	765.308	759.255	753.826
44	810.159	801.482	793.447	786.039	779.279	773.131	767.614
45	824.311	815.574	807.471	799.992	793.153	786.928	781.343
46	838.377	829.569	821.398	813.855	806.947	800.660	794.998
47	852.323	843.463	835.232	827.635	820.664	814.315	808.551
48	866.173	857.265	848.984	841.342	834.303	827.873	822.008
49	879.943	870.998	862.667	854.956	847.848	841.324	835.377

TIMES OF S IN JAPAN

Δ	Depth $h =$						
	Surface	0.00	0.01	0.02	0.03	0.04	0.05
°	s	s	s	s	s	s	s
50	967.241	958.969	946.734	935.195	924.085	913.422	903.248
51	981.079	972.796	960.531	948.954	937.820	927.123	916.906
52	994.836	986.542	974.252	962.645	951.477	940.727	930.458
53	1008.507	1000.201	987.883	976.236	965.018	954.224	943.903
54	1022.078	1013.759	1001.408	989.722	978.456	967.621	957.261
55	1035.547	1027.216	1014.831	1003.108	991.806	980.931	970.531
56	1048.915	1040.571	1028.151	1016.404	1005.065	994.155	983.708
57	1062.197	1053.843	1041.394	1029.605	1018.234	1007.294	996.812
58	1075.394	1067.030	1054.561	1042.729	1031.310	1020.289	1009.731
59	1088.483	1080.104	1067.590	1055.695	1044.221	1033.145	1022.551
60	1101.431	1093.035	1080.468	1068.533	1057.014	1045.905	1035.254
61	1114.245	1105.833	1093.239	1081.269	1069.698	1058.548	1047.856
62	1126.949	1118.525	1105.900	1093.885	1082.281	1071.084	1060.341
63	1139.548	1131.112	1118.443	1106.386	1094.744	1083.498	1072.698
64	1152.027	1143.575	1130.863	1118.771	1107.086	1095.800	1084.940
65	1164.385	1155.920	1143.178	1131.052	1119.314	1107.975	1097.080
66	1176.625	1168.147	1155.371	1143.192	1131.421	1120.041	1109.101
67	1188.745	1180.253	1167.440	1155.233	1143.406	1131.983	1121.009
68	1200.743	1192.239	1179.388	1167.146	1155.283	1143.839	1132.824
69	1212.636	1204.121	1191.241	1178.966	1167.072	1155.580	1144.516
70	1224.424	1215.896	1202.990	1190.671	1178.730	1167.174	1156.055
71	1236.083	1227.540	1214.594	1202.221	1190.229	1178.619	1167.448
72	1247.587	1239.027	1226.037	1213.616	1201.578	1189.925	1178.697
73	1258.940	1250.366	1237.326	1224.874	1212.801	1201.115	1189.853
74	1270.170	1261.583	1248.513	1236.026	1223.919	1212.202	1200.902
75	1281.287	1272.689	1259.600	1247.075	1234.936	1223.172	1211.841
76	1292.289	1283.679	1270.566	1258.007	1245.824	1234.028	1222.650
77	1303.174	1294.553	1281.404	1268.814	1256.594	1244.763	1233.342
78	1313.948	1305.317	1292.139	1279.507	1267.251	1255.375	1243.908
79	1324.595	1315.951	1302.737	1290.071	1277.772	1265.854	1254.353
80	1335.108	1326.450	1313.196	1300.501	1288.178	1276.226	1264.688
81	1345.498	1336.830	1323.558	1310.829	1298.474	1286.486	1274.924
82	1355.785	1347.107	1333.804	1321.057	1308.671	1296.644	1285.021
83	1365.952	1357.263	1343.940	1331.132	1318.703	1306.640	1294.977
84	1375.977	1367.275	1353.903	1341.071	1328.598	1316.488	1304.786
85	1385.849	1377.134	1363.729	1350.854	1338.345	1326.193	1314.445
86	1395.570	1386.840	1373.407	1360.492	1347.939	1335.744	1323.959
87	1405.142	1396.401	1382.931	1369.984	1357.393	1345.166	1333.346
88	1414.577	1405.823	1392.322	1379.351	1366.727	1354.462	1342.595
89	1423.876	1415.111	1401.581	1388.567	1375.905	1363.593	1351.688
90	1433.023	1324.245	1410.679	1397.614	1384.927	1372.583	1360.638
91	1442.012	1433.223	1419.623	1406.535	1393.807	1381.436	1369.462
92	1450.868	1442.070	1428.446	1415.342	1402.585	1390.195	1378.199
93	1459.629	1450.823	1437.185	1424.055	1411.283	1398.866	1386.839
94	1468.290	1459.475	1445.815	1432.682	1419.853		
95	1476.831	1467.997					

TIMES OF S IN JAPAN

△	Depth $h =$						
	0.06	0.07	0.08	0.09	0.10	0.11	0.12
°	s	s	s	s	s	s	s
50	893.643	884.653	876.254	868.468	861.277	854.687	848.666
51	907.256	898.200	889.737	881.883	874.623	867.968	861.875
52	920.758	911.635	903.122	895.210	887.888	881.168	875.012
53	934.151	924.988	916.417	908.451	901.074	894.288	888.003
54	947.463	938.255	929.633	921.615	914.192	907.270	900.871
55	960.692	951.431	942.779	934.677	927.126	920.128	913.643
56	973.840	964.525	955.776	947.587	939.964	932.880	926.323
57	986.854	977.457	968.628	960.381	952.694	945.538	938.899
58	999.723	990.269	981.382	973.074	965.319	958.091	951.361
59	1012.478	1002.978	994.040	985.671	977.835	970.528	963.719
60	1025.138	1015.584	1006.589	998.148	990.239	982.858	975.962
61	1037.687	1028.072	1019.018	1010.506	1002.536	995.079	988.105
62	1050.118	1040.443	1031.332	1022.761	1014.719	1007.184	1000.141
63	1062.438	1052.717	1043.528	1034.892	1026.788	1019.180	1012.057
64	1074.635	1064.854	1055.619	1046.922	1038.742	1031.073	1023.890
65	1086.720	1076.885	1067.596	1058.836	1050.608	1042.885	1035.626
66	1098.684	1088.803	1079.467	1070.668	1062.379	1054.573	1047.220
67	1110.552	1100.634	1091.240	1082.381	1074.009	1066.113	1058.666
68	1122.320	1112.346	1102.891	1093.943	1085.498	1077.524	1069.990
69	1133.954	1123.906	1114.385	1105.369	1096.848	1088.796	1081.202
70	1145.433	1135.321	1125.730	1116.660	1108.077	1099.968	1092.308
71	1156.767	1146.602	1136.963	1127.829	1119.204	1111.048	1103.321
72	1167.981	1157.779	1148.091	1138.913	1130.227	1122.014	1114.220
73	1179.089	1168.852	1159.115	1149.889	1141.141	1132.861	1125.004
74	1190.103	1179.815	1170.023	1160.746	1151.938	1143.591	1135.686
75	1200.986	1190.652	1180.820	1171.481	1162.629	1154.216	1146.231
76	1211.753	1201.378	1191.499	1182.104	1173.189	1164.719	1156.664
77	1222.417	1211.980	1202.041	1192.602	1183.625	1175.105	1166.998
78	1232.931	1222.450	1212.475	1202.987	1193.960	1185.386	1177.228
79	1243.338	1232.821	1222.795	1213.264	1204.198	1195.572	1187.347
80	1253.639	1243.078	1233.019	1223.441	1214.304	1205.611	1197.319
81	1263.838	1253.229	1243.113	1233.462	1224.281	1215.513	1207.152
82	1273.883	1263.230	1253.052	1243.354	1234.107	1225.280	1216.848
83	1283.784	1273.081	1262.857	1253.103	1243.786	1234.899	1226.400
84	1293.552	1282.793	1272.511	1262.700	1253.336	1244.379	1235.830
85	1303.161	1292.356	1282.025	1272.167	1262.753	1253.749	1245.136
86	1312.630	1301.788	1291.422	1281.511	1272.042	1262.980	1254.297
87	1321.985	1311.096	1300.677	1290.712	1281.180	1272.058	1263.319
88	1331.186	1320.241	1309.775	1299.762	1290.178	1281.004	1272.204
89	1340.237	1329.255	1318.736	1308.672	1299.044	1289.826	1280.992
90	1349.143	1338.119	1327.571	1317.474	1307.816	1298.566	1289.692
91	1357.938	1346.899	1336.319	1326.190	1316.500	1307.208	1298.340
92	1366.653	1355.584	1344.970	1334.811	1324.047		
93	1375.279	1364.129					

TIMES OF S FOR SMALL DISTANCES AND DEPTHS

Δ	Depth $h =$						
	0.00	0.005	0.010	0.015	0.020	0.025	0.030
s	s	s	s	s	s	s	s
0.0	(9.060)	16.277	23.428	30.500	37.492	44.405	51.240
.1	(9.630)	16.409	23.644	30.669	37.606	44.427	51.321
.2	(11.164)	16.934	23.993	31.012	37.882	44.779	51.519
.3	(13.331)	17.966	24.677	31.484	38.308	45.150	51.829
.4	15.846	19.442	25.653	32.206	38.875	45.628	52.250
.5	18.384	21.247	26.887	33.145	39.623	46.202	52.778
.6	20.921	23.245	28.307	34.254	40.524	46.934	53.409
.7	23.459	25.397	29.944	35.536	41.573	47.812	54.155
.8	25.996	27.623	31.700	36.975	42.750	48.815	55.016
.9	28.536	29.929	33.604	38.514	44.053	49.918	55.979
1.0	31.070	32.262	35.591	40.169	45.457	51.143	57.038
1.1	33.609	34.640	37.668	41.949	46.981	52.459	58.173
1.2	36.146	37.066	39.788	43.793	48.570	53.849	59.415
1.3	38.684	39.495	41.969	45.701	50.255	55.326	60.721
1.4	41.221	41.927	44.192	47.696	51.998	56.874	62.100
1.5	43.758	44.370	46.469	49.725	53.824	58.483	63.558
1.6	46.296	46.821	48.749	51.803	55.685	60.165	65.071
1.7	48.834	49.280	51.045	53.915	57.611	61.907	66.640
1.8	51.371	51.743	53.386	56.084	59.585	63.695	68.260
1.9	53.908	54.208	55.735	58.255	61.588	65.535	69.934
2.0	56.432	56.676	58.102	60.463	63.614	67.406	71.661
2.1	58.983	59.147	60.480	62.704	65.701	69.332	73.420
2.2	61.521	61.621	62.881	64.971	67.817	71.279	75.226
2.3	64.058	64.098	65.263	67.226	69.952	73.255	77.087
2.4	66.596	66.577	67.669	69.522	72.099	75.268	78.952
2.5	69.133	69.058	70.086	71.816	74.286	77.312	80.846
2.6	71.671	71.542	72.501	74.138	76.476	79.381	82.774
2.7	74.208	74.028	74.922	76.468	78.675	81.472	84.732
2.8	76.746	76.515	77.350	78.802	80.912	83.579	86.717
2.9	79.283	79.005	79.783	81.145	83.140	85.718	88.723
3.0	81.762	81.496	82.219	83.491	85.393	87.853	90.752
3.1	84.260	83.990	84.658	85.851	87.658	90.019	92.800
3.2	86.788	86.484	87.099	88.221	89.955	92.183	94.866
3.3	89.315	88.980	89.542	90.598	92.223	94.375	96.956
3.4	91.843	91.477	91.987	92.973	94.502	96.589	99.073
3.5	94.364	93.976	94.434	95.350	96.806	98.792	101.215
3.6	96.892	96.475	96.883	97.732	99.119	101.017	103.332
3.7	99.416	98.975	99.334	100.121	101.434	103.235	105.478
3.8	101.940	101.476	101.786	102.514	103.761	105.497	107.591
3.9	104.464	103.978	104.239	104.909	106.094	107.729	109.818
4.0	107.039	106.480	106.693	107.306	108.427	109.984	111.971
4.1	109.503	108.983	109.149	109.705	110.762	112.253	114.164
4.2	112.028	111.486	111.605	112.107	113.099	114.531	116.367
4.3	114.545	113.989	114.062	114.511	115.441	116.814	118.515
4.4	117.066	116.491	116.519	116.917	117.791	119.095	120.730
4.5	119.580	118.994	118.978	119.325	120.147	121.376	122.988
4.6	122.099	121.497	121.433	121.734	122.507	123.666	125.205
4.7	124.613	123.999	123.888	124.146	124.865	125.962	127.439
4.8	127.134	126.500	126.343	126.559	127.222	128.265	129.680
4.9	129.645	129.002	128.798	128.973	129.580	130.572	131.926
5.0	132.242	131.502	131.253	131.388	131.939	132.881	134.169



THE ANALYSIS OF P WAVES AT USSR STATIONS IN RELATION TO JEFFREYS-BULLEN TABLES*

by N. V. KONDORSKAYA

Delivered 4 October 1967 on the symposium "Travel Times" (Zürich)

Discussion of the problem of observed travel-times of P waves by first arrivals on the territory of the USSR is divided in the present paper into 2 parts :

1. The range of distances $0 < \Delta \leq 600$ km;
2. $600 \text{ km} < \Delta < 2500$ km.

I. — The range of distances $0 < \Delta \leq 600$ km.

Travel-times of P waves in this range are investigated in detail on the basis of results of the deep seismic sounding, registrations of large quarry blasts and also on the basis of precise regional investigations by observations of both stationare and expeditional seismic stations.

Deviations from Jeffreys-Bullen travel-time tables for P waves for different regions by data of DSS and large quarry blasts (GAMBURTSSEV, 1960; KOSMINSKAYA et al., 1958; TVALTVADZE et al., 1957) are given in Fig. 1.

It is possible to devide travel-time curves into two groups by the deviation character :

- 1) Those for continental regions (1, 2, 3 Fig. 1) which are shields and platforms (Kazakhstan, Turkmenia).
- 2) Those for mountain regions and deep depressions (5, 6, 7, Fig. 1).

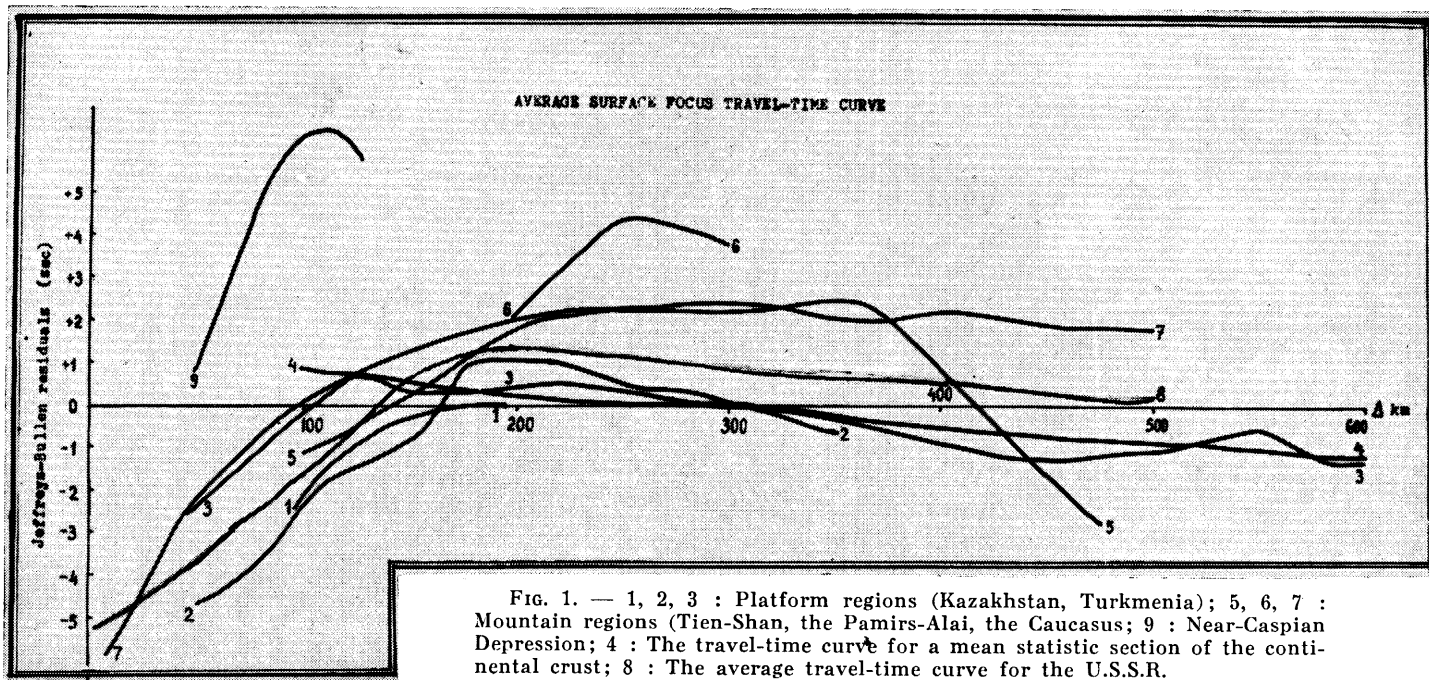
Near-Caspian Lowland occupies a detached position in the group of the travel-time curves (9, Fig. 1), that can be explained by the presence of a thick layer of loose sediments.

As one can see from Fig. 1, the character of coordination of those travel-time curves with those of J-B is different for different regions and different epicentral distances.

There are the following general regularities for different zones :

- 1) Residuals are negative at distances 0 to 100 km, and they are usually positive at distances greater than 120-140 km.

The greatest positive residuals are typical for mountain regions, in particular for the Pamirs-Alai zone with the greatest value of the earth crust thickness.



The first group of continental travel-time curves can be well approximated with a mean statistical travel-time curve constructed on the basis of a summary listed in the paper by Mc CONNEL and Mc TAGGART-COWAN "Crustal seismic refraction profiles" (1964) for a mean statistical section of the continental crust.

We have constructed an averaged travel-time curve on the basis of all the available knowledge on travel-time curves by data of the DSS and large quarry blasts on the territory of the USSR. This averaged travel-time curve coordinated observations of different zones of our country best of all and is used in the Soviet seismic service when defining a source location. (Fig. 1 (8)). It is worth to note that deviations of observed travel-time curves, constructed on the basis of near regional and expeditional stations data, from that of J-B for corresponding depth, prove to be somewhat greater than analogous deviations by the blasts and DSS data.

The comparison results are given in Fig. 2. The averaged travel-time curve by data of the DSS and large blasts is given in the same figure for comparison.

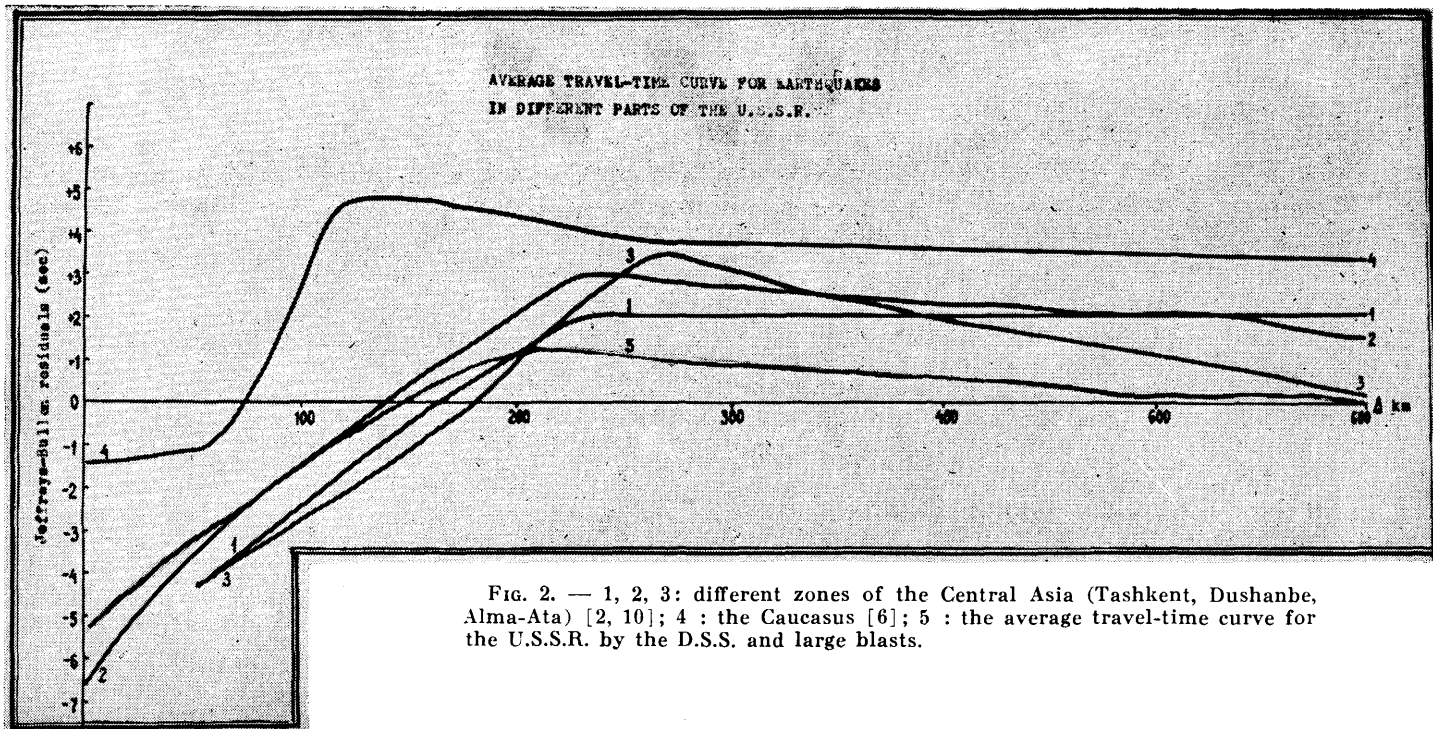
As one can see, for a distant range 150 to 200 km residuals are 2 sec less than a mean value and they are at an average by 2 sec greater for distances greater than 200 km.

A direct wave velocity for a majority of the USSR regions is at an average 6 km/sec. If there are a great number of stations near an epicenter, one can see some change of the direct wave velocity with moving away from the source. The travel-time curve corrections increase for areas with thick cover of sediments and decrease for those with outcrop of crustal rocks.

Local travel-time curves are not symmetric in different directions that was marked out in several papers (Riznichenko, edit., 1960).

II. — Distance range $600 \text{ km} < \Delta < 2500 \text{ km}$.

Travel-times at this distance range is interesting from the point of view of "the shadow zone" and especially of layers under Moho discontinuity. Accurate interpretation of records is of essential importance here, as they are conditioned by the structure peculiarities of both the earth crust and the upper mantle between a source and a station and also by characteristics of seismic instruments and a noise level.



The research of P waves at seismic stations of the USSR in relation to J-B travel-time curves can be carried out most suitably on the basis of regional investigations for earthquakes occurred on the territory of the USSR and near its frontiers. Such investigations are made more widely in the Central Asia, and materials for this region are most representative.

Accordingly, we have carried out investigation of station residuals on the basis of strong earthquakes in the Central Asia in 1956-1966, coordinates of their sources being defined with enough accuracy mainly by observations of seismic stations disposed in the vicinity of epicentral area. An error of coordinate determination by evaluation of a local station network did not exceed 5 km.

We have selected the most reliable observations of stationary seismic stations of the USSR equipped with both wideband and high response instruments. Magnitudes of earthquakes used were 5 and greater. In all, we have considered 46 shocks with origins in Hindu-Kush region, 33 of them being deep ones ($h \geq 70$ km) and the rest locating within the earth crust.

Travel-times for Tashkent's shock on 25.4.66 were studied separately, its origin position being known with accuracy 1-2 km and the origin time being defined reliably enough by data of near seismic stations.

The study of travel-times of P waves was carried out on the basis of analyses of P waves at different seismic stations in relation to J-B travel-time curves; for short distances it was made in relation to the above mentioned travel-time curve for the USSR territory.

A statistical model $t_i - t^* = f_i$ ($i = 1, 2 \dots, N$) was used, where f_i was a random value with dispersion S^2 , t^* was a travel-time to i -th station calculated by the travel-time curve and suggested to be known without an error, and t_i was an observed travel-time to i -th station. Individual values f_i and their corrections for ellipticity were carried out on ϵC on the basis of known origin parameters. (K. E. BULLEN, 1937.)

The statistical analysis was fulfilled by way of construction of normalized curves of distribution of f_i for every individual station (histogramme); calculated parameters of these histogrammes allow to evaluate both a mean correction to the standard travel-time curve and a reliability of station observations. The reliability degree for a mean correction m is conditioned by the confidence interval

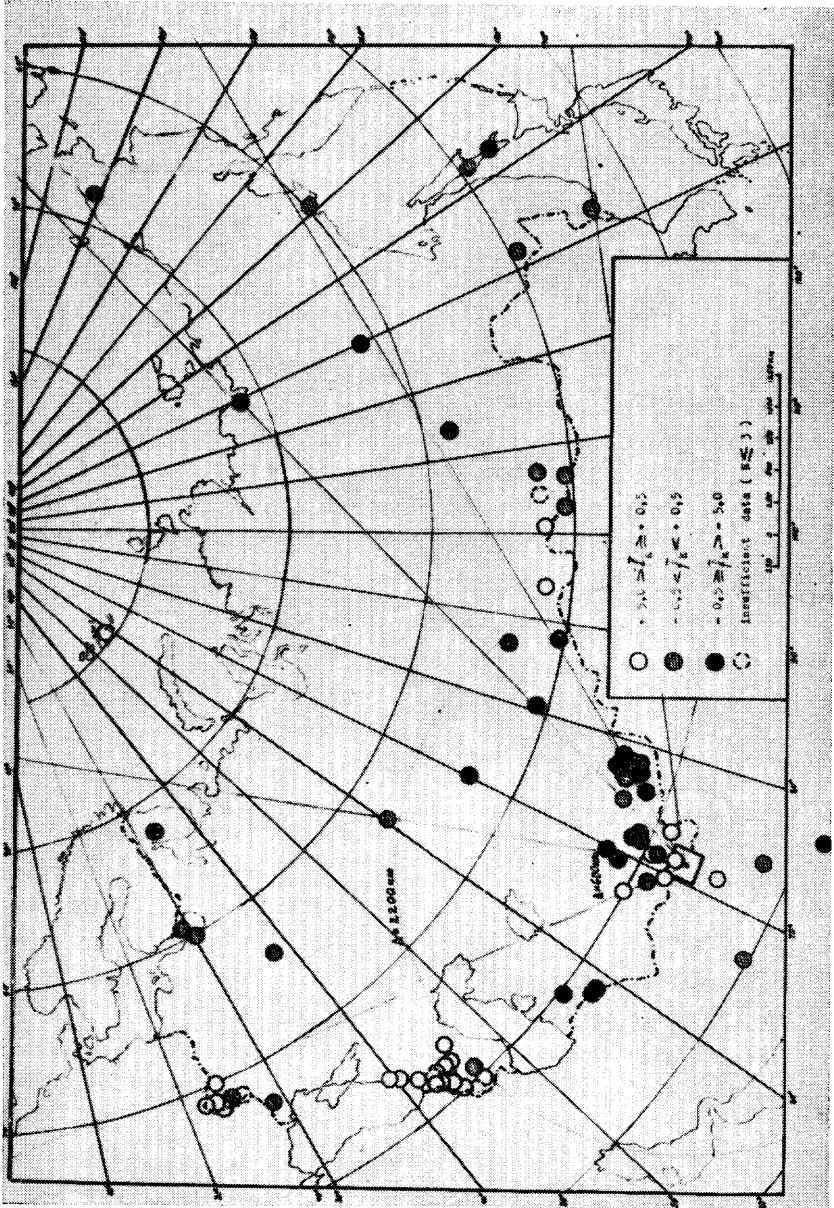


FIG. 3

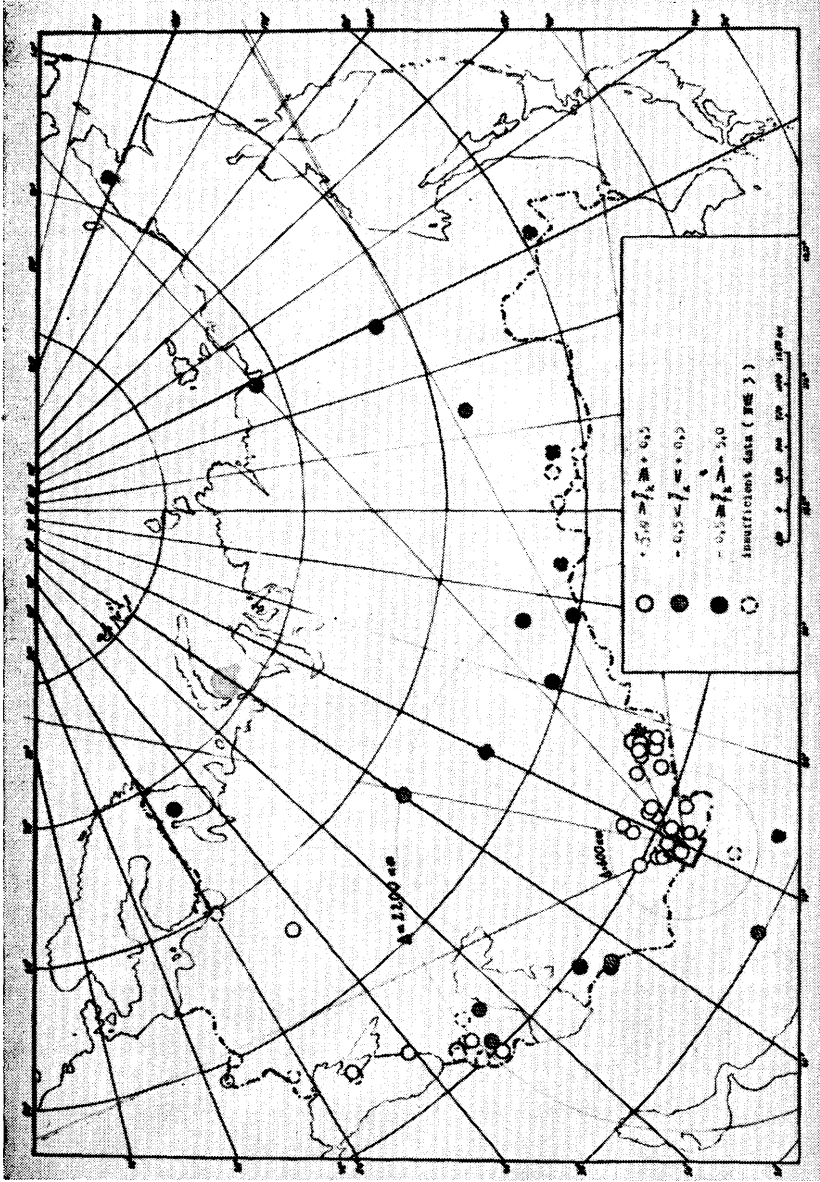


FIG. 4

in accordance with Student's distribution (SMIRNOV, DUNIN-BARKOVSKII, 1965).

Results

Mean station residuals for deep earthquakes are shown in Fig. 3.

The residuals have positive values up to 600 km, which is in accordance with travel-time curves discussed in part I. Mean values of residuals for a number of stations become negative at distances about 600 km, that is one can see earlier arrival times there; those deviations remain negative to about 2200 km independently of azimuthal position of a station relatively to an epicenter.

After 2200 km, one can see both positive and negative values of residuals, directions being marked out along which the residuals are negative (the Russian platform, Eastern Siberia) and positive (mountain regions, the Caucasus, the Carpatians).

Mean station residuals for surface earthquakes are shown in Fig. 4. Negative values of mean residuals in such a case can be observed at greater distances than those for deep earthquakes, namely at distances about 10° , it being more distinct at stations equipped with high response instruments (Vannovskaya, Eltsovka). Reversion of deviation signs has place also at distances about 2200 km.

It is interesting to note a boundary going among the Caucasian stations (so Kirovabad gives negative residuals, whereas Tbilisi, Bakuriani and others give positive ones).

Positive residuals are observed at greater epicentral distances ($\Delta > 2500$ km) in this direction as it is in the previous case of deep shocks (Fig. 4). As in the earlier case, distant stations ($\Delta > 2500$ km) give negative residuals in the direction of East Siberia and the Russian platform.

Dependence of mean residuals on epicentral distance for deep and surface sources of Hindu-Kush's earthquakes is shown in Fig. 5. Dependence of station residuals on epicentral distance for Tashkent's earthquakes on 25-4-66 is also given in this figure; arrival times of P waves have been accurately measured by records of different stations. Decrease of residual values for deep and surface sources at 20° can be clearly seen. An area of negative residuals ($\delta\Delta_-$) for deep earthquakes is wider than that for surface ones. For deep Hindu-Kush's shocks $\delta\Delta_- = 600-2200$ km, for surface Hindu-Kush's shocks $\delta\Delta_- = 900-2200$ km, for Tashkent's shock $\delta\Delta_- = 800-1700$ km.

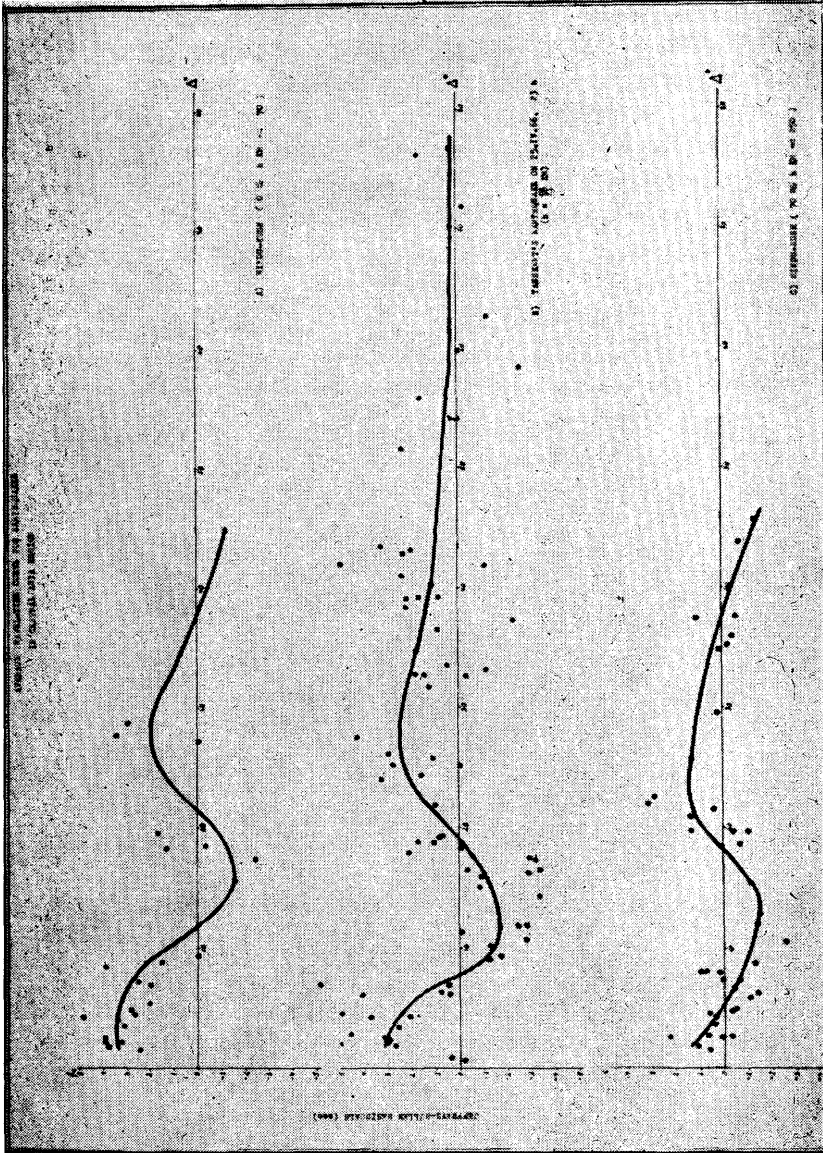


FIG. 5

Peculiarities of identification on first arrivals at distances greater than 700 km were marked out in the paper by Nersesov and Rautian (1964); their observations were made by a profile of stations disposed in direction the Pamirs — the Lena River with a general length of 3500 km.

Outrun of P waves in comparison with J-B travel-time curve is seen here at distances about 600 and more kilometers, reaching 3.5 sec. Nevertheless any sharp change of residual signals was not revealed there about 20° . It can be explained by the fact that the profile stations have got in a region of positive residuals (see Fig. 3, 4). Travel-time curves constructed by Nersesov and Rautian, don't give essential deviations from that of J-B in the direction from west to east.

So the study of station residuals for earthquakes of different regions reveals for some of them the presence of systematic deviations from J-B travel-time curve at the range 600 to 2 200 km. The distance range in which one can see a sufficient outrun of P wave, depends on the examined region.

Obtained effect can be the result of rise of P_r waves at those distances (LEHMANN, 1962); waves of this type are refracted ones at depth 200-215 km, where velocity gradient increases sharp.

It is possible to suggest also that first arrivals of longitudinal waves after a zone of interference with the direct wave can be considered as a series of reflected waves substituting each other. These reflections occur at great depths in the mantle of the Earth (NERSESOV, RAUTIAN, 1964).

It is worth to mark out an interesting experimental fact of distinct wave groups observed on seismic records made in distance range 1500 to 1700 km; these waves delay by 8-10 sec relatively to first arrivals (NERSESOV, RAUTIAN, 1964). With increasing distance the wave connected with this arrival nears the first one and appears in first onsets at distances 2100-2400 km.

By its nature, the wave can be connected with a boundary inside the mantle of the earth at the depth 900 km. Wave picture in this distance range requires a further study.

REFERENCES

1. BULLEN K. E., MNRAS G. S. N° 5, 1937.
2. BUTOVSKAYA, E. M., V. I. ULOMOV, Trudy instituta matematiki AN Uzb. SSR, 1964.
3. GAMBURTSEV, G. A., Selected works, Ed. Academy of Sciences of the USSR, 1960.

4. KOSMINSKAYA, I. P., G. G. MIKHOTA, Yu. V. TULINA, *Izv. AN SSSR, Series Geoph.* N° 10, 1958.
5. LEHMANN, I., *Bull. Seismol. Society Am.*, v. 52, N 3, July 1962.
6. LEVITSKAYA, A. Ya, T. M. LEBEDEVA, *Izd. AN Gruz, SSR, Tbilisi*, 1952.
7. MCCONNEL, I. R., McTAGGART-COWAN, *The university of Toronto, Inst. of Earth Science Scientific Report*, N° 8, 1964.
8. NERSESOV, I. L., T. G. RAUTIAN, *Trudy instituta fiziki zemli AN SSSR*, N° 32 (193), 1964.
9. RIZNICHENKO, Yu. V. (ed.), *Trudy instituta fiziki zemli AN SSSR*, N° 9 (176), 1960.
10. ROZOVA, E. A., *Trudy seismologicheskogo instituta AN SSSR*, N° 72, 1936.
11. SMIRNOV, N. V., J. V. DUNIN-BARKOVSKII, "Course of probability theory and mathematical statistics", 1965.
12. TVALTVDZE, G. K., I. P. KOSMINSKAYA, T. Ya. MURUSIDZE, G. G. IOSELIANI, Yu. V. TULINA, *Trudy inst geof. AN SSSR*, v. XVI, 1957.

SOME RESULTS OF INVESTIGATION OF P WAVE TRAVEL TIMES

by N. V. KONDORSKAYA and L. B. SLAVINA

PART II

Corrections to JEFFREYS-BULLEN travel-time curves (J-B) for a number of seismic stations of the U.S.S.R. in the distance range 20° to 100° have been studied in this paper on the basis of statistical analysis of residuals of P wave travel-times by recording earthquakes from different seismic areas. An effect of dependence of the travel-time residual curve on epicentral distance has been observed. The authors have pointed out at variations on the curve at distances of 30° , 60° , and 80° , they being connected with anomalies in the mantle at corresponding depths. A dependence of the correction value and sign upon an earthquake region has been revealed. It has been noted that P wave travel time increases to stations disposed in geosynclinal regions and it decreases to stations disposed on ancient shields and platforms.

Travel times of P waves were studied for 15 Soviet stations equipped with high response instruments of the same type and covering by their geographic disposition the whole territory of the U.S.S.R. The statistical analysis of the travel-time residuals was carried out for 1144 earthquakes ($M > 5$) occurred in the Earth's crust, their epicentral coordinates being results of calculations on electronic computer.

Residuals were defined as

$$f_i = t_i - t^* \quad (1)$$

where t_i is an observed travel time of P waves and t^* is its theoretical value. A mean value of the correction was defined by the formula

$$\bar{f} = \frac{1}{N} \sum_{i=1}^N f_i \quad (2)$$

where N is a number of observations. The confidence interval for the mean and the dispersion (S) was defined in accordance with Student's distribution (N. V. SMIRNOV et al., 1965).

$$\frac{S_f \cdot t_{\alpha, n-1}}{\sqrt{n-1}} + \bar{f} < m < \frac{S_f \cdot t_{\alpha, n-1}}{\sqrt{n-1}} - \bar{f} \quad (3)$$

where S_f is an empirical dispersion

$$S_f^2 = \frac{1}{n} \left[\sum_{i=1}^n f_i^2 - n(\bar{f})^2 \right] \quad (4)$$

where $t_{q, n-1}$ is Student's test for $n-1$ degrees of freedom and a probability $P = 1 - q/100$; m is a real mean value. We choose the confidential level of 90 per cent.

Two problems were investigated: 1) regularities conditioned by origin and station regions; 2) a character of dependence of the corrections on epicentral distance.

AVERAGED RESIDUALS FOR ALL THE REGIONS

No. No. in suc.	Name of station	Number of obs. N	\bar{f} (sec)	Conf. interv. (\pm sec)	$S_{\bar{f}}$ (sec)	$\frac{n_{\max}}{N}$
1.	Frunze	417	+ 0.36	0.08	1.02	0.38
2.	Talgar	293	+ 0.18	0.12	1.2	0.40
3.	Bakuriani	232	+ 0.56	0.13	1.2	0.40
4.	Yuzhno- Sakhalinsk	234	+ 0.20	0.11	1.03	0.48
5.	Petropavlovsk	312	+ 0.20	0.10	1.12	0.41
6.	Uzhgorod	304	+ 0.33	0.11	1.2	0.32
7.	Vannovskaya	255	+ 0.20	0.12	1.18	0.41
8.	Bodaybo	360	- 0.03	0.10	1.18	0.35
9.	Yakutsk	530	- 0.71	0.07	0.97	0.35
10.	Tiksi	482	- 0.70	0.09	1.23	0.32
11.	Semipalatinsk	285	- 0.54	0.12	1.2	0.35
12.	Sverdlovsk	560	- 0.44	0.08	1.05	0.44
13.	Vyborg	241	- 0.64	0.14	1.3	0.33
14.	Apatity	285	- 0.29	0.11	1.09	0.48
15.	Kirovabad	290	- 0.47	0.09	0.97	0.45

Mean values of corrections calculated for each station are given in table. It proved to be possible to divide the stations into groups in accordance with values of \bar{f} . P wave travel times to stations disposed on platforms and ancient shields (Sverdlovsk, Vyborg, Semipalatinsk, Apatity, and others) are less than theoretical ones ($\bar{f} < 0$). And to stations disposed in regions of active tectonic movements they are greater than theoretic times ($\bar{f} > 0$). It is in accordance with previous work by N. V. KONDORSKAYA (1957).

The station corrections were studied for different seismic origin areas. In every area, azimuth α from an origin to a station was taken to be constant. The correction values, confidential intervals for the mean, dispersion of the mean (S), parameter n/N characterizing maximal number of observations near mode are given in paper [5] for three regions — the Far East, Philippines, and Indonesia.

The analysis of these data shows that stations have selective ability when registering shocks of different regions. For each region, stations giving the best parameters (little dispersion, maximal value of n/N) are different. One can see a systematic deviation of travel times from those of J-B which is of different value and sign in dependence on station region and that of shock (that is on azimuth).

For clearing up a dependence of the residual value and sign upon epicentral distance, averaged curves $f = \phi(\Delta^\circ)$ were constructed. The averaged curves of such a dependence for stations Yakutsk and Tiksi are given as an example in Fig. 1. Averaged data by observations of 15 stations for Alaska's aftershocks are also given here. The curves were constructed on the basis of definitions of weight centres for particular intervals of the field of observed points f_i .

One can see from Fig. 1, that all the curves are below J-B by 1 to 2 seconds. Nevertheless it is possible to mark out that the curve has a set of extrema. Thus a decrease of travel times is seen for Yakutsk at distances about 30° , 60° , and 85° ; for Tiksi it is slightly displaced and seen at distances about 20° and 70° .

The presence of the extrema on the correction curve $f = \phi(\Delta^\circ)$ can be provoked by the presence of anomalies in the mantle at depths corresponding these epicentral distances. The stability of

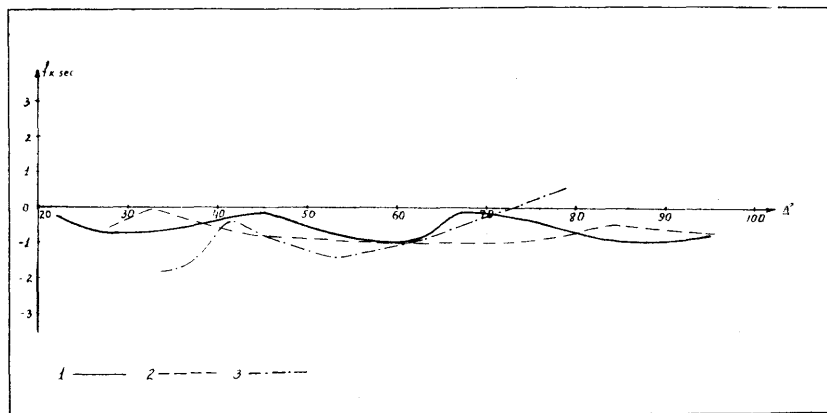


FIG. 1 : Curves of residual dependence upon epicentral distance.

Conventional marks :

————— for station Yakutsk;

----- for station Tiksi;

- . - . - . aftershocks of Alaska's earthquake for all the stations.

the extrema appearance on the correction curves for different stations points out from one hand to their non-random and

from the other hand to the fact that these anomalies in the mantle have a global character. Some displacement of extrema along the curves for different stations may be connected with variation of the anomalies with depth.

It is worth to note that the behaviour peculiarities of dynamic characteristics of P waves have been also observed about these distances (ANTONOVA, 1967; KONDORSKAYA, 1967).

REFERENCES

1. ANTONOVA, L. V. et al., Experimental regularities of dynamic characteristics of seismic waves. Publ. "Nauka" (in print).
2. KONDORSKAYA, N. V., On regional peculiarities of seismic travel times. *Izvestia AN SSSR, ser. Geofiz.*, N° 7, 1957.
3. KONDORSKAYA, N. V., T. S. ZHELANKINA, S. S. MEBEL, L. Y. VARTANOVA, Some results of use of electronic computer in the Soviet seismic service. *Collection of computational seismology*, N° 2, 1966.
4. KONDORSKAYA, N. V., L. N. PAVLOVA et al., Some results of investigation of longitudinal wave spectra of earthquakes in the Far East. *Izvestia AN SSSR, Ser. Fizika Zemli*, N° 1, 1967.
5. KONDORSKAYA, N. V., L. B. SLAVINA, Some results of investigation of travel times of P waves. *Izvestia AN SSSR, ser. Fizika Zemli* (in print).
6. SMIRNOV, N. V., I. V. DUNIN-BARKOVSKII, *Course of Probability Theory and Mathematical Statistics*. Moscow, 1965.

TRAVEL-TIMES AND AMPLITUDES OF PcP WAVES FROM SURFACE FOCI

by S. D. KOGAN (Moscow)

ABSTRACT

The residuals of the travel times of P and PcP waves from the JEFFREYS-BULLEN travel-time curves and the character of the dependence of these residuals on epicentral distance are discussed in this paper. Experimental data as to the core reflection coefficient and the phase shift due to the reflection of the longitudinal wave are given and their inconsistency with the theoretical estimates is noted.

The investigation of the core-reflected waves is of great interest as it can provide information about the properties of the transition zone from the mantle to the core.

MARTNER, ERGIN and others [1-4, 17] used the data from earthquakes in their papers, while BUCHBINDER and KOGAN [5-7] used the data from explosions. The data obtained from explosions are naturally more reliable since the initial parameters of the source are known precisely and the source itself can be considered symmetrical in contrast to an earthquake source.

This paper deals with the analysis of the kinematic and dynamic properties of PcP wave recorded at many stations from explosions in North America, Africa, Arctic, Asia and the Pacific ocean. The arrival times, amplitudes and period of PcP waves of Soviet seismic stations are taken from seismograms while the data of foreign stations are obtained from seismic bulletins and the paper by BUCHBINDER [5].

It is interesting to note that PcP waves are most often recorded at the epicentral distance from 30° to 50°. RICHTER in his book "Elementary Seismology" [8] also states that the core-reflected waves are rather intensive at 30° to 40°.

First, let us consider the kinematic properties of PcP records. The travel times of this wave (about 160 arrivals) in the distance range 19 - 88° are available. The comparison with the JEFFREYS-BULLEN tables [9] confirms the result obtained earlier [5-7] as to the fact that the observed travel times are less than the calculated ones. The corrections for ellipticity were introduced according to BULLEN [10, 11].

In table 1 distances ranges Δ° , the number of observations n , the average travel-time residuals $\delta t_{\text{PcP}} = t_{\text{PcP}}^{\text{obs}} - \tau_{\text{PcP}} - t_{\text{PcP}}^{\text{J-B}}$, the

standard errors of a single measurement σ and the errors of the average $\bar{\sigma}$ for various epicentral regions are given.

TABLE 1

Region of epicentre	Δ°	n	δt_{PcP} sec	σ	$\bar{\sigma}$
1. North America	19-88	35	-2.01	1.16	0.20
2. Africa	29-48	8	-2.76	0.32	0.11
3. Arctic	27-73	22	-3.31	1.98	0.44
4. Asia	21-67	40	-2.94	1.47	0.23
5. The Marshall Islands	33-81	24	-3.03	0.73	0.15
6. The island of Amchitka	30-84	31	-3.48	1.15	0.21

On the average the travel time of PcP wave is about 3 sec less with respect to the JEFFREYS-BULLEN tables.

Within the limits of the existing accuracy of observations the values of δt_{PcP} obtained for separate regions can be considered close except North America where they are evidently less.

The analysis of the data from separate epicentral regions does not permit to establish the dependence of δt_{PcP} on the epicentral distance [5, 7].

However if we consider all these data irrespective of epicentral regions we can notice a weak variation of the observed values of δt_{PcP} with the increase of distance (Fig. 1). If we want to establish this dependence with greater certainty we must have sufficient number of observations from separate epicentral regions.

TABLE 2

Δ°	11-20	21-30	31-40	41-50	51-60	61-70	71-80	81-90
Δ° average		27.3	35.0	46.6	55.6	64.7	75.9	84.1
n	1	21	51	41	11	23	6	5
	(-)	(11)	(40)	(37)	(9)	(21)	(3)	(3)
δt_{PcP} , sec	-2.6	-2.68	-2.46	-2.93	-3.12	-3.69	-4.11	-2.84
	(-)	(-3.54)	(-2.80)	(-2.96)	(-3.23)	(-3.60)	(-4.80)	(-3.83)
σ		1.43	1.20	0.82	0.91	1.67	2.06	1.59
$\bar{\sigma}$		0.29	0.17	0.12	0.25	0.35	0.84	0.71

Table 2 gives the averaged values of δt_{PcP} and their standard errors within 10° distance intervals. The errors include both the casual errors of observations and the systematic deviations connected with the seismic-geological conditions in the regions of the station

and epicentre. The data in brackets are the values of δt_{peP} and n without taking into account the observations from explosions in North America. Since for this region the main part of data (about 70 per cent) is obtained for the epicentral distance less than 40° , the result for $\Delta > 40^\circ$ is practically unchanged within the limits of the available accuracy.

The dependence of δt on the epicentral distance undoubtedly exists for the P wave. The example of such dependence established from the observations of the Longshot explosion is given in fig. 2. The fact that no dependence of δt_r on Δ was noticed from the observations of explosions on the Marshall islands [7] is accounted by a

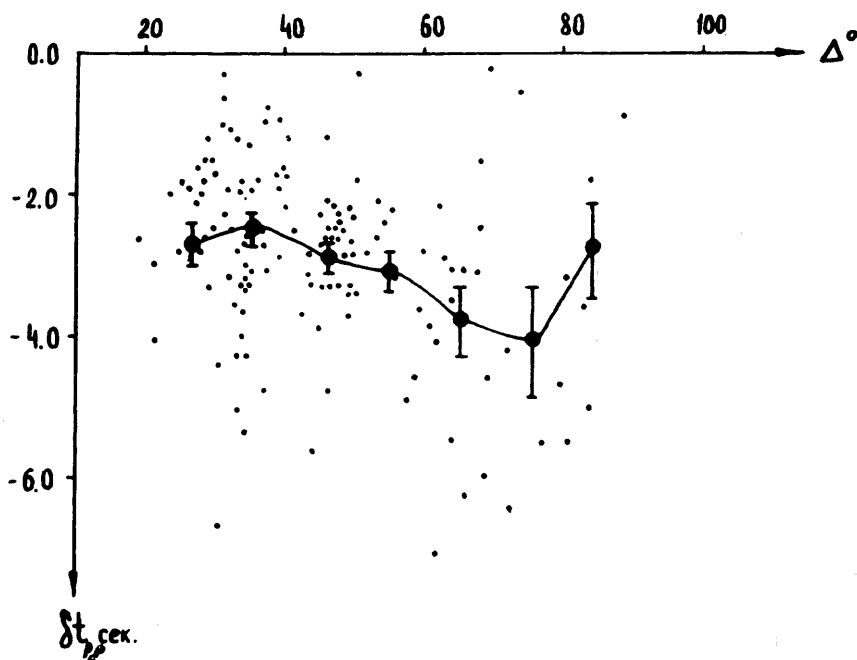


FIG. 1. — The dependence of δt_{peP} on the epicentral distance without the allowance for epicentral regions.

very small number of observations in the epicentral range $50-70^\circ$. The main peculiarity of the curve $\delta t_r(\Delta)$ is the minimum for $\Delta = 50-75^\circ$; it is preserved with the change of epicentral regions. Probably due to the peculiarities in the focal region the curves $\delta t_r(\Delta)$ are somewhat shifted as to their level for different epicentral regions. The most essential differences of the curves are noticed at epicentral distances up to 40° , which seems to reflect the peculiarities of the

crustal and upper mantle structure for various travel time paths.

The maximum difference between the observed travel times of longitudinal waves and the JEFFREYS-BULLEN tables is observed at the moment of the propagation of P at the depths of 1 300-2 100 km. The penetration of P down to the depth about 2 100-2 700 km causes the decrease of the value of δt_p . At the epicentral distances more than 90° we have few observations as yet. A further analysis of all the data will permit to obtain a more reliable curve $\delta t_p(\Delta)$.

As it seems up to now we can state that the increase of the longitudinal velocity in the mantle with the depth is not monotonous and its values are on the average somewhat greater than according to the JEFFREYS-BULLEN tables.

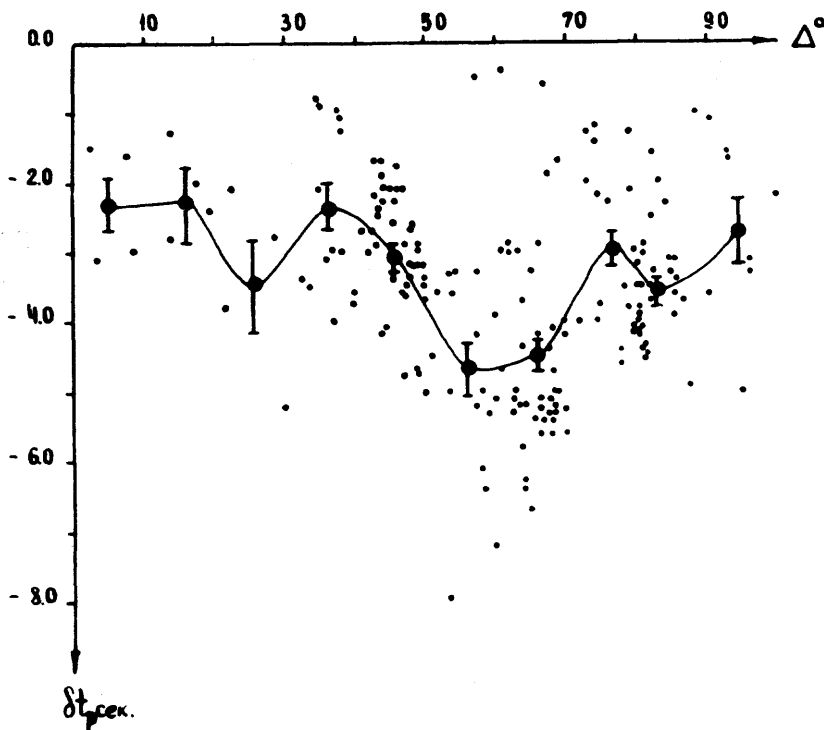


FIG. 2. — The dependence of δt_p on the epicentral distance from the observations of the Longshot explosion.

Some interesting data as to the character of the velocity variation with depth in the mantle are obtained by CHINNERY and TOKSÖZ in [12] where the slope of the travel-time curve of P is investigated. A model of the velocity variation with depth is constructed with three anomalous regions at the depths approximately 800, 1 300 and

2 000 km where the velocities change very slowly and maybe even decrease with the depth.

The previous papers of KOGAN [7] and BUCHBINDER [5] show that residual of P from the travel time curve is less than that of PcP. The observations ($n = 143$) obtained by the present time on the average give the difference $(\delta t_{\text{PcP}} - \delta t_{\text{P}}) = -0.47 \mp 0.12$ sec with the mean square error of a single measurement 1.48, about 40 per cent of observations yielding $(\delta t_{\text{PcP}} - \delta t_{\text{P}}) > 0$. Since the variation of δt_{P} and δt_{PcP} with the epicentral distance is not the same, their difference will depend on distance in a rather complicated way. However it is difficult to judge about the character of this dependence from the available data as yet, since the value of the difference $(\delta t_{\text{PcP}} - \delta t_{\text{P}})$ itself is within the accuracy of measurements. The corresponding estimates are given in table 3.

TABLE 3

Δ°	11-20	21-30	31-40	41-50	51-60	61-70	71-80	81-90
Δ° average	19.4	27.4	35.5	46.9	56.0	65.7	75.9	84.7
$(\delta t_{\text{PcP}} - \delta t_{\text{P}})$ sec	+0.1	-0.70	-0.19	-0.68	+0.31	-0.69	-1.75	-0.36
n	1	22	44	38	12	15	6	5
σ		1.49	0.96	1.23	1.33	2.75	1.99	0.59
$\bar{\sigma}$		0.32	0.14	0.20	0.39	0.71	0.82	0.26

It this fact $(\delta t_{\text{PcP}} > \delta t_{\text{P}})$, is confirmed by the analysis of a greater number of observations the reasons for it might be several : 1) a shallower depth of penetration of P as compared with PcP and hence different velocities of propagation; 2) the presence of a thin-layered transition zone at the core boundary with a higher velocity of longitudinal waves [18]; 3) a somewhat greater radius of the core than the assumed value that was used to calculate the travel-time curve, etc.

Now we shall consider the dynamic properties of the PcP wave. The data that show the change of the incident wave phase with reflection are essential for the understanding of the reflection boundary.

In Fig. 3 we used the observations obtained from seismograms and those taken from the paper by BUCHBINDER [5]. We believe that these data suggest that within the distance range 19 to 31° a change of sign is possible while the observations of such a change are not available within the range from 32 to 81°.

The conversion of the PcP wave phase near 31° was stated by BUCHBINDER [6] on the basis of his observations of the Longshot explosion. Since the data under consideration are recorded from explosions any possibility of the effect of the source direction is

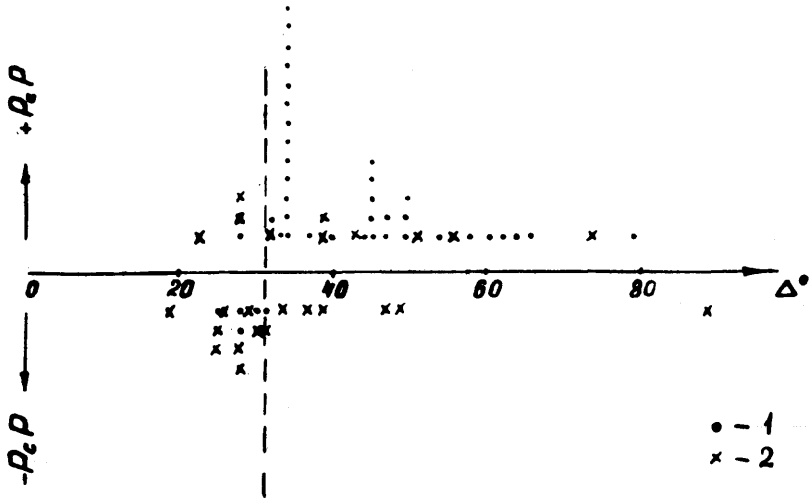


FIG. 3. — The number of observations of the compressional and dilatational motion for the PcP wave as a function of the epicentral distance : 1) according to our data from seismograms; 2) from the data of [5].

out of question. Unfortunately the observations at epicentral distances greater than 80° are scarce and they are rather unreliable due to a greater probability of the interference of PcP and P waves. BATH [13] presented a theoretical estimate made under the assumption that the transition boundary from the mantle to the core is a boundary of solid and liquid semi-spaces, and he showed at what angles of incidence to the core the PcP wave will change its phase depending on the density jump at the boundary.

According to this estimate at epicentral distances $\Delta \geq 80^\circ$ PcP must change its sign as compared with P at $\rho'/\rho \geq 1$. At $\Delta \leq 30^\circ$ the sign may change at $\rho'/\rho = 1$; with the growth of ρ'/ρ up to 1,71 the corresponding value of Δ must decrease. Hence the data from $\Delta < 32^\circ$ could have been in favour of the values ρ'/ρ close to 1 if the observed values of the amplitude ratios of P and PcP that are essentially greater than the expected theoretical ones even for $\rho'/\rho = 2.0$ [14], had not been at evident variance with this fact.

In Fig. 4 the theoretical reflection coefficients of PcP are obtained for the ratio ρ'/ρ equal to 1 and 2 under the assumption that the mantle-core boundary is a boundary of solid and liquid semi-spaces.

The parameters of the medium were the following for the mantle : $v_p = 13.7$ km/sec, $v_s = 7.25$ km/sec; for the core : $v'_p = 8.0$ km/sec, $v'_s = 0$. The reflection coefficient will be still lower if the shear modulus for the outer core is taken not equal to 0.

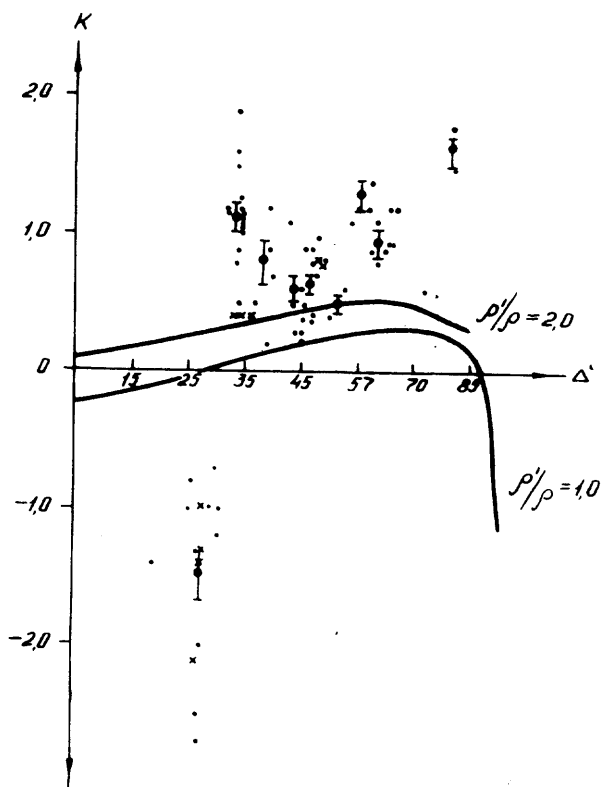


FIG. 4. — The comparison of the experimental and theoretical values of the reflection coefficient of the PcP wave : × — the values of K taken with the sign reverse to the observed one.

The dots in Fig. 4 represent the experimental reflection coefficients; the circles are the averaged values within 5° distance intervals. The reflection coefficients were calculated from the formula :

$$K^2 = \left(\frac{A_{PcP}}{A_P} \right)^2 \cdot \frac{T_P}{T_{PcP}} \cdot \left(\frac{\mathfrak{H}_P}{\mathfrak{H}_{PcP}} \right)^2 \cdot \frac{M_{PcP}}{M_P}$$

where A and T are experimental values of the amplitude of the vertical ground motion and the corresponding period of a given wave, \mathfrak{H} is a coefficient allowing for the effect of the free surface and the reflecting boundaries in the Earth's crust [15], $M = \frac{\sin \Delta \operatorname{tge}}{de / d\Delta}$ is the function allowing for the geometric divergence of the wave

[16]. This formula is derived from the ZOPPRITZ-WIECHERT formula but the allowance for the fact that the motion duration in a given wave on our records is actually equal to one period.

The fact that the values of K are sometimes greater than 1 seems to be due to the errors of M function for the inaccuracy of the travel-time curve of the P and PcP waves and the inaccuracy of the calculation technique of the reflection coefficients from the amplitudes of waves with different shapes. The difference of P and PcP shapes is sharply manifested in the difference of their periods. The periods corresponding to the maximum trace amplitudes of PcP are on the average less than the periods of P . The average value of $T_P/T_{PcP} = 1.23 \pm 0.06$.

The fact of a significant difference between the experimental and theoretical reflection coefficients of PcP was stated by us as far back as in 1958 when we interpreted the data from the explosions on the Marshall islands but our results were not published as the scarcity of data and relatively small trace amplitudes were likely to give errors. By now the number of observations had increased and the quality had improved. Similar data are obtained by other authors both from explosions [5] and earthquakes [1-4, 17].

At first one of the reasons for such difference seemed to be the difference in the absorption of P and PcP waves due to the decrease of absorption with depth. Such estimates recently made by H. KANAMORI [17] show that the allowance for the difference in the absorption of P and PcP waves permits to diminish the values of the observed ratios (A_{PcP}/A_P) but does not do away with the fact that the experimental data exceed the theoretical ones. The difference in the periods of T_P and T_{PcP} may also be partly connected with the difference in absorption.

The contradictory character of the data concerning the experimental reflection coefficients from the core and the phase change of reflected longitudinal waves as well as their incomparability with the estimated values are most likely an indication of an incorrect theoretical model assumed for the estimates. The transition zone from the mantle to the core seems to be more complicated and the reflection boundary can not be considered as simply a boundary of two semi-spaces. BERZON I. S. [18] suggest that the observed experimental data are likely to be explained if the boundary of two semi-spaces is substituted by a thin-layered model of the transition zone. At present estimates of such models are being carried out.

Some additional data of PcP as well as ScS and PcS will probably

permit to construct a more correct model of the mantle-core transition zone.

The number of reliable data of the PcP amplitude is still insufficient for an independent construction of an experimental amplitude curve. The first tentative curve $\left(\frac{A}{T}\right)_{\text{PcP}}(\Delta)$ (Fig. 5, I) was drawn by means of the multiplication of the experimental curve of the ratio $\left(\frac{A}{T}\right)_{\text{PcP}} : \left(\frac{A}{T}\right)_P$ (Fig. 5, III) obtained from the data of [1, 2, 5] and presented in the paper by BERZON, KOGAN and PASSECHNIK [18] and

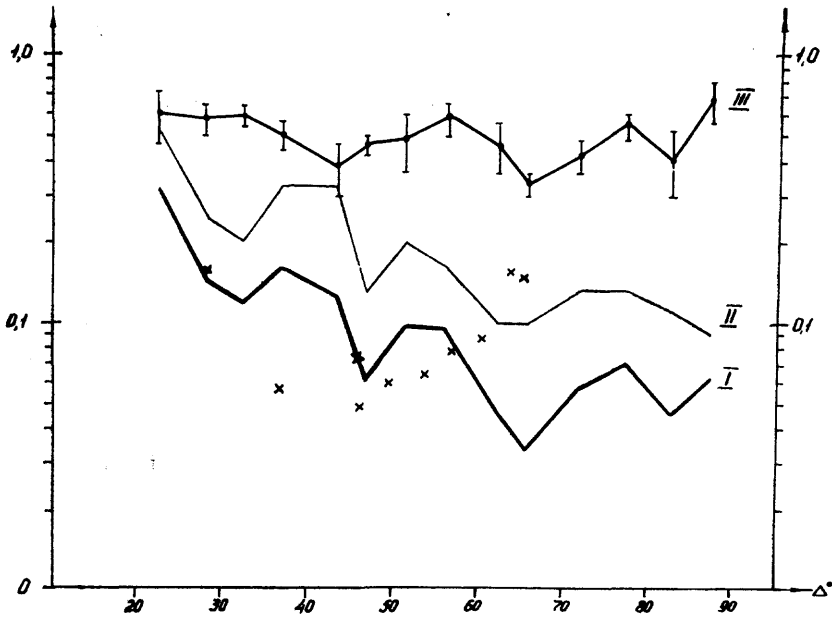


FIG. 5. — The dependence of the ratio of A/T for the PcP wave on the epicentral distance : I — the curve $\left(\frac{A}{T}\right)_{\text{PcP}}$; II — the curve $\left(\frac{A}{T}\right)_P$ according to [19]; III — the curve $\left(\frac{A}{T}\right)_{\text{PcP}} : \left(\frac{A}{T}\right)_P$ according to [18]; x — the values of $\left(\frac{A}{T}\right)_{\text{PcP}}$ for the Longshot explosion.

the amplitude curve of GUTENBERG and RICHTER [19] for P at $m = 6$ (Fig. 5, II) at the points which correspond to the averaged values of curve III. The crosses in Fig. 5 represent our data of the values of $\left(\frac{A}{T}\right)_{\text{PcP}}$ for the Longshot explosion. The agreement is satisfactory.

The comparison of the curves I and II seems to imply that the character of the amplitude change of PcP with distance is roughly similar to that of P and if the reflection coefficient from the core is close to 1, the smaller amplitude of PcP as compared with P is mainly accounted for a greater geometric divergence of the PcP wave front.

REFERENCES

- [1] MARTNER (S. T.). Observations on seismic waves reflected at the core boundary of the earth. *Bull. Seism. Soc. Am.* 40, N 2, 1950.
- [2] ERGIN (K.). Amplitude of PcP and PcS and ScP in deep-focus earthquakes. *Bull. Seismol. Soc. Am.*, 43, N 1, 1953.
- [3] GRUDEVA (N. P.). On problem of earth's core boundary properties. *Izv. AN SSSR, series geophys.*, N 5, 1964 (in Russian).
- [4] BALAKINA (L. M.), VVEDENSKAYA (A. V.), KOLESNIKOV (Yu. A.). Investigation of the outer boundary of the earth's core by means of the spectral analysis of seismic waves. *Izv. AN SSSR, Earth's Physics*, N 8, 1966 (in Russian).
- [5] BUCHBINDER GOETZ (G. R.). PcP from the nuclear explosion Bilby, September 13, 1963. *Bull. Seism. Soc. Am.*, 55, N 2, 1965.
- [6] BUCHBINDER GOETZ (G. R.). PcP Travel times from Longshot and the density ratio of the mantle-core boundary, *Trans. Am. Geophys. Union*, 47 N 1, 1966.
- [7] KOGAN (S. D.). Travel times of longitudinal and transverse waves, calculated from the data of nuclear explosions in the region of the Marshall islands., *Izv. AN SSSR, geophys. series*, N 3, 1960 (in Russian).
- [8] RICHTER (C. J.). *Elementary Seismology*, Moscow, 1963.
- [9] JEFFREYS (H.), BULLEN (K. E.). *Seismological Tables*, London, 1940.
- [10] BULLEN (K. E.). Ellipticity corrections to earthquake waves reflected at the central core, *MNRAS, Geophys. Suppl.*, v. 4, N 5, 1938.
- [11] BULLEN (K. E.). A suggested new seismological latitude, *MNRAS, Geophys. Suppl.*, N 4, N 2, 1937.
- [12] CHINNERY (M. A.) and NAVI TOKSÖZ (M.). P-waves velocities in the mantle below 700 km. *Bull. Seism. Soc. Am.*, v. 57, N 2, 1967.
- [13] BÄTH (M.). The density ratio at the boundary of the Earth's core *Tellus*, v. 6, N 4, 1954.
- [14] MOLODENSKY (M. S.). Density and elasticity in the Earth's interior, *Trudy Geophys. Inst. AN SSSR*, N 26, 1955 (in Russian).
- [15] KOGAN (S. D.). Dynamic parameters of the foci of deep earthquakes, *Trudy Geophys. Inst. AN SSSR*, N 30, 1955 (in Russian).
- [16] KOGAN (S. Ya.). On problem of the determination of the energy of body waves, *Acta Geophys. Sinica*, N 8, N 1, 1956 (in Russian).
- [17] KANAMORI (H.). Spectrum of P and PcP in relation to the mantle core boundary and attenuation in the mantle. *Journal Geophys. Research*, v. 72, N 2, 1967.
- [18] BERZON (I. S.), KOGAN (S. D.), PASSECHNIK (I. P.). On the possibility of the construction of the thin-layered model in the transition zone from the mantle to the core, *DAN SSSR*, v. 178, N 1 1968 (in Russian).
- [19] GUTENBERG (B.), RICHTER (C. F.). Magnitude and energy of earthquakes. *Annali di geofis.*, v. IX, N 1, 1956.

TIMES OF P IN PACIFIC EXPLOSIONS

by Sir Harold JEFFREYS and M. L. GOGNA

Data for arrivals of P from nuclear explosions have been published and studied by several authors. The fullest list is by *CARDER* and *BAILEY*, and is used by *GOGNA* in this paper. *CARDER* and *BAILEY* have made corrections for the heights of the stations above sea level, but *GOGNA* has preferred not to make these corrections, leaving them to be absorbed at a later stage into station corrections, which might arise in several ways. The residuals against the J.B. 1940 times were classified at small intervals; after allowance for the means they gave a standard deviation for one observation of 0.45 s. In well-observed natural earthquakes about 1.2 s. is usual. In *Jeffreys's* study several possible explanations of the difference were considered, the most likely appearing to be that the P arrivals from the explosions were in fact unusually sharp. Allowance for departure from the normal law of error made the weight decrease to less than 0.1 at a residual of ± 1.6 s.

Up to 18.6° a linear form

$$t = 4.27 \pm 0.20 + (13.628 \pm 0.0189) \Delta$$

was found to fit.

Beyond 25.5° the method was to take 15° intervals and three distances in each, fit a quadratic to them, and take residuals against this quadratic. This eliminates the greater part of the curvature. Then in each interval two distances were found such that the errors would be independent of each other and of a possible additional square term in Δ , and the corresponding times were estimated by least squares. Then from 28° to 94° the table was completed, first at 5° and then at 1° intervals, by divided differences.

Beyond 94° the data are scanty. Five points from 90° to 94° were fitted by a quadratic: this agreed with the observed time at 97° ; and then the times were extrapolated linearly.

There was a strong group of observations from 17.0° to 20.0° at Rabaul and Guam, and interpolation based on 18° , 20.0° , 28° and 36° filled in the gap from 18° to 28° . The final χ^2 was 44, based on 39 degrees of freedom, which is satisfactory.

The data used are all first arrivals. There are some late arrivals in the range 13.9° to 20.6° . It was found that if the straight line fitted up to 18.6° is extended to 20.55° it passes through some of the late arrivals in 20.3° to 20.55° . A quadratic fitted to five points from

19.0° to 23.0° was taken back to 13.88° and was found to agree with some of the late arrivals in 13.88° to 18.55°. But there were many late arrivals not explained in this way, and the data are not sufficient to decide on the existence of these possible branches.

Mean residuals for stations against the corrected times were found. 21 out of 60 exceeded twice the standard error, but if there were no further complications we should expect about 3. So presumably most of them represent genuine station anomalies. They show no noticeable correlation with height above sea level, or with the difference between island and continental stations, as we should have expected. The direct effect of height would reach about 0.2 s per km. If there is isostatic compensation the variation of the depth of the Moho would increase this to about 0.5 s per km. Actually Baguio, a high station in the Philippines, has the largest negative mean.

Δ°	1940	Europe-JB	Japan (Arnold)-JB	Pacific (Gogna)-JB
0	0 (6.8)	(+ 0.7)	(+ 0.8)	(- 2.5)
5	1 18.1	- 2.0	+ 0.9 \pm 0.2	- 5.7 \pm 0.1
10	2 28.0	- 3.6	+ 0.8 \pm 0.2	- 7.4 \pm 0.1
15	3 35.0	- 2.3	+ 0.1 \pm 0.2	- 6.3 \pm 0.2
20	4 37.0	- 3.8	- 2.6	- 2.8
25	5 26.8	- 2.3 \pm 0.3	- 1.7 \pm 0.4	- 3.0 \pm 0.2
30	6 12.5	- 1.6	- 2.1	- 2.5 \pm 0.4
35	56.1	- 1.1 \pm 0.4	- 2.0	- 2.2 \pm 0.1
40	7 38.1	- 1.0	- 1.7	- 1.6
45	8 18.9	- 1.0	- 1.8	- 0.9 \pm 0.2
50	58.0	- 1.0 \pm 0.5	- 1.7 \pm 0.3	- 1.2 \pm 0.1
55	9 35.4	- 0.9	- 1.5	- 2.4
60	10 10.7	- 0.7	- 1.2	- 3.4 \pm 0.1
65	44.0	- 0.7 \pm 0.8	- 0.9	- 3.1 \pm 0.1
70	11 15.4	- 1.1	- 0.7	- 1.6 \pm 0.04
75	45.0	- 1.6 \pm 0.5	- 0.6	- 1.0
80	12 12.7	- 1.7	- 0.9	- 1.2 \pm 0.06
85	38.5	- 1.5	- 0.9 \pm 0.3	- 1.6
90	13 2.7	- 1.2	- 0.9	- 1.9
95	25.7	- 0.5 \pm 0.7	- 0.9	- 2.0 \pm 0.1
100	48.4			- 2.4
105	14 10.6			

Standard errors are quoted as for the nearest summary value.

The velocity at short distances is practically the same as in Europe and Central Asia, but the constant term is nearly 4 s. less. This might be attributed to smaller thickness of the outer layers, but if this was the only reason for the difference we should expect the difference to increase with distance. Actually it diminishes.

The negative corrections about 60° found by **CARDER** and **BAILEY** are confirmed. But **Arnold's** study of deep Japanese shocks and **Jeffreys's** of European and Central Asian shocks do not show them. **S. S. ALEXANDER** (Paper 11 at this Assembly) finds regional differences down to the core boundary. It seems that regional differences extend to much greater depths than have yet been considered.

Gogna's work has since been published in the *Geophysical Journal of the Royal Astronomical Society*, 13, 1967, 503-28; **Jeffreys's** comparison of stations will be in a later number of the same journal.

DISCONTINUOUS VELOCITY CHANGES IN THE MANTLE AS DERIVED FROM SEISMIC TRAVEL TIMES AND AMPLITUDES

by I. LEHMANN

ABSTRACT

Departure from normal behaviour of the velocity of seismic body waves is reflected in the travel time curves, but it is rarely, if ever, possible to determine from observations the complete time curve, including retrograde branches. Therefore the velocity function cannot be derived directly. A model has to be chosen and adapted to available observations. In the uppermost mantle velocities are not everywhere the same and observations should, preferably, be taken on profiles on which the structure does not vary significantly. It is shown on three examples how discontinuous velocity changes are indicated by observations. The travel times are in agreement with those derived from velocity models previously considered having a discontinuity at about 215 km depth.

It is of considerable interest to find where the seismic velocity departs from what may be termed "normal" behaviour and especially where discontinuous changes occur. Using body wave data we derive how departures from normal behaviour are reflected in the time curve. Loops are produced if the velocity increases abruptly or very strongly. An abrupt or strong gradual decrease of the velocity breaks off the time curve. We can find under what circumstances caustics arise. The question is whether features of this description can be recognised in the travel time curves we determine from observations, and if so, whether we can derive the corresponding velocity function.

A loop may be indicated by a sudden change of slope of the time curve of first arrivals, but we shall rarely, if ever, be able to trace the complete loop, part of the corresponding onsets being due to second or third arrivals of small amplitude. Similarly, when there is a break in the time curve of first arrivals indicating a decrease of velocity with depth, it will not be possible to determine the complete time curve including the retrograde branch of small second or third arrivals. Thus, when the velocity function does not have normal behaviour, we may see indications of this, but we shall not be able to determine the velocity directly from the travel times we derive from observations.

It was in 1910 that A. Моноровиѣрѣ found the upper boundary of the mantle clearly indicated by the branching off of the time

curve. The determination of its depth and the velocity contrast on it met with difficulties.

MOHOROVIČIĆ took the time curves for small distances to curve slightly and the velocity to vary according to the exponential law. The procedure was complicated and JEFFREYS pointed out that the travel times fitted on to straight lines just as well. This led up to the habitual practice of fitting travel times to straight line segments of time curves, especially in crustal studies, but also sometimes, and again recently, in mantle studies. Correspondingly, the velocity would be increasing stepwise. But this is only one type of many possible velocity models. It is accepted as the simplest and is quite satisfactory provided too much significance is not attached to the discontinuities determined from it.

In the course of time various discontinuous changes of mantle velocity have been determined, most of them from time-curves that have undergone smoothing processes of some kind. The most important and the only one I shall mention here is the 20° discontinuity which emanated from the work done by JEFFREYS and BULLEN when they constructed their time-curves. The P curve has a stronger curvature around 20° than elsewhere, and it seemed to set in rather abruptly. A discontinuous change of the velocity gradient and possibly of the velocity itself at about 400 km depth would account for this. However, later some of the observations used for the smallest distances were found to be in error, and when the travel times were corrected the increase of curvature around 20° became more gradual. Correspondingly, the velocity increase would be gradual and it would become strong around 200 km depth. It appeared from many studies carried out by Sir Harold JEFFREYS that upper mantle velocities were not everywhere the same. In some regions there was a more or less well-marked 20° discontinuity in the time-curve for P, but the corresponding velocity function would not have a discontinuity at the depth originally determined. It is a curious fact that now-a-days the 20° discontinuity is often spoken of as a discontinuity in the velocity at about 400 km depth with no regard to the behaviour of the time-curve around 20° .

GUTENBERG maintained that there was no discontinuity anywhere in the mantle, but his velocities did show a behaviour departing from normal. The P_n time curves broke off, sometimes at quite small distances, indicating the presence of a low-velocity layer. GUTENBERG believed that the decrease of the velocity was gradual and so was the increase that terminated the low-velocity layer. If this were so, there would be a caustic at the lowest point of the

upper branch of the time curve, but the existence of such a caustic has never been convincingly demonstrated.

Around 1950 nuclear explosions began to provide seismology with far more accurate data than those obtained from earthquakes. It had been found already that mantle velocities were not everywhere the same, but it now appeared that they differed far more than found previously from one region to another. The GNOME shot was the first one to bring this out clearly and convincingly. Then mantle investigations had to be modified. It could no longer be considered advisable to combine the travel times obtained in different azimuths from the source. Profiles had to be taken as in crustal studies, but since the profiles had to be long the structure would, perhaps, not always be the same along a profile and this would complicate matters. However, results have been obtained from many studies on profiles. I shall comment on three examples here.

One is the GNOME-NE. Fig. 1 presents the travel times observed on this profile and time curves calculated on certain velocity

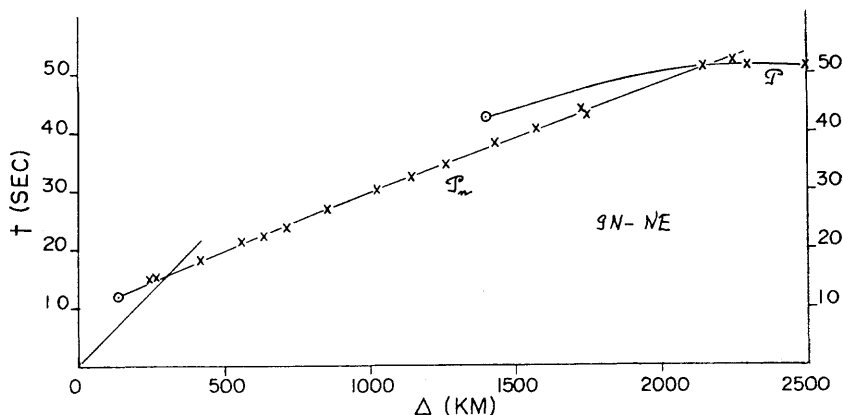


FIG. 1. — P travel times reduced by 0.1Δ to stations northeast of the GNOME site and corresponding time-distance curves.

assumptions to which the travel times fit on extremely well (See LEHMANN, 1964, pp. 136-7). The Pn curve bends slightly while the upper P curve bends rather strongly. There is a cross-over at about 2100 km distance where the slopes of the two curves differ distinctly. Taking the observations by themselves, neglecting the calculated curves, it is clear that there is no way of fitting them all on to one continuous curve bending gradually. First

arrivals, and they are all I have, therefore do not determine the complete time curve. There is a bunch of rays with angles of emergence in between those of the two different rays emerging at the cross-over, and unless their travel times can be determined we cannot trace the complete time curve. I have not seen the GNOME records and do not know whether later arrivals are readable. I have, however, seen a beautiful series of Lake Superior W records. The P_n and P travel time curves have a cross-over at a similar distance and for ranges of distance both before and after the cross-over there are well marked second arrivals. Whether third arrivals could be read I cannot say, but I feel that even with these excellent records there is no way of tracing the complete time curve with any accuracy.

This means that we cannot deduce the velocity function directly from the travel times as we have them. We have to choose a model for it more or less arbitrarily and adapt it to our travel times. There are, of course, a great many possible ways of doing this.

Before it is explained how the model that produced the travel times here calculated was chosen, results derived from explosions on the NTS recorded to the east of the test site are presented, one of them being the strong Bilby shot (See LEHMANN, 1967, pp. 18-19). The travel time curves differ a great deal from

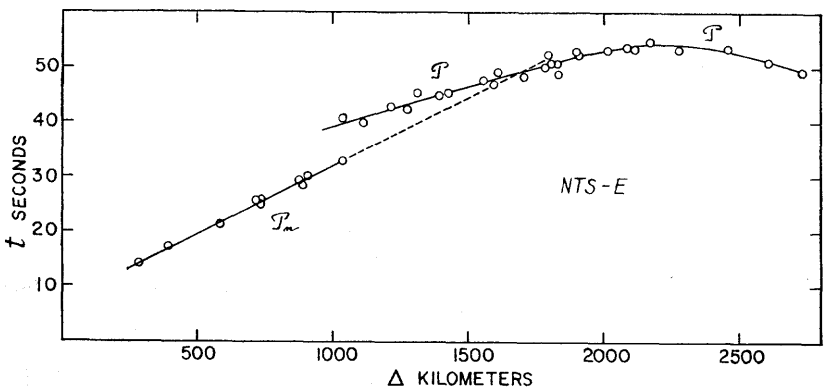


FIG. 2. — P travel times reduced by 0.1Δ to stations east of the Nevada Test Site and corresponding time-distance curves.

those of the GNOME-NE. We have again a nearly straight P_n curve and a bending P curve, but P_n breaks off a little beyond 1000 km so the two curves do not meet. P is observed as the

first arrival from the distance at which P_n breaks off. It is delayed against P_n at first, but the bending P curve is intersected by the continuation of the P_n line at about 1700 km distance. From the smallest distance at which P is observed, the P travel times can be represented by one continuous curve. It is clear that no significantly better fit is obtainable by adapting different curves or straight lines to different segments.

The observations are taken from a great many different shots on the NTS, Bilby being the strongest. Bilby P is recorded clearly as far away as 9100 km, so the absence of P_n beyond 1039 km on our profile indicates the presence of a low-velocity layer. This is regional. To the ENE and NE of NTS P_n is recorded in the range where it is missing here.

Here as for the GNOME shot the complete time curve cannot be determined from observations. The angle of emergence is greater for the first P ray than for the last P_n ray and so the travel times of a bundle of rays are missing. They would belong to the retrograde branch of the time curve with small amplitudes on it, and they are not likely ever to be observable. So here again we cannot derive the velocity function directly from observations. We have to choose a model and adapt it so as to fit the observations we have.

There is agreement between GUTENBERG's results and recent results of JEFFREYS about the velocity increase being strong about 200 km depth. This is responsible for the strong curvature of the P curve around 20° and for the large amplitudes there. They both take the velocity increase to be gradual.

My travel time curves for the NTS-E bear resemblance to those of GUTENBERG in that the P_n curve breaks off, but there is a very important difference between the P curves. When calculated on the GUTENBERG velocity assumptions the P curve begins between 1600 and 1700 km distance, and GUTENBERG never had good P observations at smaller distances, partly because instrumentation had been inadequate and partly because observations had not been obtained on separate profiles. He had some scattered observations of small amplitude that would fit on to the P curve as drawn here, but he took them to be due to diffraction. With the P curve we have here it becomes imperative to find a velocity distribution that will make the P curve begin at a much smaller distance than the GUTENBERG curve. This is hardly possible unless we take the velocity to increase abruptly at some depth so that reflections go back to small distances and refractions begin there. I have there-

fore assumed that there is a discontinuous increase of velocity at depth, and I have placed it a little below 200 km depth where according to JEFFREYS and GUTENBERG the velocity increase is strong.

The amplitudes of P increase with distance and correspondingly the velocity is taken to increase below the discontinuity. The amplitudes are relatively small at the smallest distances at which the phase occurs, but it sometimes is very well marked. I have here (Fig. 3) the Bilby record from 1039 km distance in which P_n and P both occur. P (or P_r) is seen to be a clear phase.

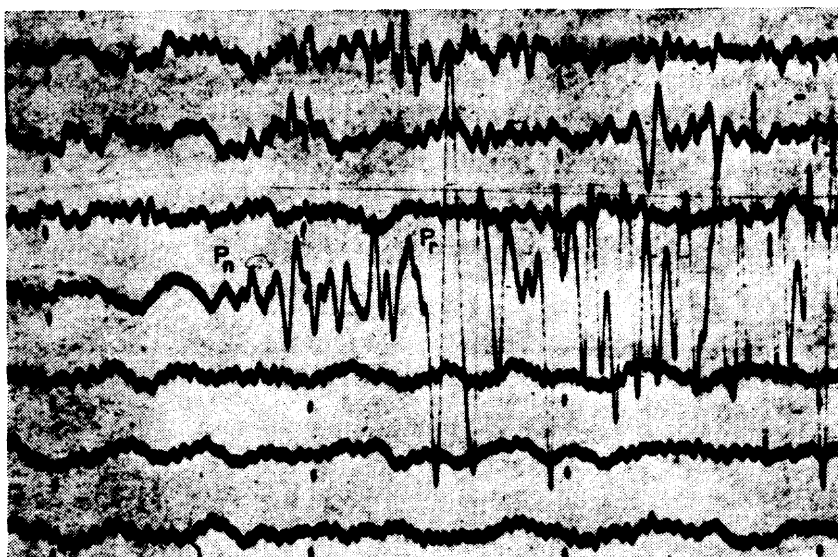


FIG. 3. — RT NM Bilby Z record, $\Delta = 1039$ km.

There is a parallel between the present development and the story of PKP at distances smaller than 143° . In the early days faint and scattered observations were obtained and they were taken to be due to diffraction. But when short-period seismographs of high magnification had been installed at many stations, clear PKP observations were obtained and had to be explained more adequately. It was found that an abrupt velocity increase deep in the core would account for the phases.

I believe that if GUTENBERG had seen the observations presented here, he would have felt that his velocity assumptions had to be modified and that an abrupt velocity increase would be required.

With a discontinuous velocity increase at a depth a little more

than 200 km, time curves can be calculated that fit the observations here presented. But it is also possible to calculate time curves to fit the travel times for other regions. The velocity below the discontinuity can be taken to be practically the same in all cases. The differences are in the uppermost mantle. Returning to the GNOME travel times and comparing them with those of the NTS-E (Fig. 4), we see that the P_n curve is lower down, i. e., the velocity

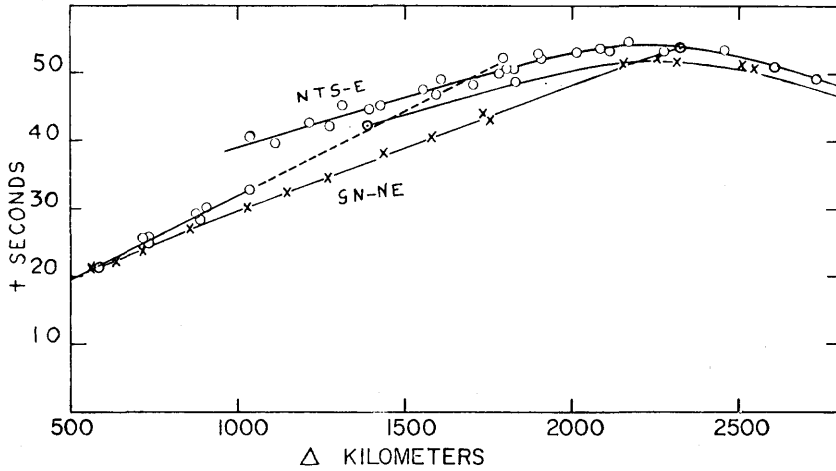


FIG. 4. — Comparison between GN-NE and NTS-E travel times of P.

is higher, and there is no shadow for P_n at distances smaller than that of the cross-over. But the P curves do not differ a great deal.

I have compared the travel times of the SALMON shot, as published by JORDAN et al. (1966), with those of GN-NE and NTS-E (Fig. 5).

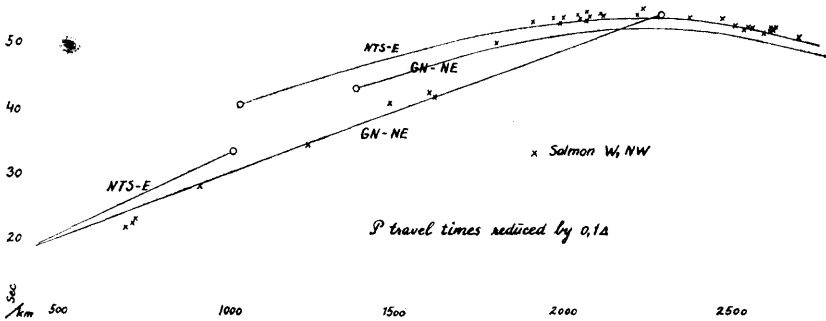


FIG. 5. — P travel times reduced by 0.1Δ to stations W and NW of the Salmon site and time-distance curves for GN-NE and NTS-E.

In figure 5 the SALMON travel times to the W and NW are marked by crosses. The paths to individual stations have this in common that at a distance of between 1 800 and 1 900 km they cross the Rocky Mountain frontier. There are few P_n observations because of lack of stations. At the smallest distances they are earlier than the GNOME times, but for somewhat greater distances they agree with them. Between 1 800 and 1 900 km, where the Rocky Mountain frontier is crossed, the P_n breaks off and it is P that is the first arrival for greater distances. This may indicate the presence of a low-velocity layer. While the SALMON P_n fits the GN-NE P_n curve, the SALMON P fits approximately the P curve of NTS-E.

REFERENCES

- JORDAN (J. N.), MICKEY (W. V.), HELTERBRAN (W.) and CLARK (D. M.). 1966. Travel times and amplitudes from the Salmon explosion. *J. Geophys. Res.* 71, 3469-3482.
- LEHMANN (I.). 1964. On the travel times of P as determined from nuclear explosions. *Bull. seismol. Soc. Amer.* 54, 123-139.
- LEHMANN (I.). 1967. On the travel times of P as obtained from the nuclear explosions Bilby and Shoal. *Phys. Earth Planet. Interiors* 1, 14-23.

J.F. IMPRESSIONS, 14, RUE IDRAC — TOULOUSE — 4718 2-69

PRINTED IN FRANCE

